NASA/TP—2004–213339

Solar Variability and the Near-Earth Environment—Mining Enhanced Low Dose Rate Sensitivity Data From the Microelectronics and Photonics Test Bed Space Experiment

T. Turflinger, W. Schmeichel, J. Krieg, and J. Titus
NAVSEA Crane, Crane, Indiana

A. Campbell and M. Reeves
Naval Research Laboratory, Washington, DC

P. Marshall
Consultant, Brookneal, Virginia

August 2004

The NASA STI Program Office…in Profile

Since its founding, NASA has been dedicated to the advancement of aeronautics and space science. The NASA Scientific and Technical Information (STI) Program Office plays a key part in helping NASA maintain this important role.

The NASA STI Program Office is operated by Langley Research Center, the lead center for NASA's scientific and technical information. The NASA STI Program Office provides access to the NASA STI Database, the largest collection of aeronautical and space science STI in the world. The Program Office is also NASA's institutional mechanism for disseminating the results of its research and development activities. These results are published by NASA in the NASA STI Report Series, which includes the following report types:

- TECHNICAL PUBLICATION. Reports of completed research or a major significant phase of research that present the results of NASA programs and include extensive data or theoretical analysis. Includes compilations of significant scientific and technical data and information deemed to be of continuing reference value. NASA's counterpart of peer-reviewed formal professional papers but has less stringent limitations on manuscript length and extent of graphic presentations.

- TECHNICAL MEMORANDUM. Scientific and technical findings that are preliminary or of specialized interest, e.g., quick release reports, working papers, and bibliographies that contain minimal annotation. Does not contain extensive analysis.

- CONTRACTOR REPORT. Scientific and technical findings by NASA-sponsored contractors and grantees.

- CONFERENCE PUBLICATION. Collected papers from scientific and technical conferences, symposia, seminars, or other meetings sponsored or cosponsored by NASA.

- SPECIAL PUBLICATION. Scientific, technical, or historical information from NASA programs, projects, and mission, often concerned with subjects having substantial public interest.

- TECHNICAL TRANSLATION. English-language translations of foreign scientific and technical material pertinent to NASA's mission.

Specialized services that complement the STI Program Office's diverse offerings include creating custom thesauri, building customized databases, organizing and publishing research results…even providing videos.

For more information about the NASA STI Program Office, see the following:

- Access the NASA STI Program Home Page at ***http://www.sti.nasa.gov***

- E-mail your question via the Internet to help@sti.nasa.gov

- Fax your question to the NASA Access Help Desk at (301) 621–0134

- Telephone the NASA Access Help Desk at (301) 621–0390

- Write to:
  NASA Access Help Desk
  NASA Center for AeroSpace Information
  7121 Standard Drive
  Hanover, MD 21076–1320
  (301)621–0390

NASA/TP—2004–213339

Solar Variability and the Near-Earth Environment—Mining Enhanced Low Dose Rate Sensitivity Data From the Microelectronics and Photonics Test Bed Space Experiment

T. Turflinger, W. Schmeichel, J. Krieg, and J. Titus
NAVSEA Crane, Crane, Indiana

A. Campbell and M. Reeves
Naval Research Laboratory, Washington, DC

P. Marshall
Consultant, Brookneal, Virginia

National Aeronautics and
Space Administration

Marshall Space Flight Center • MSFC, Alabama 35812

August 2004

Acknowledgments

The microelectronics and photonics test bed (MPTB) bipolar experiments would not have been possible, nor the earlier data analyses performed, without the continuing support of Lew Cohn and the Defense Threat Reduction Agency Radiation Tolerant Microelectronics program. In addition, Ron Pease, RLP Research, has been involved in this project from the beginning, and kindly assisted in the editing of this Technical Publication. Jake Tausch, Hugh Barnaby, and Dave Sleeter, Mission Research Corporation, did a superb job in the design and construction of the bipolar boards, which continue to function and record data over 5 yr into an anticipated 2-yr mission.

Clive Dyer and Karen Hunter, QinetiQ, and Bernie Blake, Joe Mazur, and Joe Fennell, The Aerospace Corporation, were all extremely helpful in interpretation and analysis of the data from their instruments, and understanding the radiation environment of the MPTB. Scott Messenger and Rob Walters, National Research Laboratory, assisted in discussions on proton displacement damage.

This effort was accomplished with resources provided by NASA's Living With a Star (LWS) Space Environment Testbeds (SET) Program.

TRADEMARKS

Trade names and trademarks are used in this report for identification only. This usage does not constitute an official endorsement, either expressed or implied, by the National Aeronautics and Space Administration.

Available from:

NASA Center for AeroSpace Information
7121 Standard Drive
Hanover, MD 21076–1320
(301) 621–0390

National Technical Information Service
5285 Port Royal Road
Springfield, VA 22161
(703) 487–4650

TABLE OF CONTENTS

TABLE OF CONTENTS (Continued)

LIST OF FIGURES

LIST OF FIGURES (Continued)

LIST OF FIGURES (Continued)

LIST OF FIGURES (Continued)

LIST OF FIGURES (Continued)

LIST OF FIGURES (Continued)

LIST OF TABLES

LIST OF ACRONYMS

Co60	Cobalt–60
COTS	commercial-off-the-shelf
CREDO	cosmic radiation environment and dosimetry
DTRA	Defense Threat Reduction Agency
ELDRS	enhanced low dose rate sensitivity
GTO	geosynchronous transfer orbit
LPNP	lateral PNP
MOS	metal oxide semiconductor
MPTB	microelectronics and photonics test bed
NAVSEA	Navel Sea Systems Command®
NIEL	nonionizing energy loss
NRL	Naval Research Laboratory
NSREC	Nuclear Space Radiation Effects Conference
SPE	solar particle event
SPNP	substrate PNP
TP	Technical Publication

NOMENCLATURE

I_B	base current
I_C	collector current
I_{ib}	input bias current
I_{os}	offset current
m	slope
V_{BE}	base-to-emitter voltage
V_{os}	offset voltage
x	total dose for a given orbit
y	corresponding input bias current of the device

TECHNICAL PUBLICATION

SOLAR VARIABILITY AND THE NEAR-EARTH ENVIRONMENT—MINING ENHANCED LOW DOSE RATE SENSITIVITY DATA FROM THE MICROELECTRONICS AND PHOTONICS TEST BED SPACE EXPERIMENT

1. INTRODUCTION

The microelectronics and photonics test bed (MPTB) space experiment was launched in November 1997 with multiple electronics experiments aboard a host satellite that has now completed over 3,700 12-hr geosynchronous transfer orbit (GTO) revolutions. The MPTB space experiment consists of 24 individual electronic and photonic device boards integrated into three panels. Most experiments have been successful, and there are many published results from this experiment.

This study was a detailed analysis of existing MPTB satellite data from one experiment—the bipolar test board (A4)—looking to improve our understanding of the enhanced low dose rate sensitivity (ELDRS) phenomenon. NAVSEA Crane and Mission Research Corporation, as a part of the Defense Threat Reduction Agency (DTRA) ELDRS program, constructed the bipolar test board and collected supporting ground test data. Over the past several years, extensive total dose irradiations of bipolar devices (hereafter, referred to as ground-based testing) have demonstrated that many of these devices exhibited ELDRS.[1–9] In sensitive bipolar transistors, ELDRS produced enhanced degradation of base current (I_B), resulting in enhanced gain degradation, at dose rates <0.1 rd(Si)/s compared to similar transistors irradiated at dose rates >1 rd(Si)/s. In 1994, several bipolar linear integrated circuits were demonstrated to exhibit enhanced degradation of input bias current (I_{ib}), offset current (I_{os}), and/or offset voltage (V_{os}) when irradiated at dose rates <0.1 rd(Si)/s compared to similar circuits irradiated at dose rates >1 rd(Si)/s.[3–5]

Until late 1997, ELDRS research had been limited to ground-based testing. The applicability of ground-based observations to space environments was questionable because of the complex nature of the space environment and the lack of known system failures attributed to ELDRS. In 1996, an experiment was initiated to acquire space-based measurements to begin examining the effects of a complex environment and to compare these data to ground-based data. This experiment was designed to characterize the total dose response of several bipolar devices during space flight. These RF25 transistors and three types of bipolar linear integrated circuits—LM124A, LM139J, and PM139Y—were selected as test vehicles. To accomplish this task, two test boards were designed and built to allow parametric measurements on these devices while being flown in a highly elliptical orbit in space as part of the MPTB satellite experiment.

After its deployment, the electrical responses of several bipolar transistors and linear circuits have been, and continue to be, recorded once during every 12-hr orbit. System dosimeters are monitored to establish an average accumulated dose per orbit. With this information, the electrical parameter data are correlated with the dosimetry data to determine the total dose response of each device. An initial paper

highlighting the ELDRS boards was presented and published in 1998 (app. A),[10] and a subsequent paper was presented and published in 1999 (app. B).[11] As of this date, the experiment has been in flight for a period of 5 yr and has accumulated an approximate dose of 45 krd(Si).

For comparison, devices—specifically, linear circuits with the same date code—were irradiated using Cobalt–60 (Co60) sources, herein defined as ground-based tests. The ground-based tests were used to evaluate two hardness assurance tests—a room-temperature irradiation test at 10 mrd(Si)/s and an elevated temperature irradiation test at 100 °C and 10 rd(Si)/s—and to evaluate the ELDRS response. Irradiations were performed at room temperature (≈22 °C) at fixed dose rates of 100, 1, and 0.01 rd(Si)/s, and at an elevated temperature of ≈100 °C at a fixed dose rate of 10 rd(Si)/s. Currently, irradiations are being performed at room temperature at a fixed dose rate of 0.001 rd(Si)/s. Comparing the ground-based data to the flight data clearly demonstrates that enhanced parametric degradation has occurred in the flight parts. The two hardness assurance screens predicted ELDRS, but the design margin for the elevated temperature test may not be adequate.

The Naval Research Laboratory (NRL) constructed the MPTB space experiment. The design and construction of board A4 was executed by NAVSEA Crane and Mission Research Corporation with DTRA funding. While the data have been downloaded from the satellite and collected by the NRL, analysis was up to individual experimenters and not directly funded as part of the MPTB program. The DTRA funded NAVSEA Crane to analyze the initial data, resulting in two publications in *IEEE Trans. Nucl. Sci.*[10,11] In addition, the DTRA funded an extensive ground test program to complement the space data. Board A4 is a self-contained analog parametric test system that maintains bias on the test devices and performs measurements of critical parameters once per orbit. It was the first ELDRS experiment to fly in space, and its demonstration of ELDRS in a space environment has had a significant impact on spacecraft development. The experiment contains two variations of an operational amplifier and two variations of a voltage comparator, described in detail in section 2.

This Technical Publication (TP) provides updated information about the test devices, the in-flight experiment, and both flight- and ground-based observations. Flight data are presented for the past 5 yr of the mission and are compared to ground-based data taken on devices from the same date code lots. Information about temperature fluctuations, power shutdowns, and other variables encountered during space flight are documented. This work continues to leverage on the existing DTRA program at NAVSEA Crane in support of ELDRS research.

Comparisons of the flight data to ground-based data irradiated at dose rates of 1 and 10 mrd(Si)/s clearly demonstrate that ELDRS effects do indeed occur in space and produce enhanced degradation.

2. EXPERIMENTAL DETAILS

Details of the two experimental test boards—the MPTB transistor board B1 and the linear integrated circuit board A4—built as part of the DTRA ELDRS program for inclusion on the MPTB are described in this section.

2.1 Orbital Information

The satellite carrying the MPTB payload was launched in November 1997 and placed in a highly elliptical orbit with an orbital period of ≈12 hr. Most of the accumulated dose per orbit occurs when the spacecraft traverses the proton and electron belts. These belt traversals last ≈70 min per orbit, or ≈10 percent of the total orbital time.

Figure 1 shows one of the three panels of experiment boards that comprise the MPTB experiment. NAVSEA Crane and Mission Research Corporation built two different experiment boards for the MPTB. For completeness, section 2 describes the experimental detail on both boards, even though this study only analyzes the data for the linear integrated circuit board A4. As described in the 1998 paper (see app. A), only limited data were utilized, primarily due to temperature effects that were very difficult to eliminate from the data.

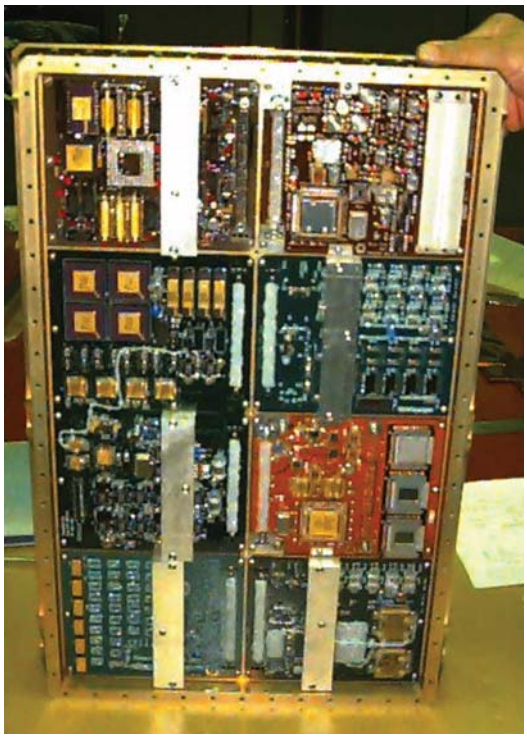

Figure 1. One of three MPTB panels.

2.2 Transistor Board B1

2.2.1 RF25 Transistor Board Description

One of the two test boards was designed to characterize the bipolar transistors. A digital-to-analog output on the motherboard provides the base-to-emitter voltage (V_{BE}). Onboard resistors allow direct measurements of the I_B and collector current (I_C), which are then processed by the motherboard for subsequent downloading. V_{BE} is swept from 0.1 to 0.9 V in 0.02-V increments. I_B and I_C are measured at each voltage increment. This board is designated as B1 on the MPTB experiment. Figure 2 shows transistor board B1, which clearly highlights the spatial location of the six mounted RF25 transistor packages.

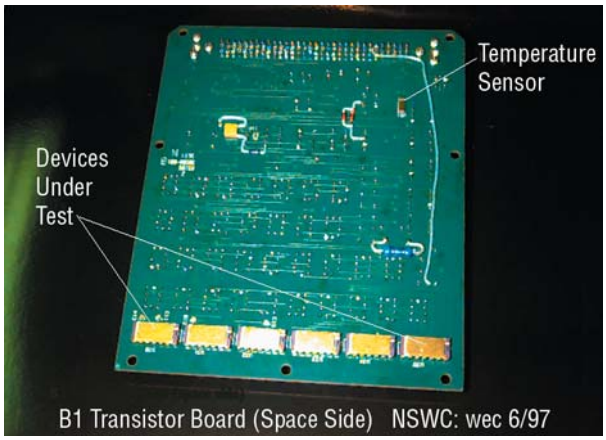

Figure 2. MPTB board B1.

2.2.2 RF25 Process/Transistor Description

The RF25 transistor is manufactured by Analog Devices and was developed for low noise amplifiers, power amplifiers, mixers, and radio frequency switches that are used in many communication applications.[10] Test dies from wafer fabrication lot No. 350569.1 contain a large, lateral PNP (LPNP), a small LPNP, a substrate PNP (SPNP), and a vertical NPN. Dies were mounted in a 14-pin, dual in-line ceramic package and date coded DC94. The small LPNP and SPNP use a square geometry with an emitter area of 1.2×1.2 μm. The large LPNP uses a square geometry with five parallel emitter areas of 1.2×1.2 μm each.

2.2.3 RF25 Transistor Biasing Description

Figure 3 shows the in situ bias configuration for the RF25 transistor package during flight. The substrate is always at ground. The emitters of the PNP transistors have an in situ bias of 2.5 V while the base and collector are floating. The collector of the NPN transistor has an in situ bias of 2.5 V while the base and emitter are floating. The bias conditions were determined, in part, by constraints imposed by the test board and the satellite system, such as size and power requirements.

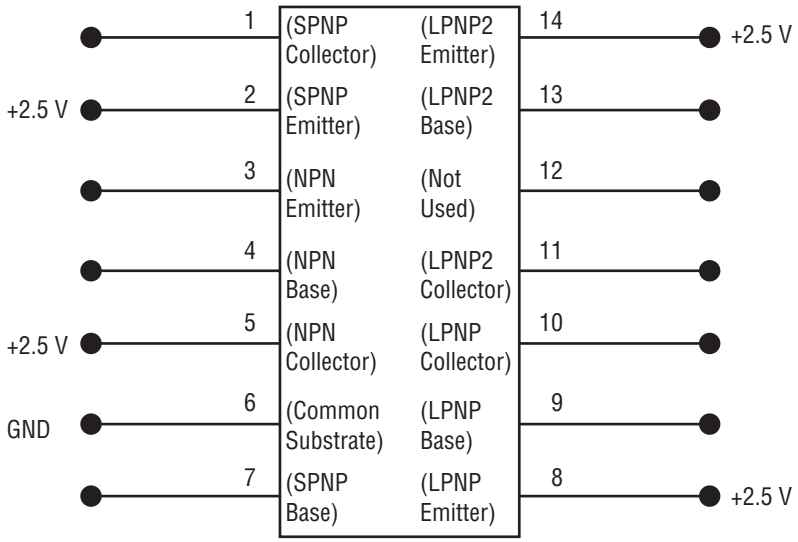

Figure 3. RF25 transistor package in situ bias configuration.

2.3 Linear Integrated Circuit Board A4

2.3.1 Circuit Board Description

The second ELDRS test board (A4) on the MPTB experiment was designed to characterize the linear integrated circuits, specifically the LM124A, LM139J, and PM139Y. The onboard op amp and comparator circuitry allowed three sets of measurements for each circuit, which are then processed by the motherboard for subsequent downloading. These three measurements are used to calculate the three circuit parameters: V_{os}, I_{os}, and I_{ib}. The measurement technique is similar to that described in MIL–STD–883, Test Method 4001.[12] The op amp and comparator require slightly different test configurations due to the different output stages in each circuit type. Figure 4 shows board A4, which clearly highlights the spatial location of the eight linear integrated circuit packages consisting of four op amp and four comparator packages mounted along both sides of the board.

2.3.2 Circuit Description

The four LM124A op amp packages are manufactured by National Semiconductor. The two commercial-off-the-shelf (COTS) packages that have a date code of 9524 were manufactured in Greenock, UK. The other two packages that have a date code of 9520 are class S-type devices and were manufactured in Santa Clara, CA. Each LM124A package consists of four independent op amp circuits. I_{ib} is temperature compensated in these devices.

The two LM139 comparator packages are also manufactured by National Semiconductor, Greenock, UK, and have a date code of 9530. The two PM139 comparator packages are manufactured by PMI—now Analog Devices—and have a date code of 9522. Each LM139 and PM139 package consists of four independent comparators. The input structures of the National Semiconductor LM124 and LM139 are fabricated using an SPNP and LPNP hybrid structure.

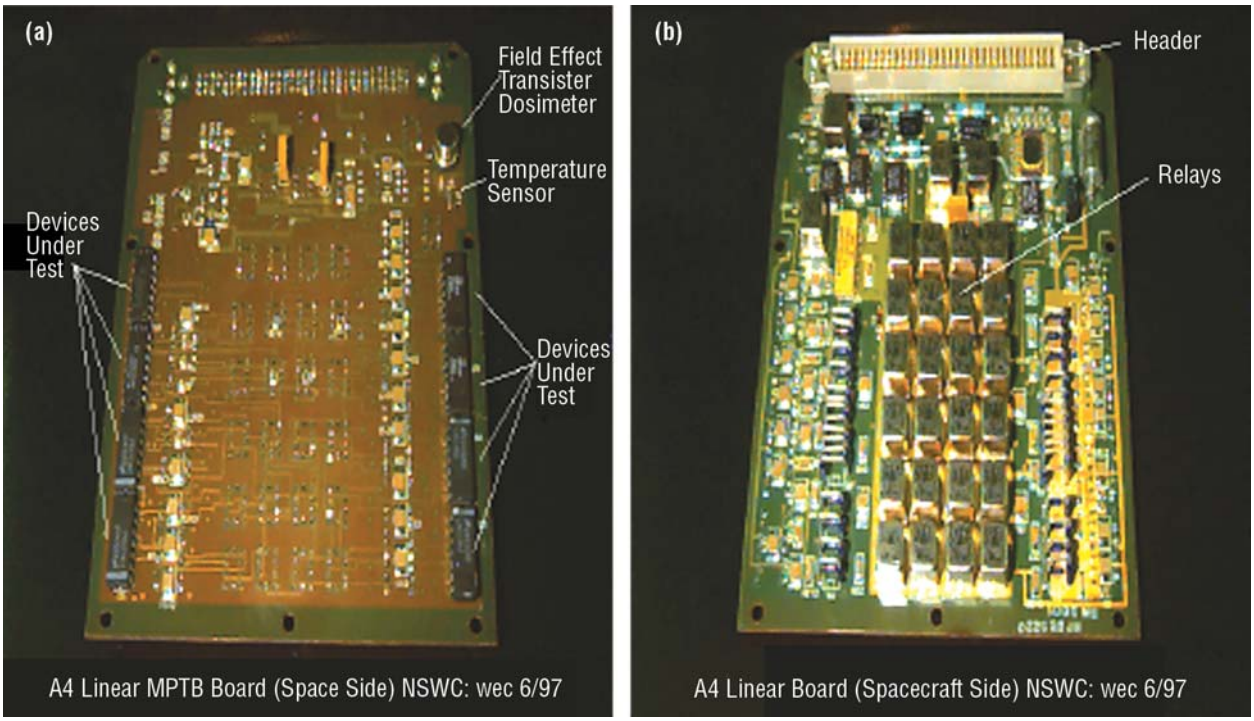

Figure 4. MPTB board A4: (a) Space side and (b) satellite side.

2.3.3 Circuit Biasing Description

Figure 5 is representative of an in situ bias configuration for the LM124 package (voltage follower with gain of 1), and figure 6 is representative of an in situ bias configuration for the LM139 and PM139 packages (basic comparator with inputs at ground potential). These configurations were selected because of certain test system constraints, and to define the input bias condition. The inputs were identified as containing the sensitive structures to be controlled during the experiment. In general, ground test data have shown these bias configurations produce worst-case degradation in the I_{ib} parameter, but not necessarily worst-case for offset parameters. Preference was given to the I_{ib}, which was anticipated to degrade a greater amount.

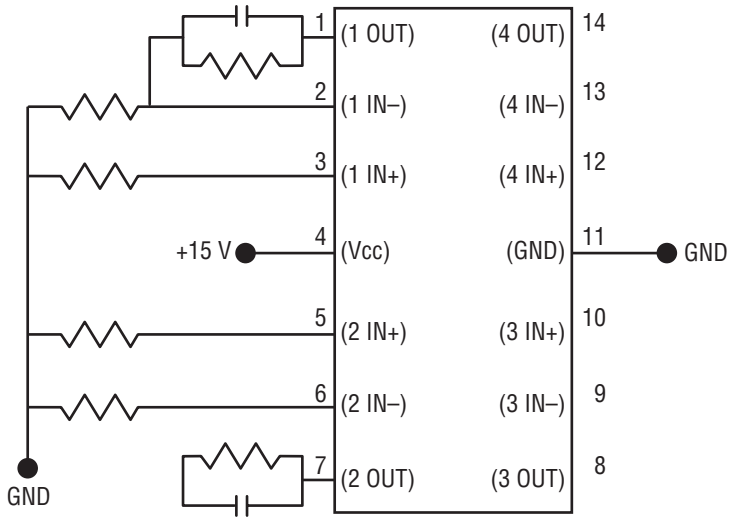

Figure 5. In situ bias configuration for the LM124 package.

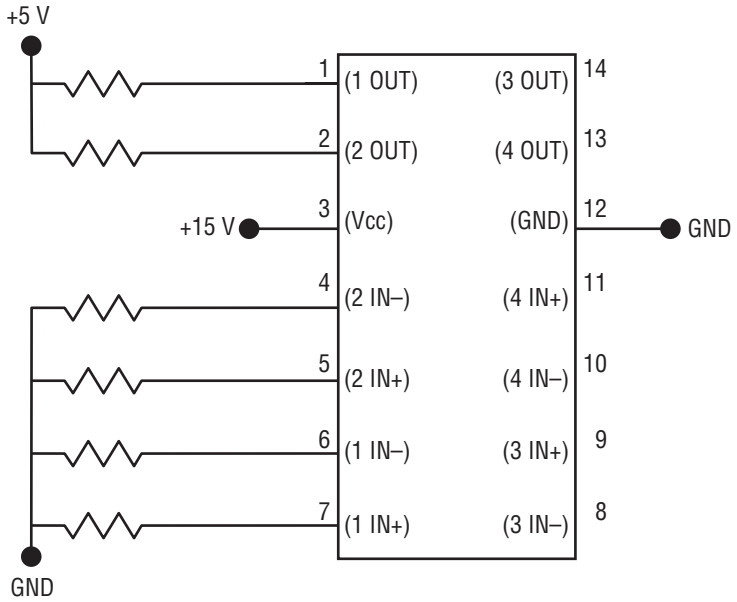

Figure 6. In situ bias configuration for the LM139 and PM139 packages.

3. ORBIT AND EXPERIMENT DOSIMETRY

The radiation environment for the MPTB consists of electrons and protons trapped in the Earth's radiation belts, cosmic ray ions—mostly protons, and solar event particles that arrive as the result of activity at the Sun's surface. The MPTB is linked to instruments used to measure this environment, including associated dose appropriate to the expected effects on devices. Because of the dynamics of the Earth's radiation belts, solar events can disturb the magnetosphere without directly injecting particles but which can result in changes in the time arrival and magnitude of particles, so it is important that these data are available continuously. The MPTB contains three primary radiation environment monitoring systems. Each experiment board includes at least one metal oxide semiconductor (MOS) (p-channel) transistor dosimeter, a proton telescope, and a particle detector. These PMOS dosimeters are from a batch of 4,007 test transistors procured for the purpose of developing space dosimeters. They have been flown in space since the 1970's.[13] Initial data analysis utilized the PMOS dosimeters exclusively, but problems were found with these data, as will be explained below. A key component of this study has been new analyses by the NRL of all available data from the MPTB to establish the best estimate of accumulated dose on board A4. This section explains how data from each of these instruments was used to establish this estimated dose, and how to determine the proton fluence on the board so possible displacement damage effects can be examined.

3.1 Orbit and Radiation Environment

The MPTB flies in a highly elliptical GTO. Each orbit is very close to a 12-hr duration; the perigee is ≈1,000 km, while apogee is beyond geosynchronous. Nearly 9 hr of the orbit are in deep space, with the remaining 3.5 hr comprised of a rapid drop to perigee and a climb back to deep space. Thus, the orbital path transits directly through the inner (proton) and outer (electron) Van Allen belts twice each orbit. As the spacecraft descends towards perigee, it spends ≈1 1/2 hr within the belts. It is below the belts for 20 to 30 min as it passes perigee, and then spends a slightly longer period in the belts again as it climbs back towards apogee. Over the mission life, there has been significant variation in these orbital parameters, due to details of the orbital mechanics and changes in orbit. As such, the above numbers should be considered a representative model. Better detail on the orbit can be found in Dyer et al.[14,15]

In normal times, when solar activity is low, the great majority of the dose absorbed in each orbit occurs during descending and ascending belt transitions. The test devices on the MPTB are shielded by an equivalent of 60–70 mil of aluminum. As such, both electron and proton doses reach the devices. During a solar particle event (SPE), the spacecraft receives significant doses outside the belts, and the belts may also be enhanced for a period of hours to many days. The transit through the proton belt is observed clearly in figure 41 (sec. 5), which shows the proton flux for three different proton energies for part of one orbit in April 2002. The descending and ascending transitions are not exactly symmetrical, with the ascending transition taking several minutes longer than the descending transition. Solar activity can also cause wide variations in dose per orbit through geomagnetic disturbances of the outer electron belts. Depending on shielding, protons from an SPE may make a small contribution to the total dose.

In addition, an asymmetry in particle count between even and odd orbits occurs because of differences in the tilt and displacement of the Earth's magnetic field. This difference means that even-numbered orbits experience more inner belt protons while odd-numbered orbits are more exposed to cosmic rays and SPEs at perigee.[14,15] The spacecraft is always fully exposed to cosmic rays when outside the belts. This asymmetry is not significant to the basic ELDRS experiment, but the even/odd orbit asymmetry caused problems with some analysis, as discussed further in section 5.

Published data have shown that dose rates >50 mrd(Si)/s do not simulate low dose rate test data well, with major inconsistencies often reported with the 100 mrd(Si)/s data. During much of the experiment's life, the average dose rate has been within bounds of established ground data, but there have been significant excursions outside the 1–10 mrd(Si)/s window predominately used in ground test. During the high dose rate periods, the rate of damage should slow. Extremely limited ground data taken at dose rates <1 mrd(Si)/s indicate that the rate of damage should probably increase, though the required lower bound to this increase in damage rate has not been established. Examining the impact of these changes on the parametric data is a prime purpose of this study (see sec. 7).

3.2 Radiation Measurement Instruments

Each experiment board included at least one MOS (p-channel) transistor dosimeter, which is sensitive to both proton and electron doses. The PMOS devices are test transistors from RCA CD 4007 integrated circuits. These PMOS dosimeters were developed by Leon August, NRL, in the late 1970's and early 1980's and were flown on a number of spacecraft. The dosimeters used for the MPTB are residuals from that same batch and were packaged at the NRL in that era. The bias method used in orbit affects the usable life of the PMOS dosimeters. For the MPTB, the board dosimeters are unbiased during exposure to get the maximum range available. PMOS dosimeter fading, which was noted in earlier analysis of these data, has been studied. Details can be found in references 16–18. Considering that most of the dose of the ≈12-hr orbit time is delivered in a couple of hours or so, except for flare periods, and that the parts are unbiased, one might well expect ≈10-percent recovery from the electron dose in each orbit but almost no recovery from the proton dose.

In addition to the PMOS dosimeters, two instruments flying with the MPTB are being utilized to provide measurements of the radiation environment at the same time that the radiation-induced changes and ELDRS measurements are being made on the test devices. One instrument is the cosmic radiation environment and dosimetry (CREDO) board from Clive Dyer, QinetiQ. The other is The Aerospace Corporation's DSU instrument, flying on the same satellite with data from Bernie Blake. CREDO is a particle coincidence counter using a solid-state detector that measures the flux of protons with energies >38 MeV and a variable time resolution. As such, it is a particle telescope with a limited field of view. Electron counts are also established on CREDO when noncoincident counts are observed.[15] The DSU measures proton fluxes in four energy regions and the dose behind several shield thicknesses over a hemispherical geometry. For this study, the proton fluxes with energies greater than 6.5, 15, and 25 MeV and doses behind 50 and 125 mil of equivalent aluminum shielding are being analyzed. The dose is delivered from trapped protons and electrons and solar event particles. These instruments are described in detail in references 14, 15, 19–32.

3.3 Integrated Dose Curve

As noted above, the PMOS dosimeter data were used exclusively in previous studies of these MPTB data. Since the PMOS transistor dosimeter characteristics are measured once per orbit—at apogee, the data have been integrated as proton fluence per orbit or dose per orbit. Intraorbit fluctuations are being considered because of changes in the spectrum and time delivery of particles as a function of solar cycle and solar activity. Analyses and correlations of the test circuit parametric changes and the dose and proton fluence per orbit are provided in this TP. Particle fluence is also being considered because of possible displacement damage effects in some device types.

The PMOS dosimeter on board A4—the ELDRS experiment—has been nonfunctional in flight. Data have been used from an adjacent board. This should provide only a small source of error. Apparent PMOS dosimeter fading was noted in earlier analysis by approximately orbit 2,000, which left questions of data interpretation. The dosimeters have been shown to respond accurately during periods of relatively high dose rates but underrespond during periods of minimal dose rate. The PMOS board dosimeters, as implemented on the MPTB, are not sensitive enough to give accurate orbit-by-orbit dose rate information. Such an analysis was attempted. The data were averaged and fit to smooth curves and then differentiated, but these dose rate data were shown to be too noisy to be useful for this analysis.

It was necessary to get access to data from the DSU instrument—a scientific instrument that provides, besides the particle spectra, dose as a function of shielding depth with a time resolution of about four per minute. Bernie Blake, The Aerospace Corporation, provided the DSU data for this effort. The DSU data have been averaged for this work to provide an average dose per orbit. It must be noted that because of the GTO during periods with no solar activity, most of the dose is provided during short periods of <1 hr during belt passage. However, during several solar events that have been seen by the MPTB, the orbit average dose goes up dramatically because dose arrives during the entire orbit period. For this TP, the PMOS data have been normalized to the DSU dosimeter data, since they provide an additional source of integral dose. These data have shown dose rates from <10 rd(Si) per orbit to ≈500 rd(Si) per orbit, depending on solar activity. Data from these instruments are available as simple orbit averages or dose and proton flux measured periodically, typically every 15 s, during each orbit. By analysis and correlation of early orbit PMOS dosimeter data with the data from the CREDO and DSU instruments, the first major result of this study is a high-confidence integral dose curve for the MPTB board A4.

The corrected dosimetry curves developed for this study are shown in figure 7(a)–7(d). All bipolar test board parametric data analyses are based on these four graphs. The basic period for data collection on the MPTB is during the orbit, so figure 7(a) displays the average dose rate per orbit (12-hr period). If these data are examined statistically, the average dose rate per orbit over these 3,700 orbits is 0.27 mrd(Si)/s, with a standard deviation of 0.51 mrd(Si)/s. The lowest recorded per orbit dose rate was 0.01 mrd(Si)/s, and the highest single orbit dose rate was 10.20 mrd(Si)/s. The integral total dose curve is shown in figure 7(b). As discussed, PMOS dosimeter fading had been observed by approximately orbit 2,000, which raised doubts about the accuracy of these data that could not be quantified with only the PMOS dosimeters. While the corrections did not turn out to be large, the new total dose curve, based on all available instruments, is a crucial result of this study and allows recent orbital data to be presented with confidence. From the analysis of the dosimetry, the electron-to-proton ratio dose is in the range of 4 to 5 behind the 60–70 mil equivalent shielding thickness found on the MPTB experiments.

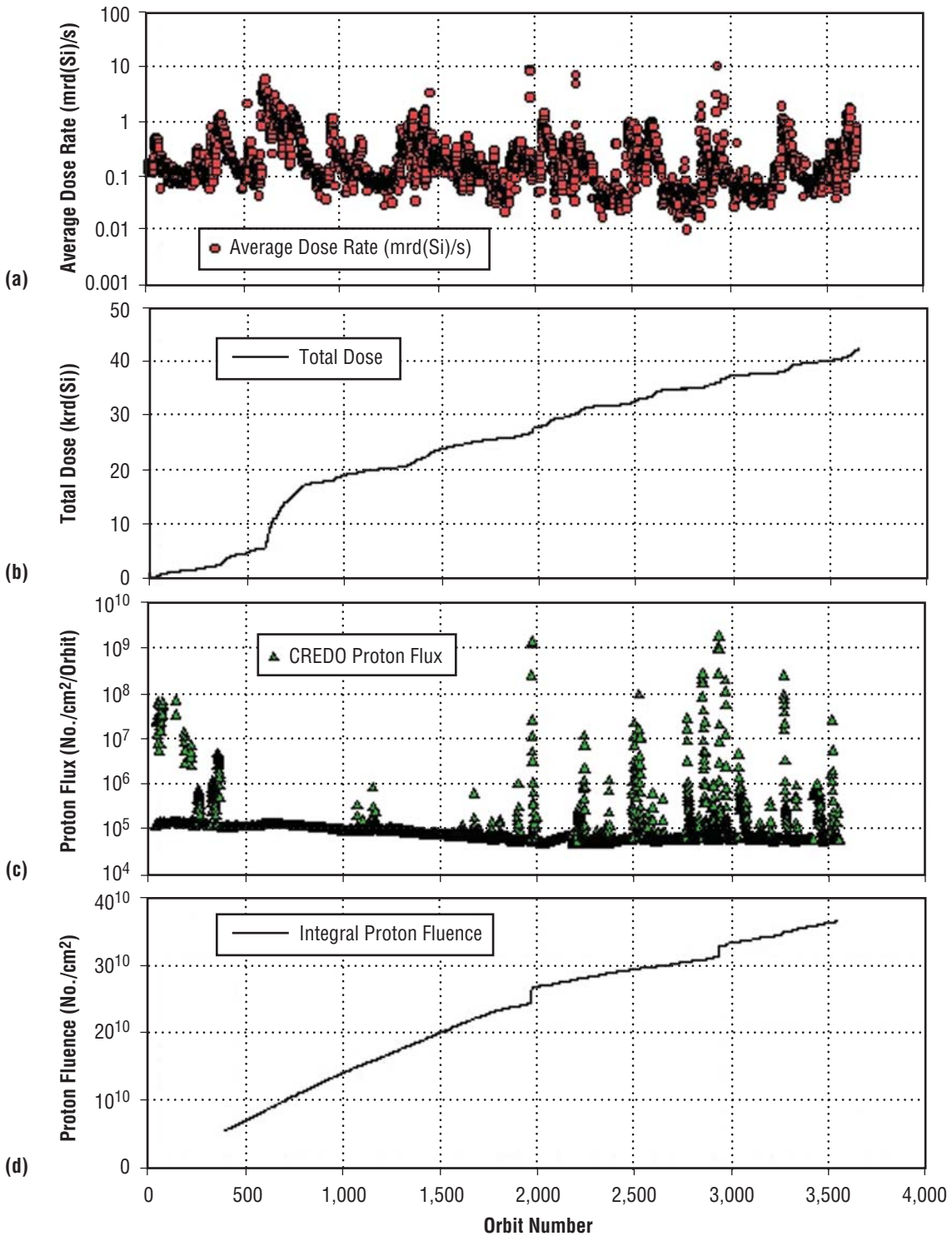

Figure 7. Dosimetry curves as a function of orbit: (a) Average dose rate per 12-hr orbit, (b) corrected integral dose curve, (c) CREDO proton flux, excluding proton belt transition flux (indicator of solar activity), and (d) integral total proton fluence.

When these data are combined with similar data provided by Clive Dyer, QinetiQ, from the CREDO instrument, integral proton fluences can also be provided to look at the effects of displacement damage.

3.4 Proton Results Curve

A curve of proton fluence per orbit from the CREDO instrument, omitting the proton flux accumulated during the proton belt passes, is shown in figure 7(c). These data are generally a good indicator of periods of enhanced dose rate due to solar particle events, though the major event that occurred about orbit 600 resulted in few solar protons but had a large dose increase. This event which rapidly accumulated nearly 10 krd(Si) has turned out to be the only major solar event during the MPTB mission where protons did not dominate, as discussed in detail in Dyer et al.[14,15]

The CREDO instrument has been calibrated in the coincidence mode to respond only to protons >38 MeV. In the singles (noncoincidence) mode, it is also sensitive to high-energy electrons during solar events.[19,20] To develop an integral proton fluence curve for analysis of the ELDRS data, it was determined that the penetration depth of protons >38 MeV have sufficient penetration depth to assure they will fully interact with the MPTB bipolar devices on board A4. This makes the coincident CREDO data the best available source of proton fluence. Figure 7(c) demonstrates that the proton fluence varies by more than 4 orders of magnitude from orbit to orbit. Compilation of these data required some interpolation because of missing orbits. Since the MPTB experiment continues to collect data, technical discussions will continue beyond this TP on energy cutoff and allowance for spacecraft shielding. The NRL worked with Karen Hunter, QinetiQ, to obtain additional data. In addition, the NRL worked with Bernie Blake, The Aerospace Corporation, to get similar data from the DSU instrument to obtain multiple energy channels. See figures 41 and 42 in section 5 for sample DSU data. The final proton fluence data are shown in figure 7(d) and are used to plot I_{ib} against proton flux to investigate the impact of displacement damage on this experiment, as discussed in section 6.

4. BASIC EXPERIMENTAL DATA

Section 4 updates all existing parametric data from the MPTB bipolar test board (board A4) through orbit 3719, which occurred on December 4, 2002. The last widely disseminated report of data from this board occurred in 1999 after orbit 1,100, so this TP represents a major expansion of previously reported results. Board A4 contains two variations of the LM124 quad op amp—COTS and class S—and two variations on the LM139 quad voltage comparator—LM139 and PM139. Three basic parameters—I_{ib}, I_{os}, and V_{os}—are measured once each orbit. In this section, the average parametric degradation as a function of orbit will be shown, and the observed degradation correlated to (1) accumulated dose, (2) orbital average dose rate, and (3) solar activity as measured by proton flux. Next, the individual device response is shown for all parts again as a function of orbit. These data are also plotted versus accumulated dose and compared to ground data.

NAVSEA Crane, as part of the ongoing DTRA ELDRS program, has been downloading and plotting data from the A4 board since launch in 1997. Extensive analysis was performed in the first 3 yr, which yielded the 1998 and 1999 papers[10,11] presented at the Nuclear Space Radiation Effects Conference (NSREC), and published in *Trans. Nucl. Sci.* (see apps. A and B). Since 1999, data have continued to be downloaded, but the level of effort was reduced. Only the I_{ib} parameter which, as expected, displays the greatest degradation, was updated. These data have not been widely disseminated. This NASA project has been leveraged off the ongoing DTRA ELDRS program, and not only updates the data to current times but also improves the dosimetry from earlier work and attempts detailed analyses of certain aspects of the data for the first time.

Figures 8–10 show the average parametric degradation (I_{ib}, I_{os}, and V_{os}, respectively) of both the COTS and class S LM124 parts as a function of orbit. These data are the average response of the four op amps tested for each type of LM124. Each figure consists of four graphs that share orbit number as a common abscissa, so the data can be studied in relation to the radiation environment accumulated in orbit: (a) parametric degradation for the two part types; (b) accumulated dose, as described in section 3; (c) average dose rate over the 12-hr orbit in millirads per second (mrd(Si)/s); and (d) uses CREDO proton data where the flux accumulated during the proton belt transitions has been excluded to demonstrate major solar flare activity over this 5-yr period. Graphs (b)–(d) were shown in figure 7, and are repeated for each graph, but allow the data to be correlated to its space environment. As might be expected in a space experiment, there are gaps and apparently anomalous data points on these graphs. One benefit of this extended study is the ability to reexamine the data set and explore anomalies and the impact of using an orbital environment for a long-term ELDRS radiation experiment. These interferences are studied and are reported on in section 5.

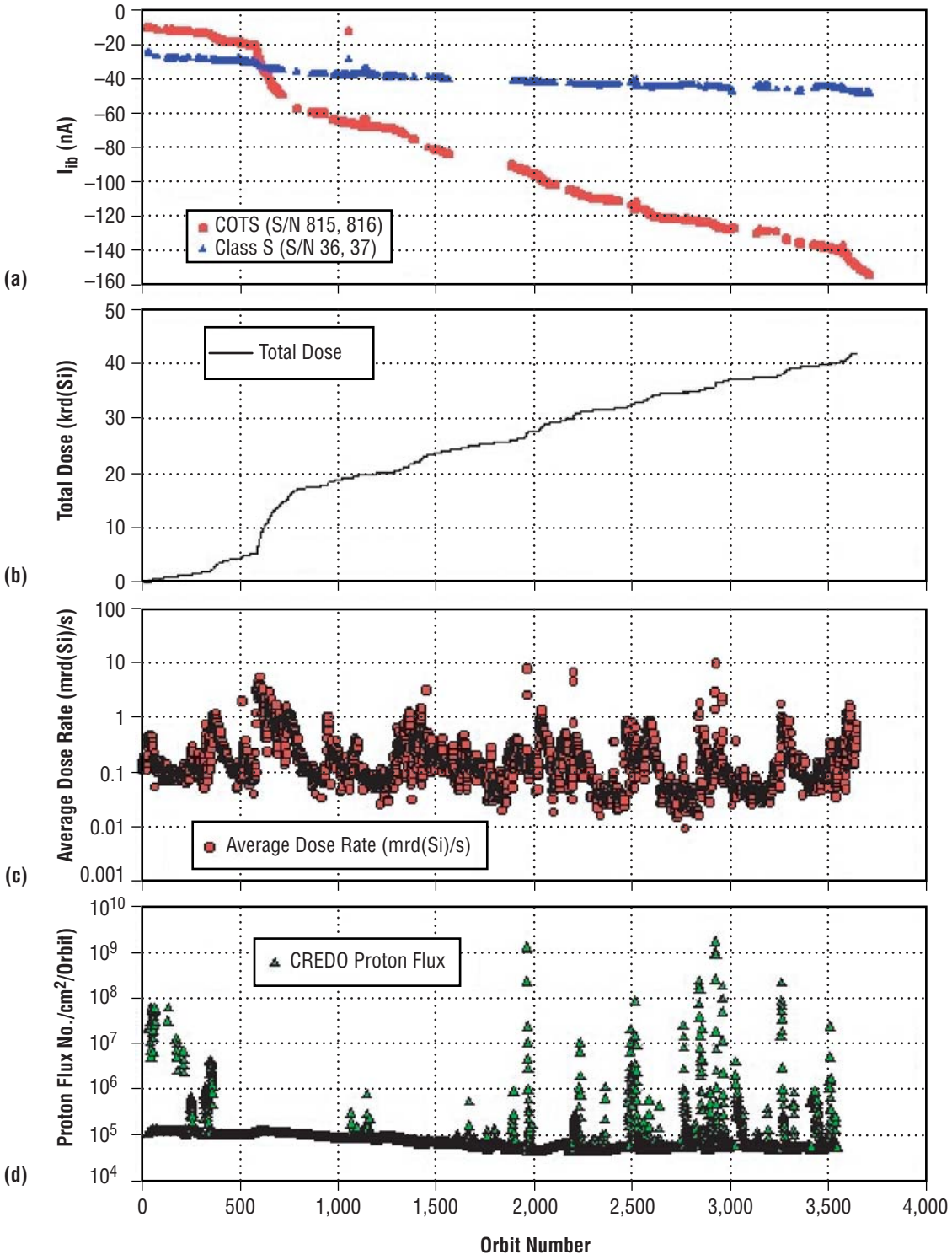

Figure 8. (a) I_{ib} for COTS and class S LM124 op amps, (b) total dose, (c) average dose rate, and (d) proton flux versus total dose. The curves show the average of all the I_b data for each part type.

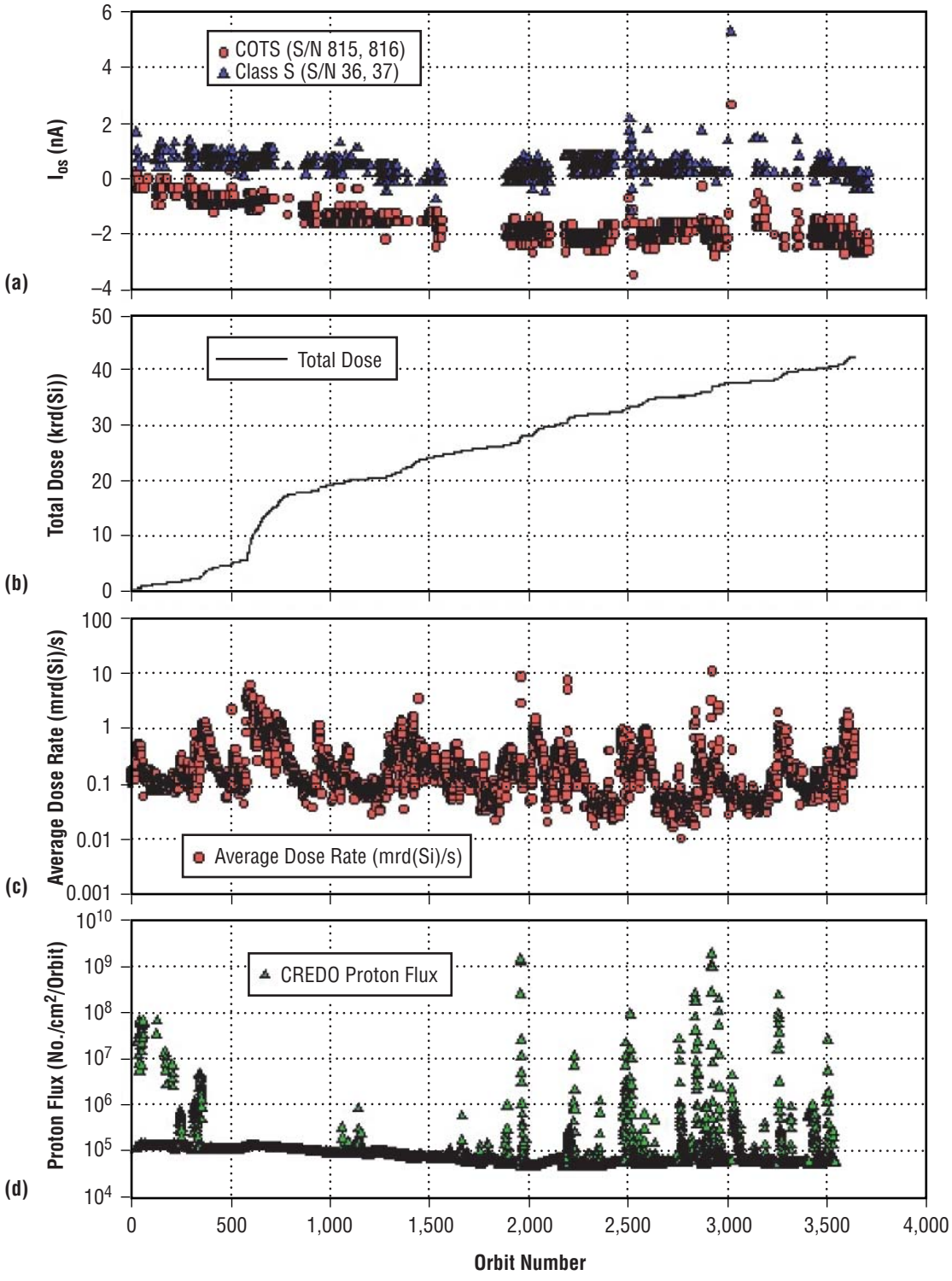

Figure 9. (a) Input I_{os} for COTS and class S LM124 op amps, (b) total dose, (c) average dose rate, and (d) proton flux versus orbit. The curves show the average of all I_b data for each part type.

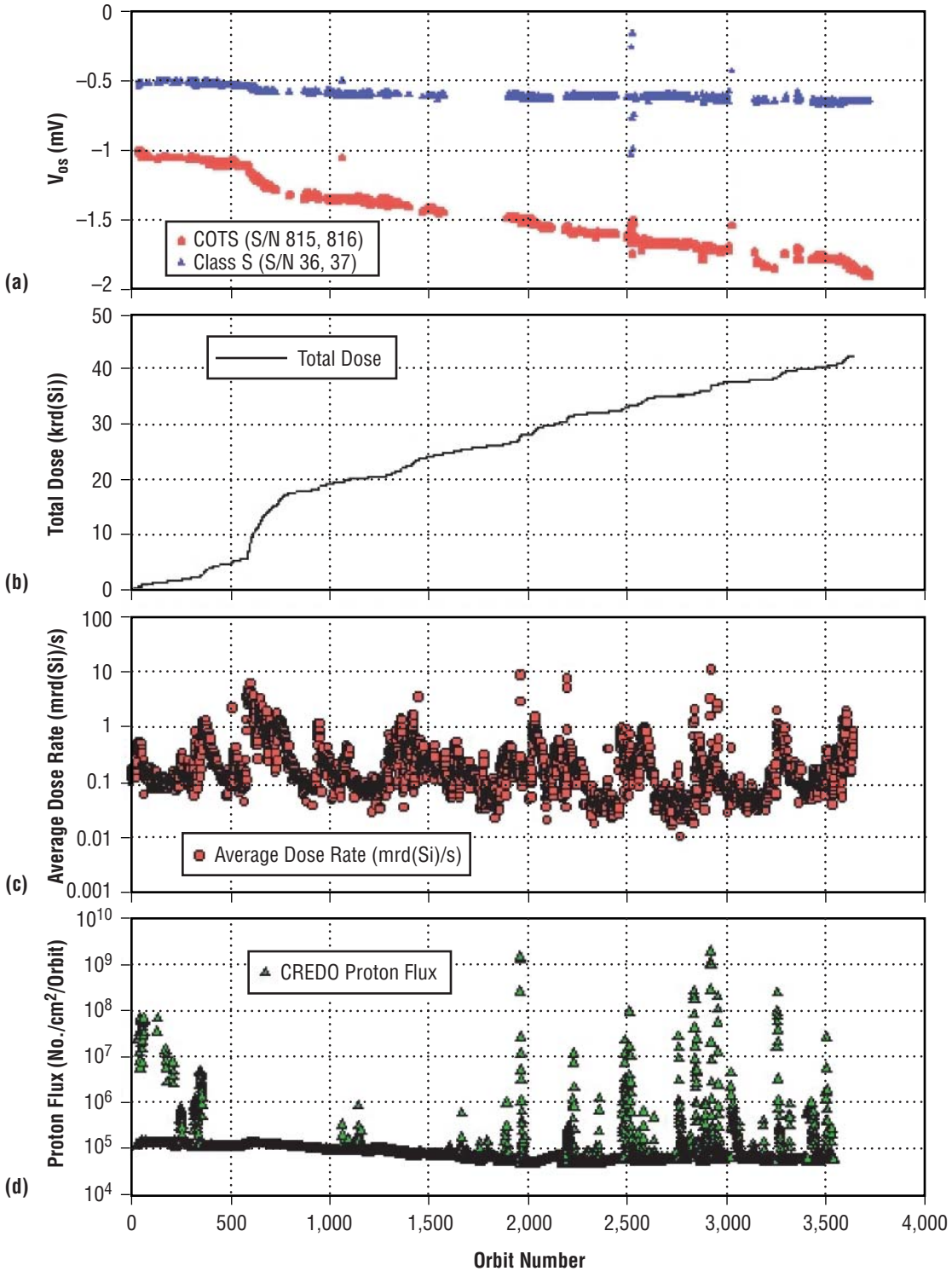

Figure 10. (a) Input V_{os} for COTS and class S LM124 op amps, (b) total dose, (c) average dose rate, and (d) proton flux versus orbit. The curves show the average of all I_b data for each part type.

Figures 11–13 display the LM139 and PM139 data in the same format used for the LM124 data in figures 8–10. The interesting I_{os} response is a function of limits in the range of the test circuit, and will be discussed in section 4.

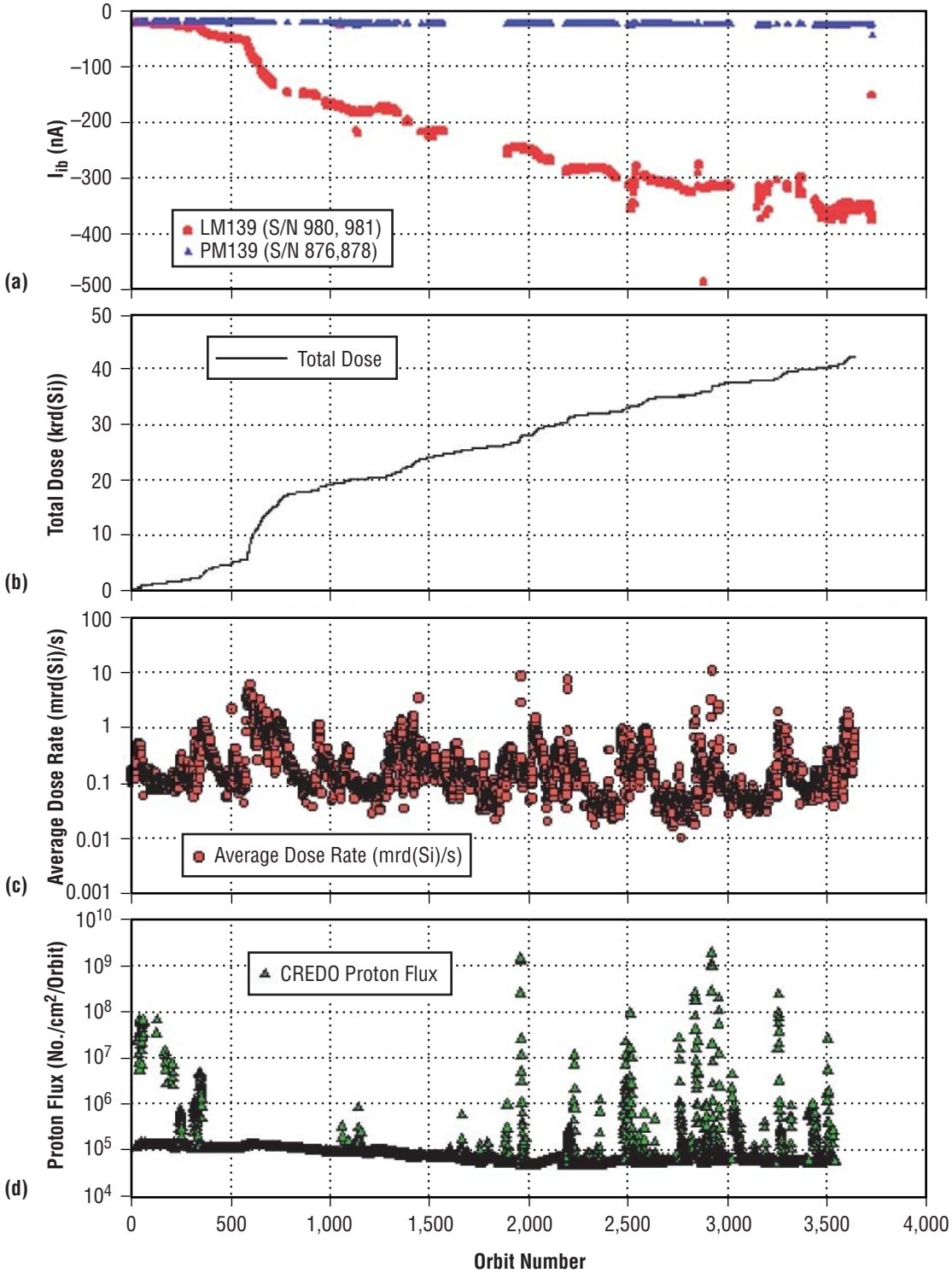

Figure 11. (a) I_{ib} for LM139 and PM139 comparators, (b) total dose, (c) average dose rate, and (d) proton flux versus orbit. The curves show the average of all I_b data for each part type.

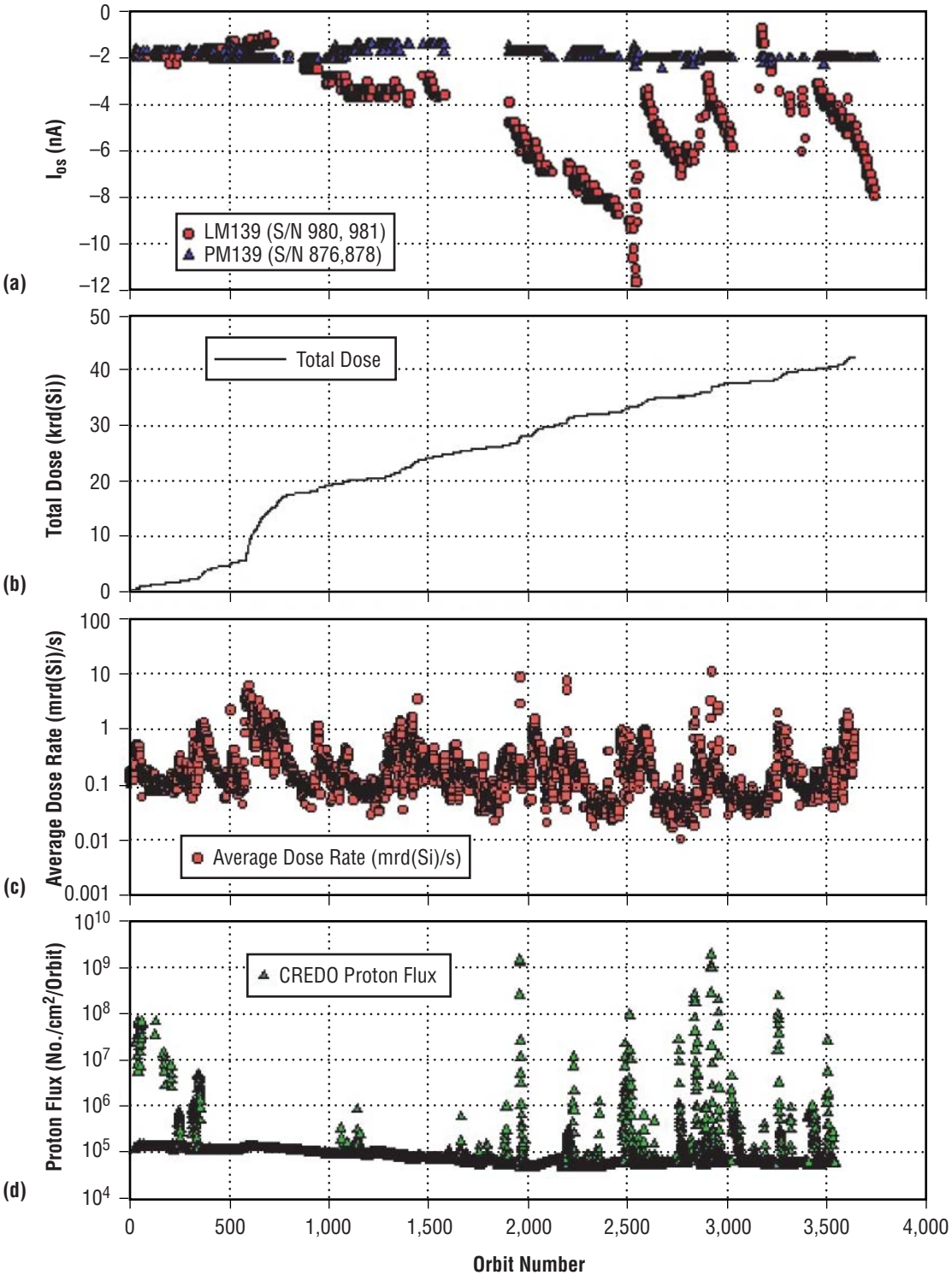

Figure 12. (a) Input I_{os} for LM139 and PM139 comparators, (b) total dose, (c) average dose rate, and (d) proton flux versus orbit. The curves show the average of all I_b data for each part type.

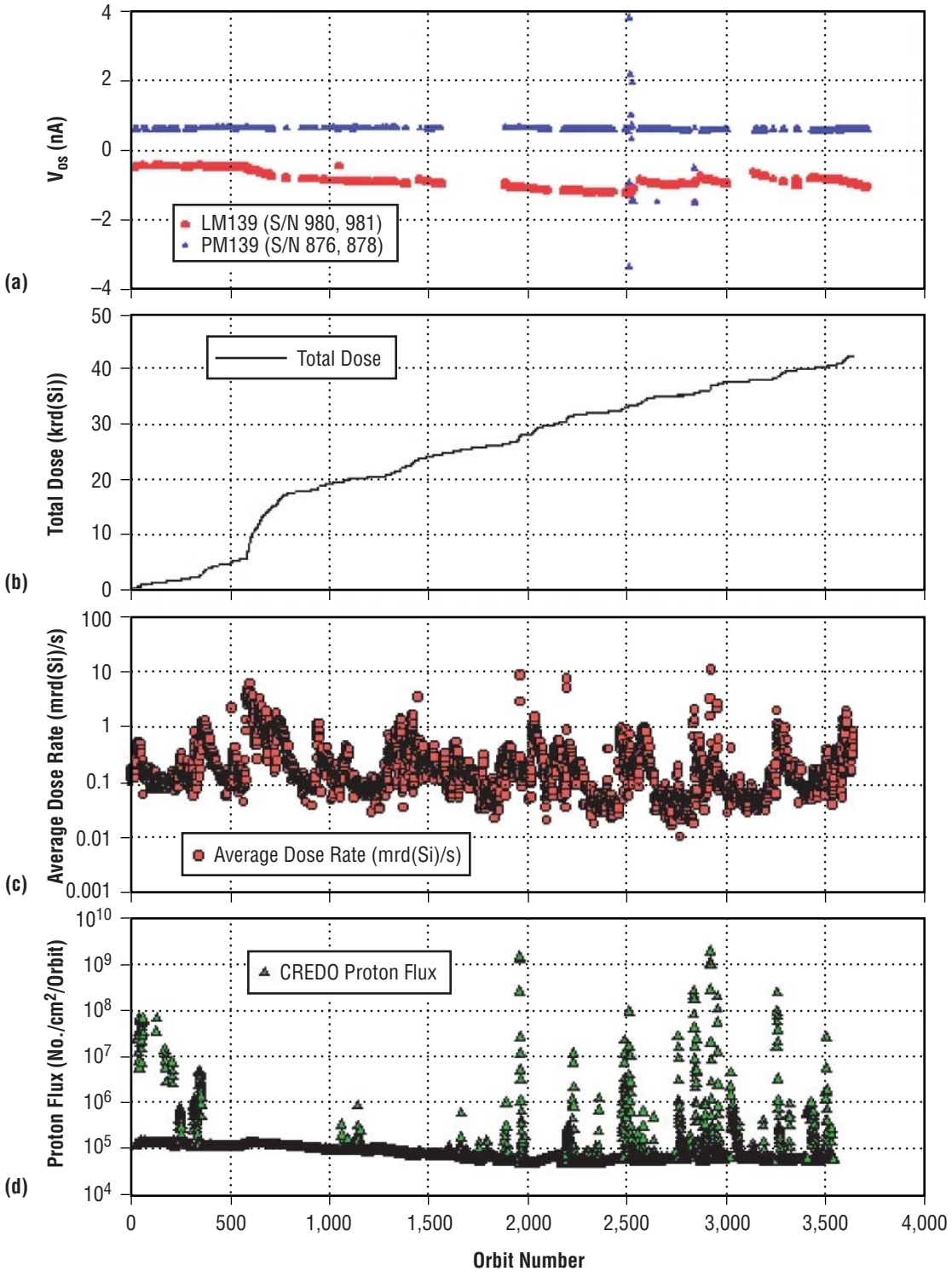

Figure 13. (a) Input V_{os} for LM139 and PM139 comparators, (b) total dose, (c) average dose rate, and (d) proton flux versus orbit. The curves show the average of all I_b data for each part type.

Figures 14–25 show the individual response of each device in the four-part groups on the experiment board as a function of orbit. These individual response data are important to allow the reader better insight into the range of responses observed in the four individual devices that comprise each part type. The experiment only collects data for two of the four circuits in each quad package, and there are two packages for each part type. Each graph displays the data from these four devices. Each circuit is referenced by its package serial number and "A" or "B" for the individual circuit.

The data for I_{ib} for each device type on the board are shown in figures 14–17. Similar data for input I_{os} are shown in figures 18–21 and input V_{os} is shown in figures 22–25. These graphs demonstrate that the parts in each group are heterogeneous in response, and that the average data used in the rest of this TP is a reasonable representation of individual part response.

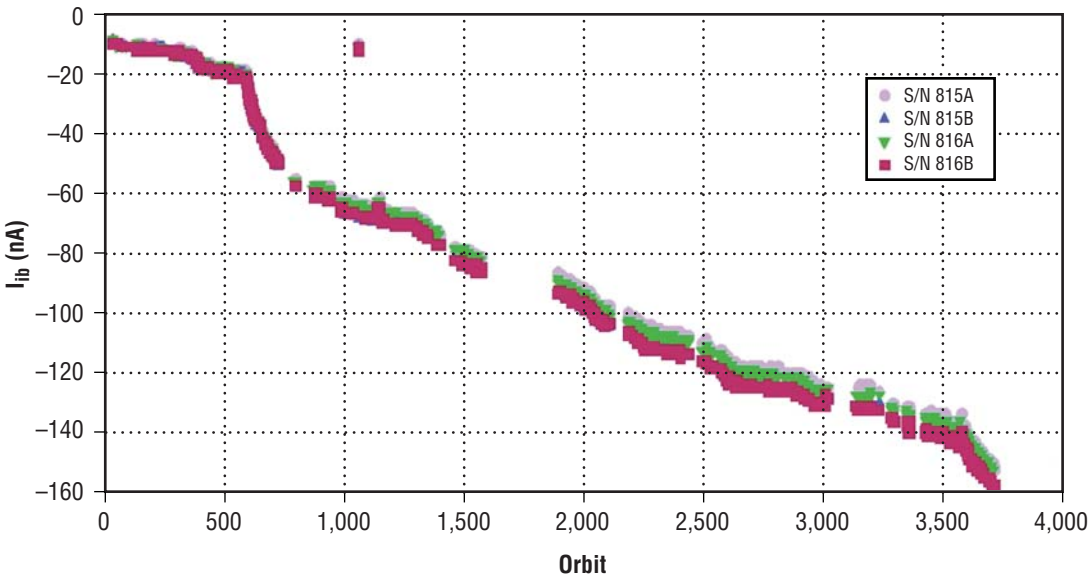

Figure 14. I_{ib} for COTS LM124 op amp versus satellite orbit. The curves show the I_b data for two devices (A and B) within each part (S/N 815 and 816).

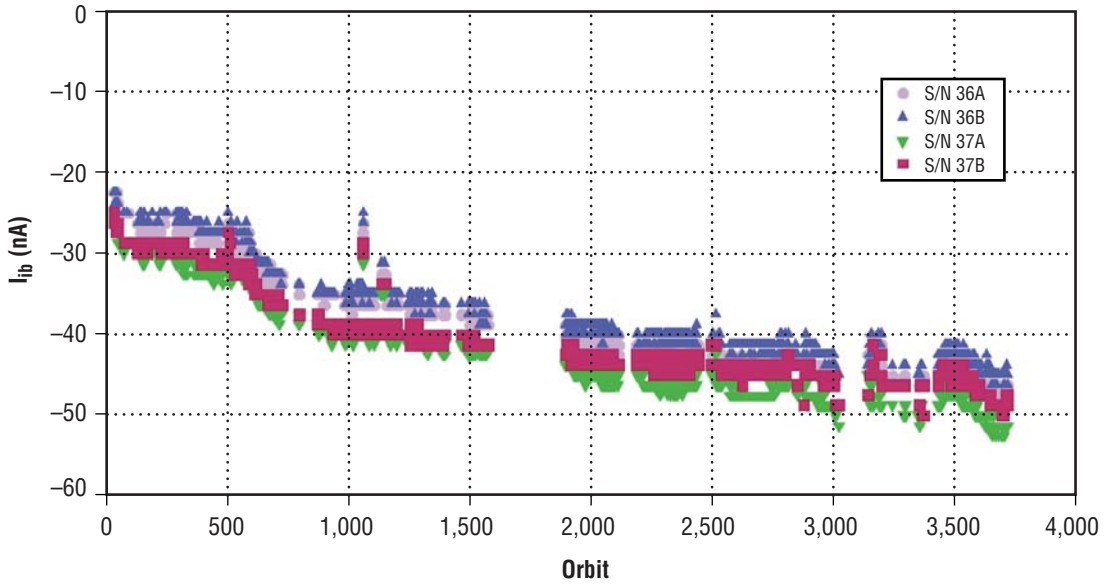

Figure 15. I_{ib} for class S LM124 op amp versus satellite orbit. The curves show the I_b data for two devices (A and B) within each part (S/N 36 and 37).

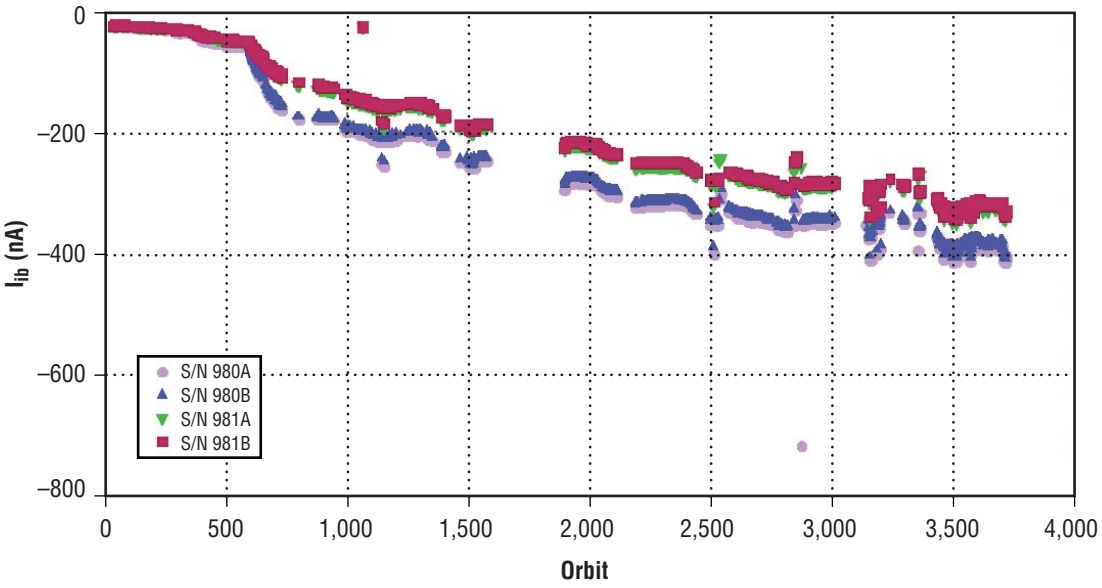

Figure 16. I_{ib} for LM139 comparator versus satellite orbit. The curves show the I_b data for two devices (A and B) within each part (S/N 980 and 981).

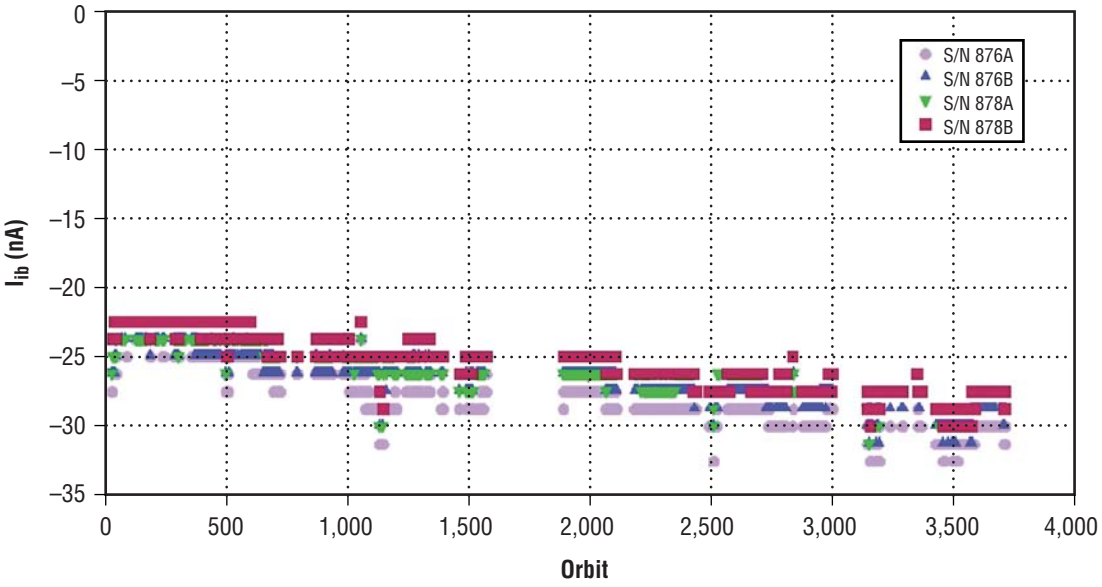

Figure 17. I_{ib} for PM139 comparator versus satellite orbit. The curves show the I_b data for two devices (A and B) within each part (S/N 876 and 878).

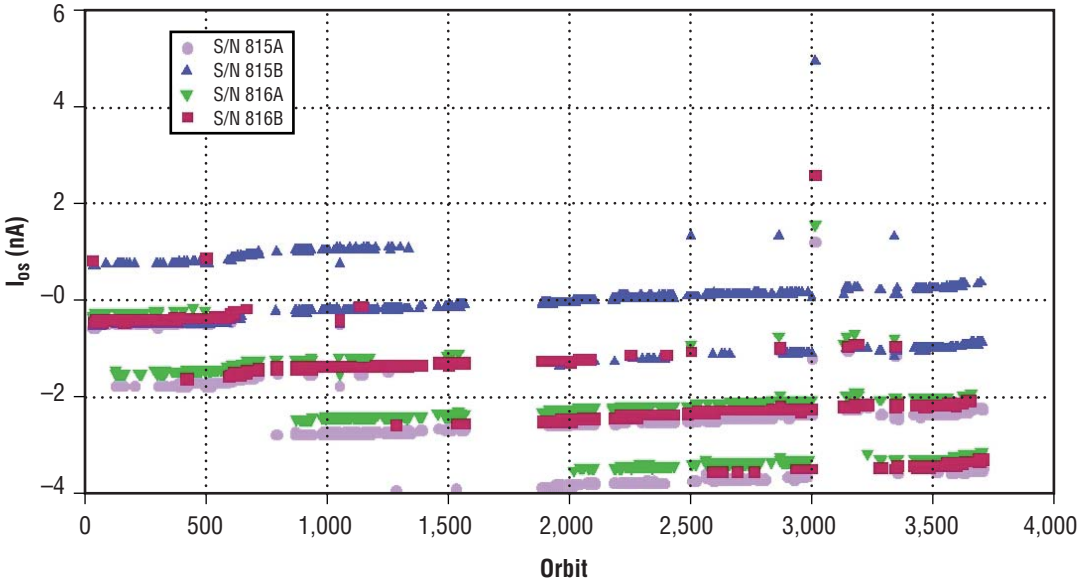

Figure 18. Input I_{os} for COTS LM124 op amp versus satellite orbit. The curves show the I_b data for two devices (A and B) within each part (S/N 815 and 816).

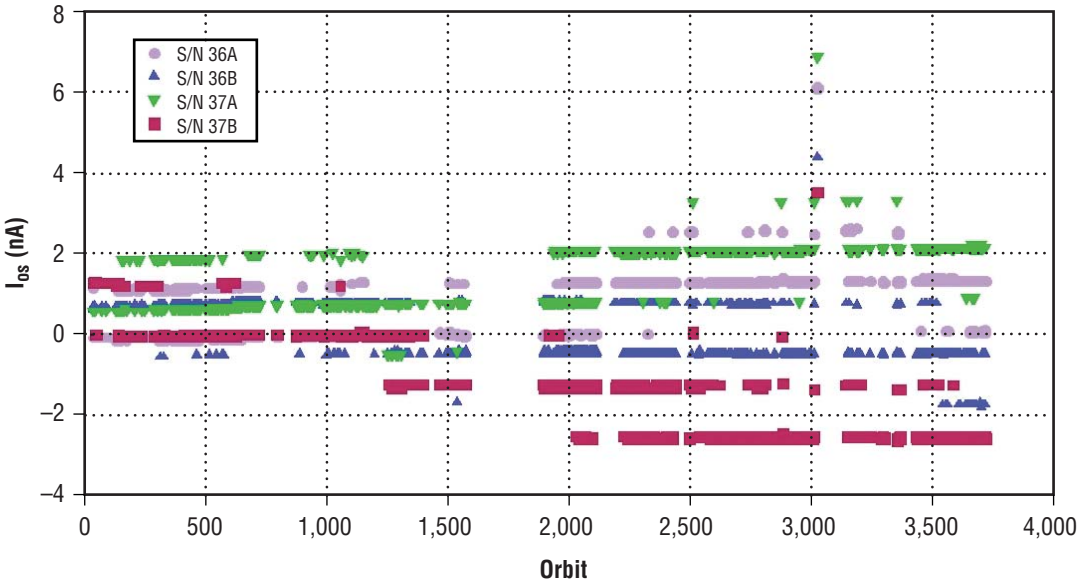

Figure 19. Input I_{os} for class S LM124 op amp versus satellite orbit. The curves show the I_b data for two devices (A and B) within each part (S/N 36 and 37).

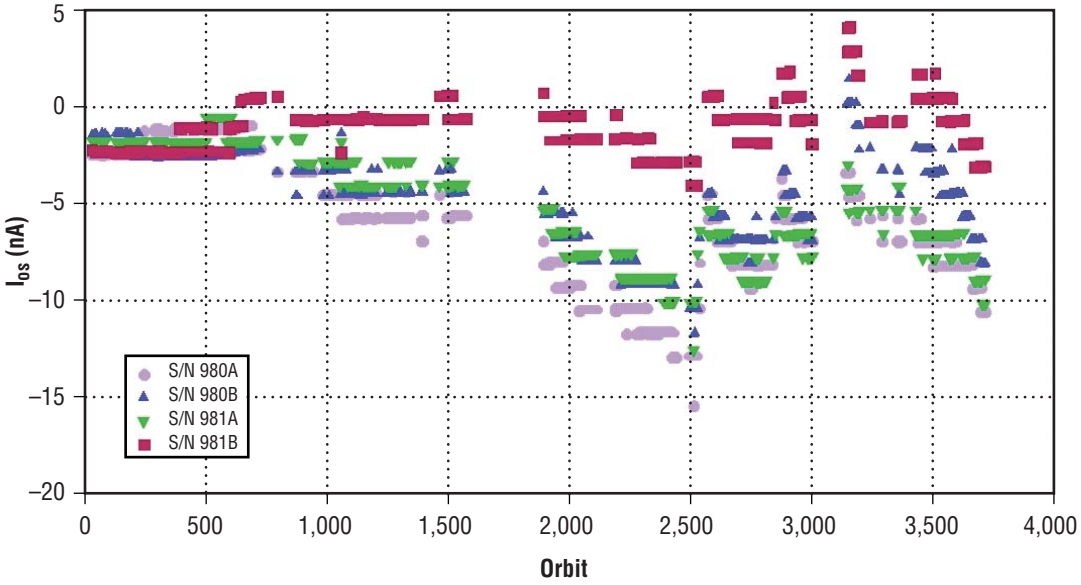

Figure 20. Input I_{os} for LM139 comparator versus satellite orbit. The curves show the I_b data for two devices (A and B) within each part (S/N 980 and 981).

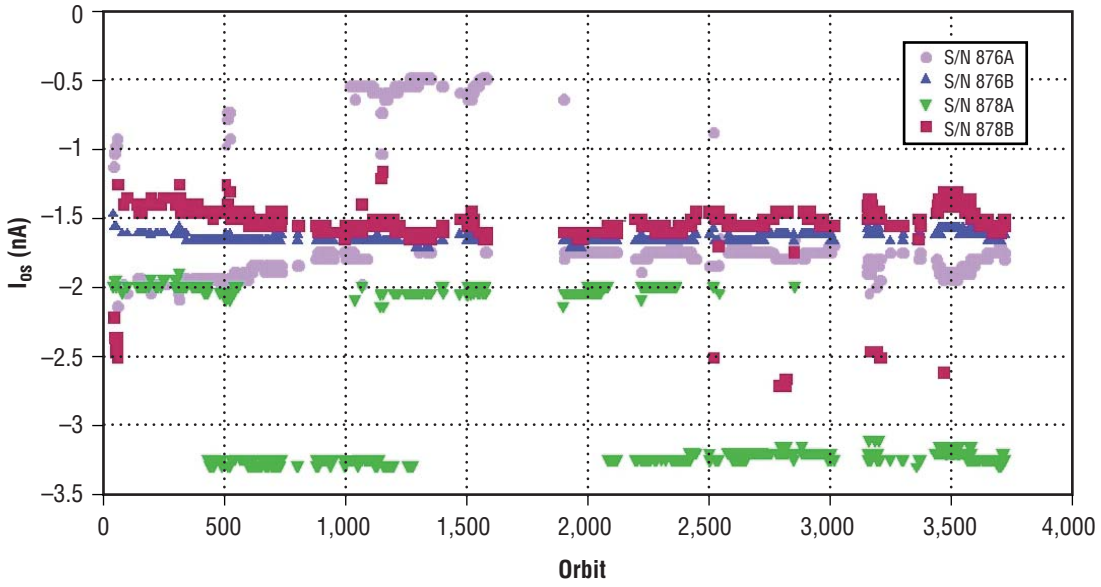

Figure 21. Input I_{os} for PM139 comparator versus satellite orbit. The curves show the I_b data for two devices (A and B) within each part (S/N 980 and 981).

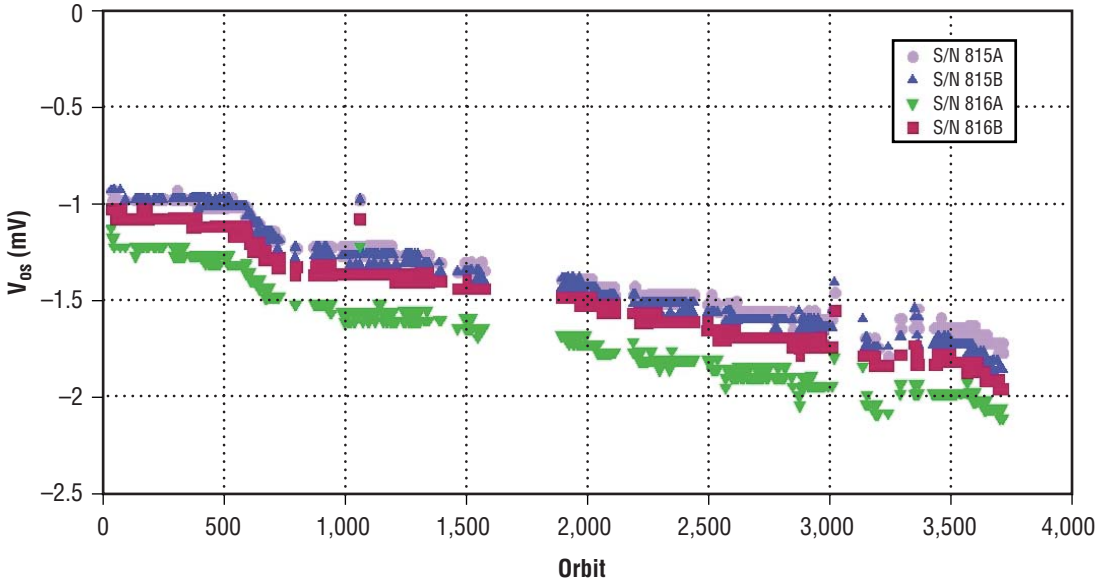

Figure 22. Input V_{os} for COTS LM124 op amp versus satellite orbit. The curves show the I_b data for two devices (A and B) within each part (S/N 815 and 816).

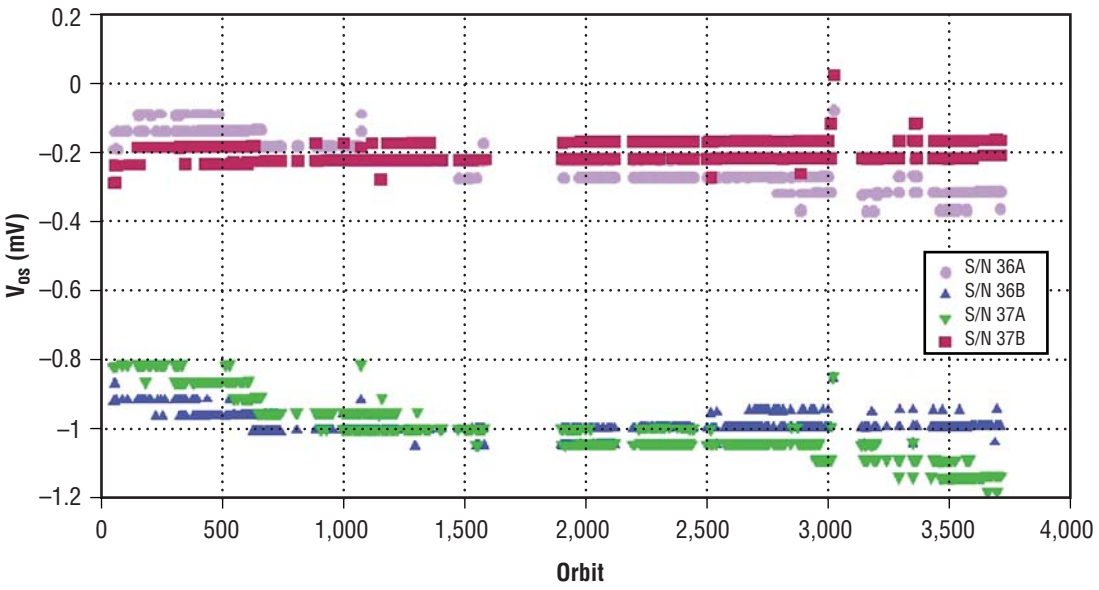

Figure 23. Input V_{os} for class S LM124 op amp versus satellite orbit. The curves show the I_b data for two devices (A and B) within each part (S/N 36 and 37).

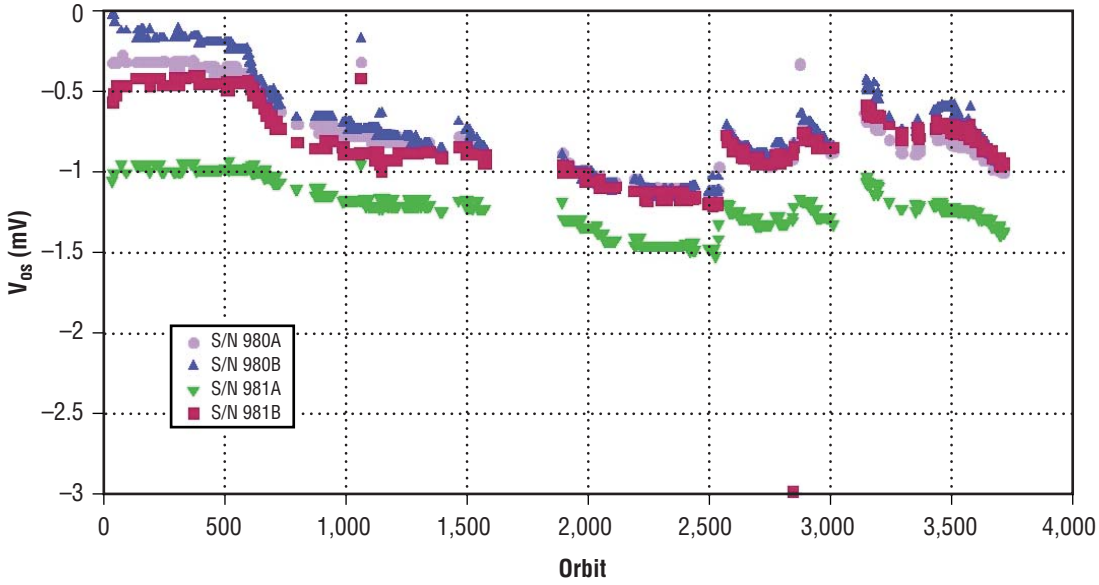

Figure 24. Input V_{os} for LM139 comparator versus satellite orbit. The curves show the I_b data for two devices (A and B) within each part (S/N 980 and 981).

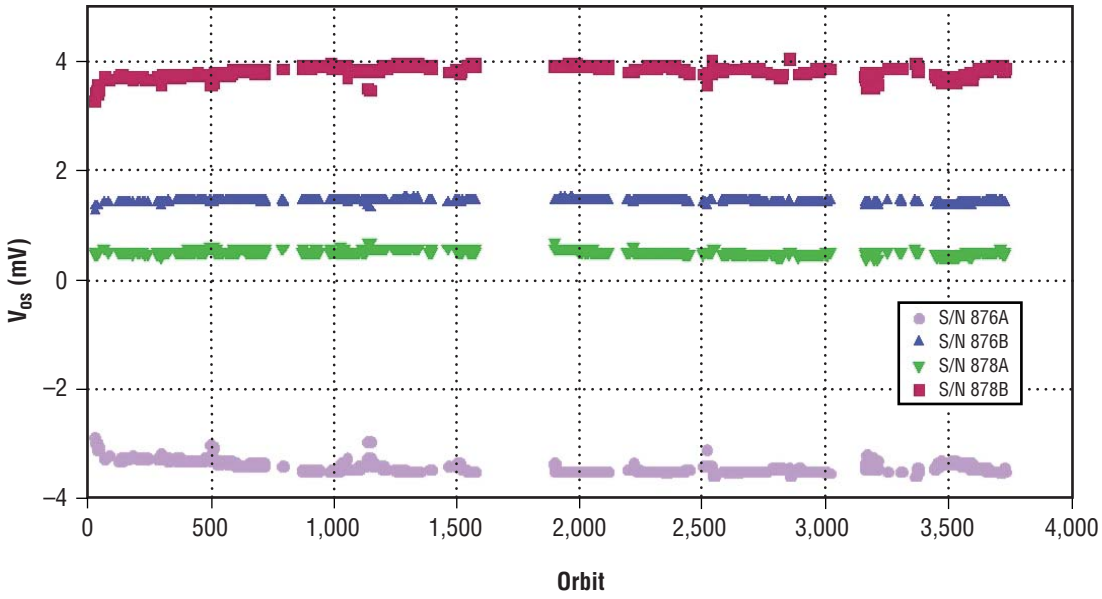

Figure 25. Input V_{os} for comparator PM139 versus satellite orbit. The curves show the I_b data for two devices (A and B) within each part (S/N 876 and 878).

Figures 26–31 show the average response of each of the four part types—COTS LM124, class S LM124, LM139, and PM139—as a function of total dose, as corrected by the dosimetry reported in section 3.

The difference in response in the ELDRS parts—COTS LM124 and LM139—and the non-ELDRS parts—class S LM124 and PM139—is readily apparent. This response provided first verification that ground test methods could be used to qualitatively predict ELDRS response in space. Subsequent analysis and comparison to ground data established that the relationship can be quantitative, as will be discussed.

The repetitive sawtooth pattern observed in the I_{os} data for the LM139 in figure 29 appears to demonstrate a limit of the test circuitry. For I_{os} to demonstrate this behavior, significant changes would have to be noted in I_{ib} as well, as the two parameters are interrelated. A repetitive sawtooth pattern is indicative of overranged digital data.

The measurement circuitry on board A4 uses a closed-loop circuit response to provide an indirect measurement of the actual parametric data. This system emulates the techniques described in MIL–STD–883, test method 4001.[12] In addition, both the op amp and the comparator tests use slightly different circuitry, as the digital comparator output cannot provide a linear signal in the feedback loop. For this reason, the comparator I_{os} data cannot be directly compared to the op amp data. For each part type, a voltage measurement of the closed-loop test circuit is made in three different circuit configurations defined with five resistors, but only two values, and two relays. From these three measurements, the three desired parameters are calculated.

From review of the original test circuitry, it appears that the LM139/PM139 test circuit was optimized to maximize the range of I_{ib} data, at the expense of a limited range for I_{os}. Given that I_{ib} was considered to be the major variable, it was a reasonable compromise. The ground data for these parts had not been completed prior to launch, and the relatively large shift in I_{os} for the LM139 with both inputs grounded was not anticipated. The ground data, as seen in figure 36, does demonstrate a relatively large shift similar to space data. It is not known, but doubtful, that the test circuit was exercised to its limits during construction and checkout.

Thus, it is most probable that the observed I_{os} data for the LM139 is an artifact of an overrange condition for the test circuit. It is not possible to determine if the large solar event that occurred in orbit 2,499, nearly coincident with this I_{os} anomaly, also resulted in the MPTB being power cycled twice in the next 10 orbits could have had any impact on these data. This scenario seems unlikely, as no other data appear to be impacted, and the PM139 data, which uses the same test circuit, is unaffected.

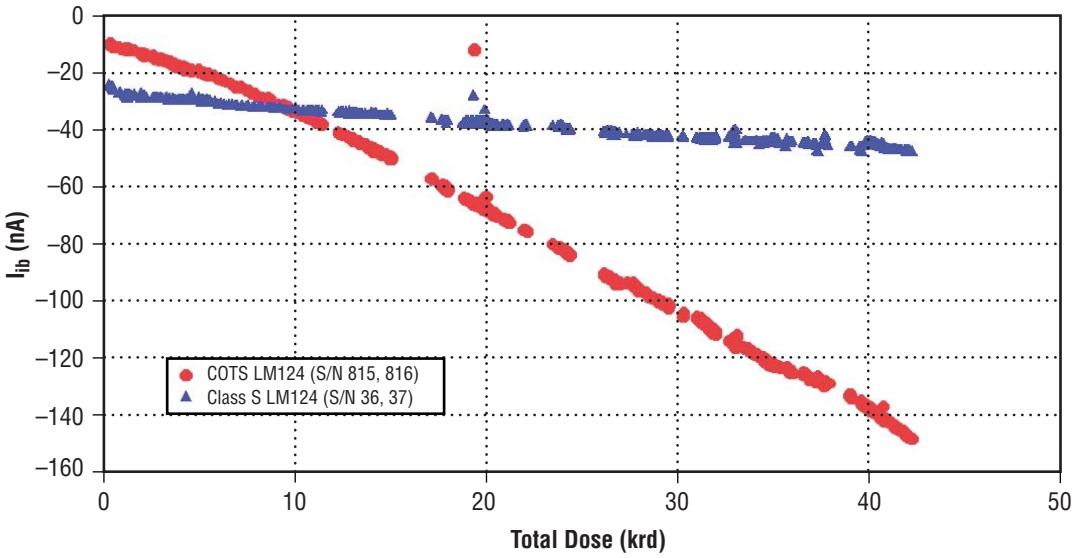

Figure 26. I_{ib} for COTS and class S LM124 op amps versus total dose. The curves show the average of all I_b data for each part type.

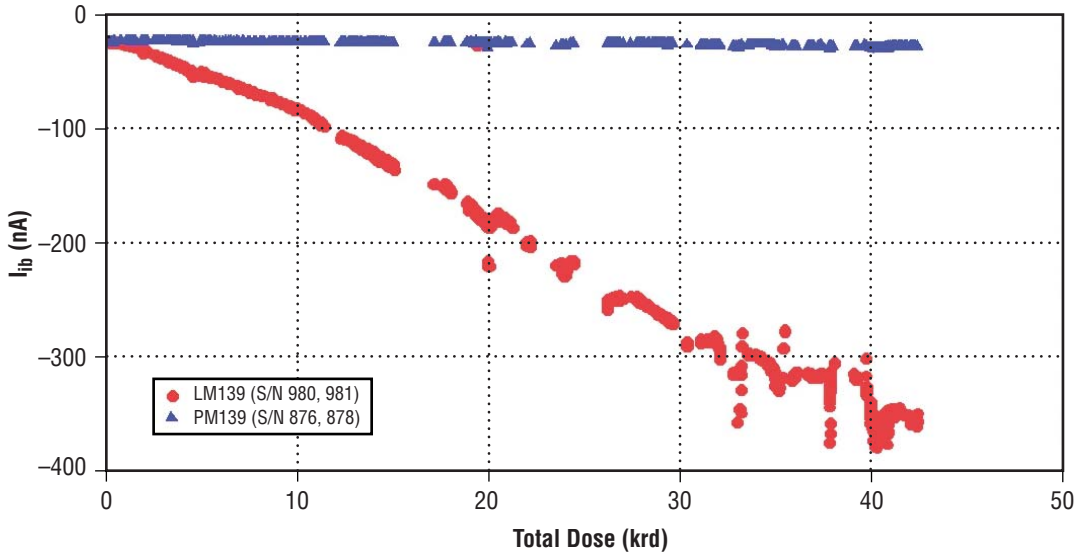

Figure 27. I_{ib} for LM139 and PM139 comparators versus total dose. The curves show the average of all I_b data for each part type.

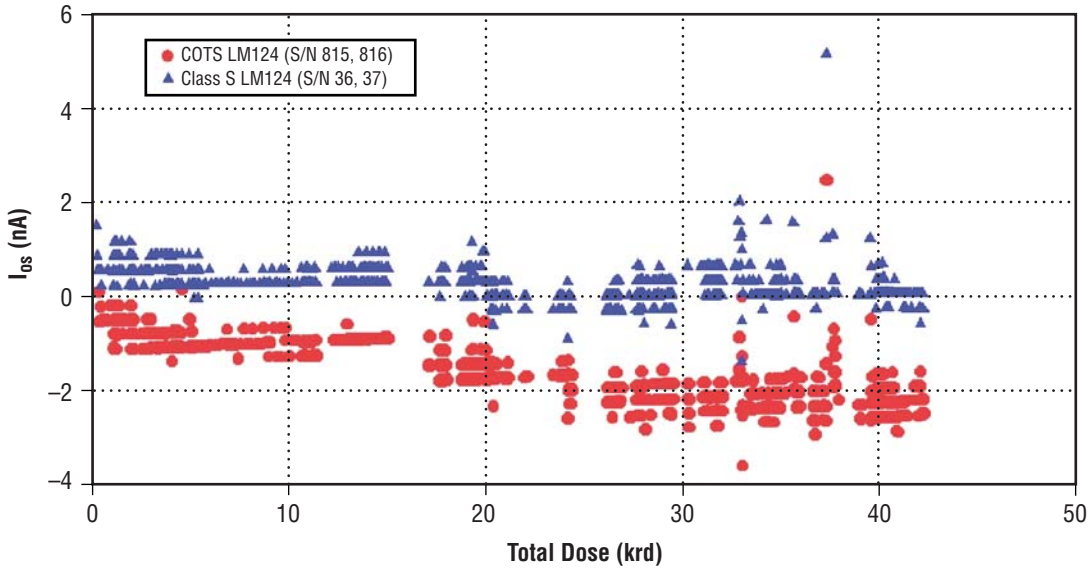

Figure 28. Input I_{os} for COTS and class S LM124 op amp versus total dose. The curves show the average of all I_{os} data for each part type.

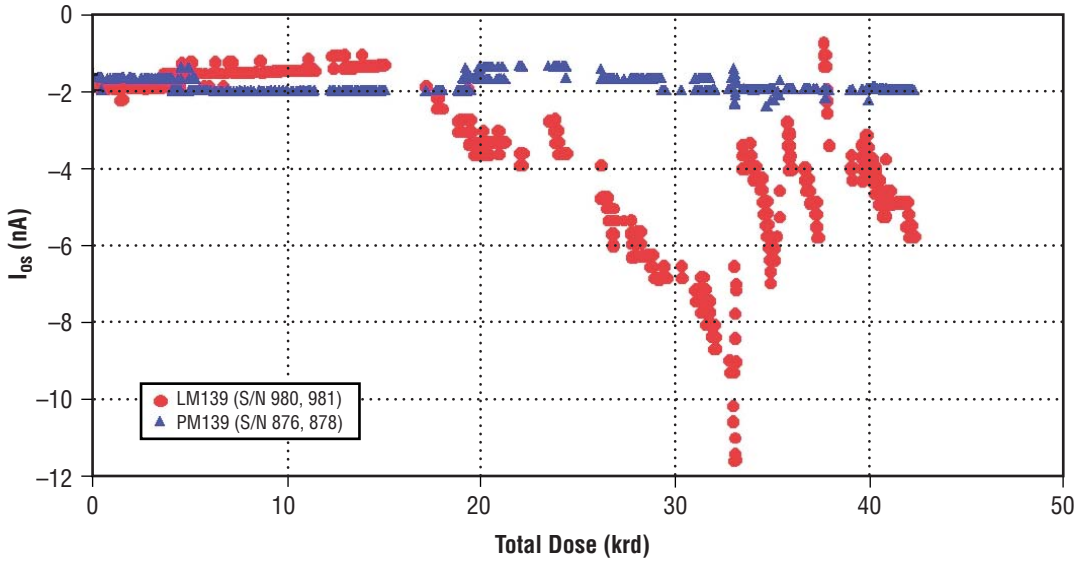

Figure 29. Input I_{os} for LM139 and PM139 comparators versus total dose. The curves show the average of all I_{os} data for each part type.

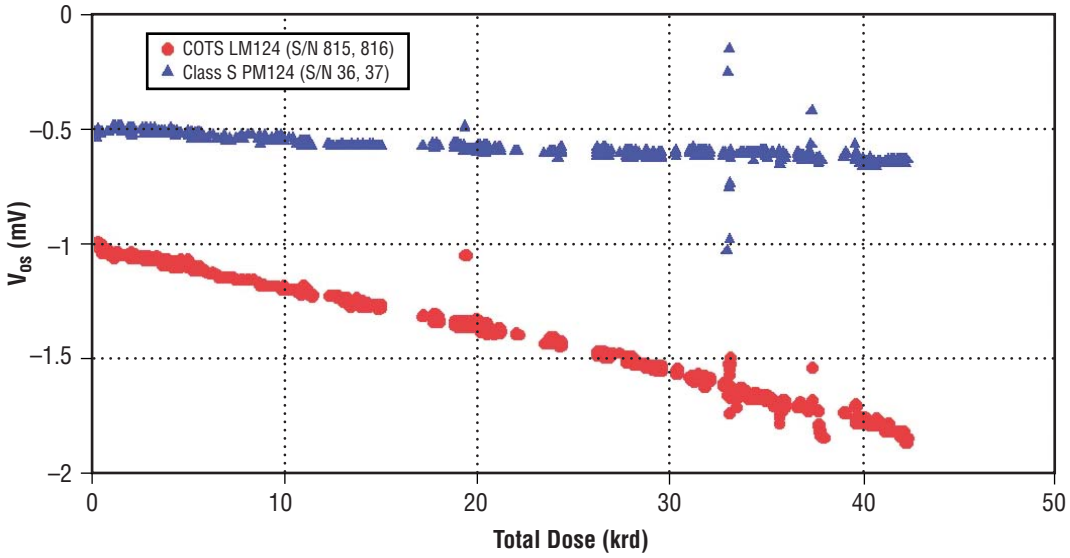

Figure 30. Input V_{os} for COTS and class S LM124 op amp versus total dose. The curves show the average of all input V_{os} data for each part type.

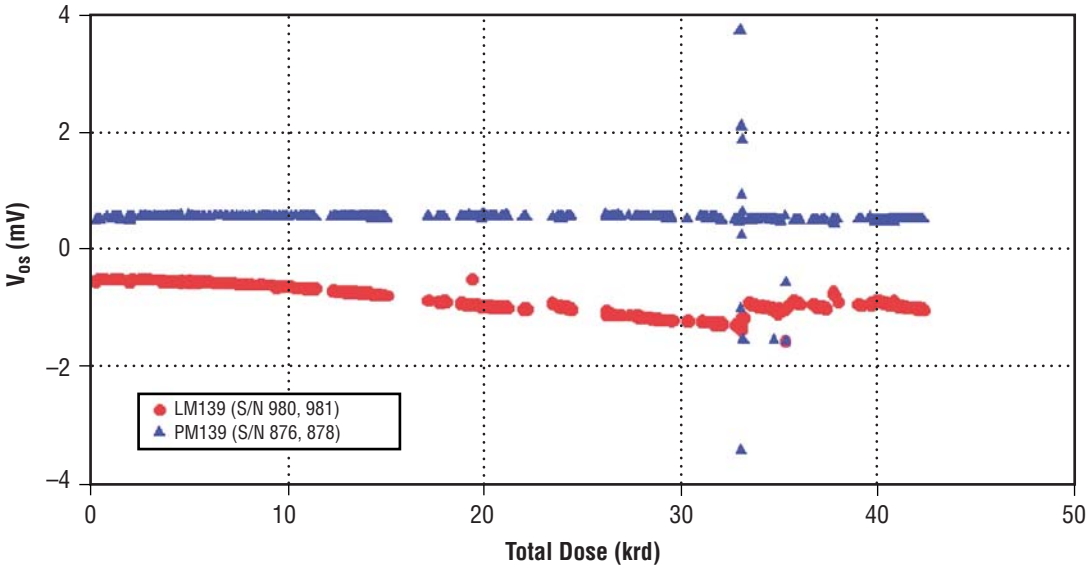

Figure 31. Input V_{os} for comparators LM139 and PM139 versus total dose. The curves show the average of all input V_{os} data for each part type.

Figures 32–40 superimpose ground test data taken as part of the DTRA ELDRS program on the A4 orbital data for the COTS LM124, LM139, and the PM139. There were no ground test data taken on the class S LM124 due to insufficient quantity of parts.

For the I_{ib}, the ground data at 1 and 10 mrd(Si)/s continues to be a very good representation of the degradation observed in space, through the current dose of >42 krd(Si). I_{ib} was expected to be the most important, and the most reproducible, data to be taken on the MPTB, and this has been the case throughout the 5-yr mission.

Issues arise in the input I_{os} and voltage data. First, there is significant scatter in the ground data. While the test technique used in both the Eagle tester and the MPTB board may contribute some degree of scatter, these parameters, when measured in this manner, do demonstrate scatter, and this scatter is highly dependent on the initial conditions found in each individual op amp or comparator. The slight mismatches in the differential pairs are amplified and impact the direction and magnitude of the parametric shifts measured. The graphs in figures 14–25 show that the individual devices on the MPTB also demonstrate significant variability, comparable to that seen in the ground test data. The comparisons herein are well within the bounds one can anticipate in data scatter. It is not nearly as easy to directly do the comparison with these variables, but it is fair to say the space data are well bounded by the ground test data. Also refer to the discussion in this section concerning test problems in space with the LM139 I_{os}.

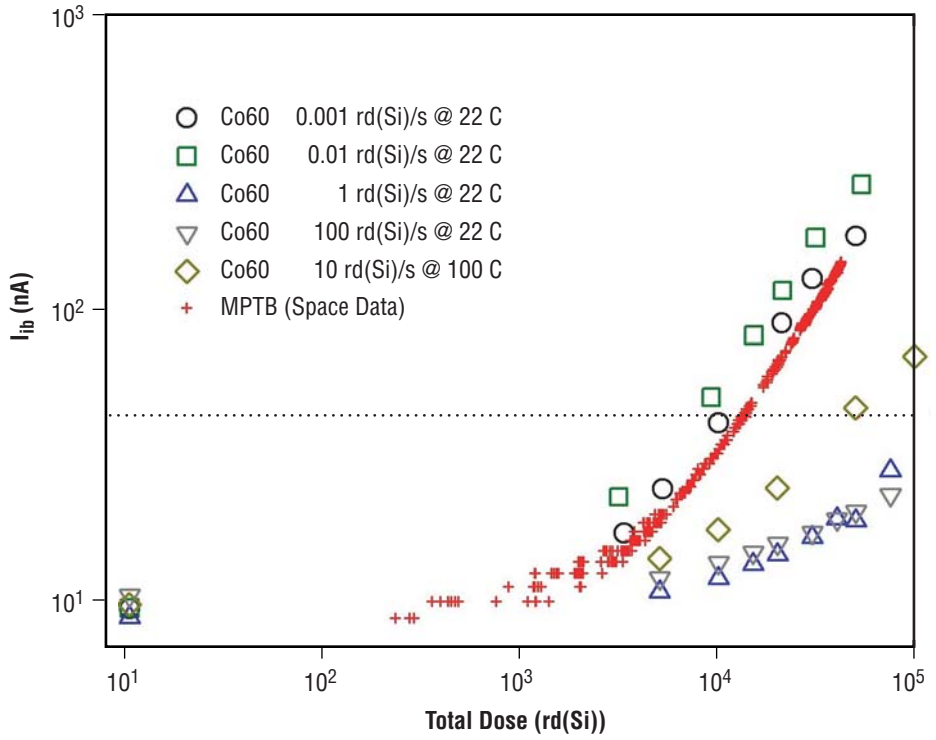

Figure 32. Comparison of MPTB space data to ground test data I_{ib} for COTS LM124 quad op amp (DC9524).

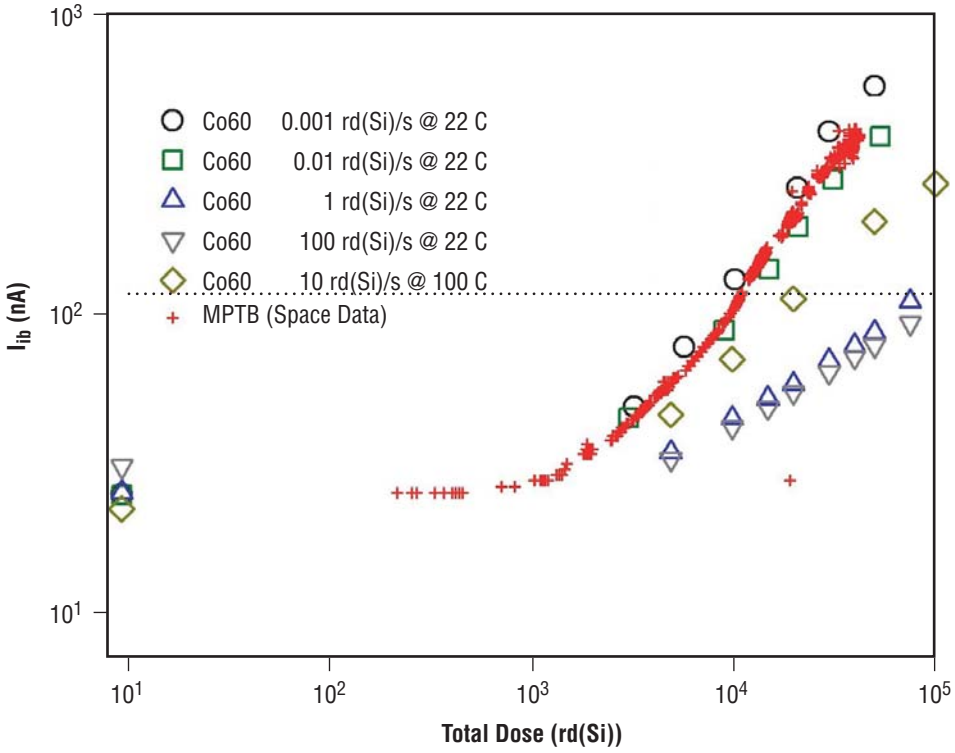

Figure 33. Comparison of MPTB space data to ground test data I_{ib} for COTS LM139 quad comparator (DC9530).

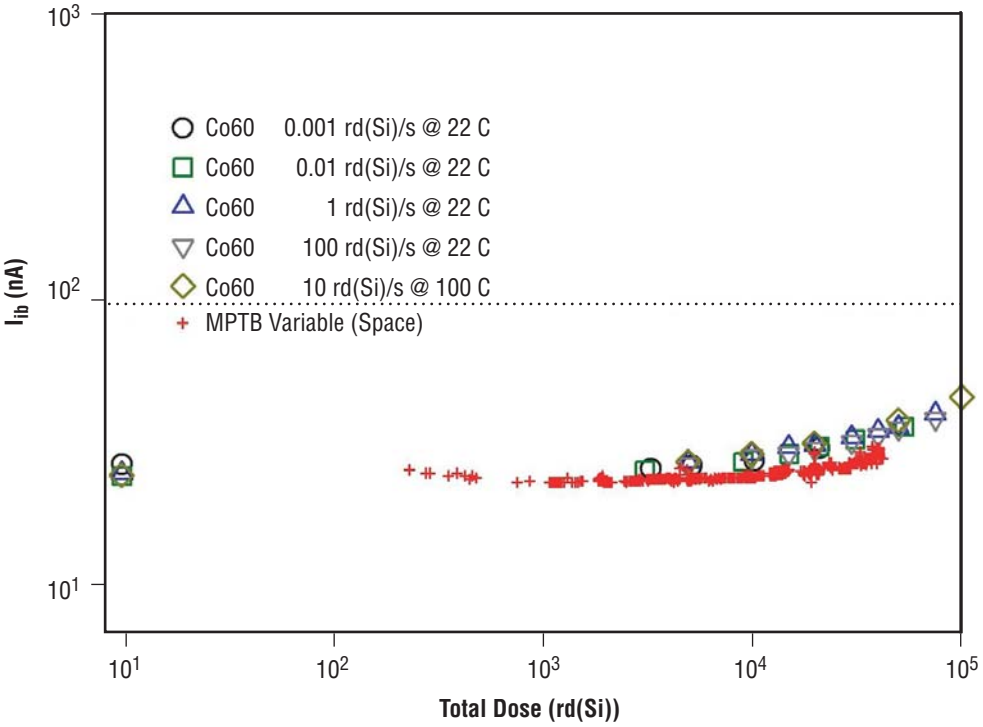

Figure 34. Comparison of MPTB space data to ground test data I_{ib} for COTS LM139 quad comparator (DC9522).

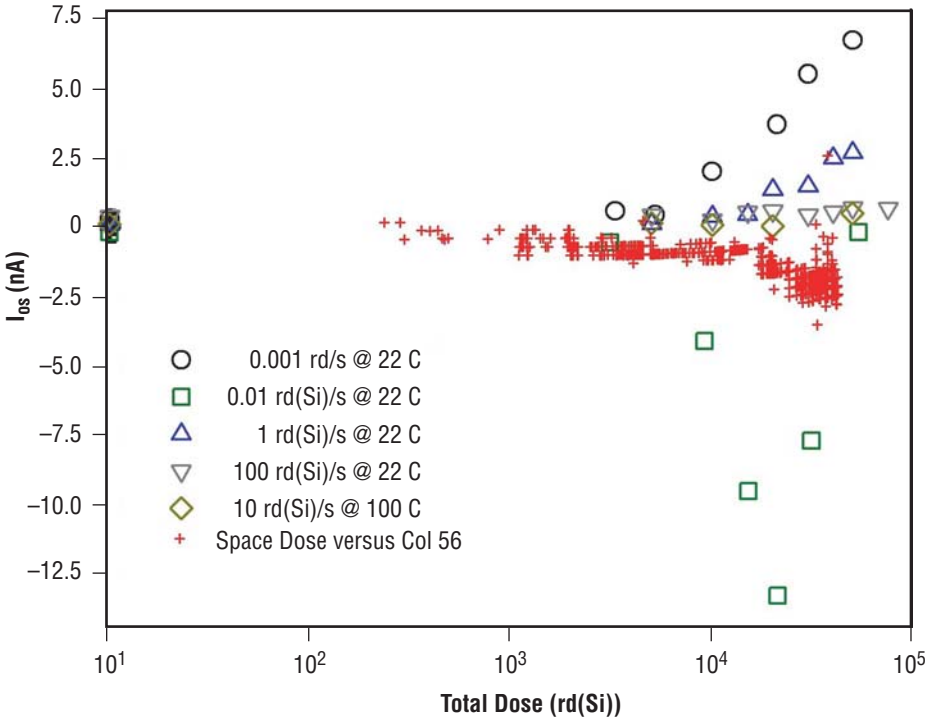

Figure 35. Comparison of MPTB space data to ground test data input I_{os} for COTS LM124 quad op amp (DC9524).

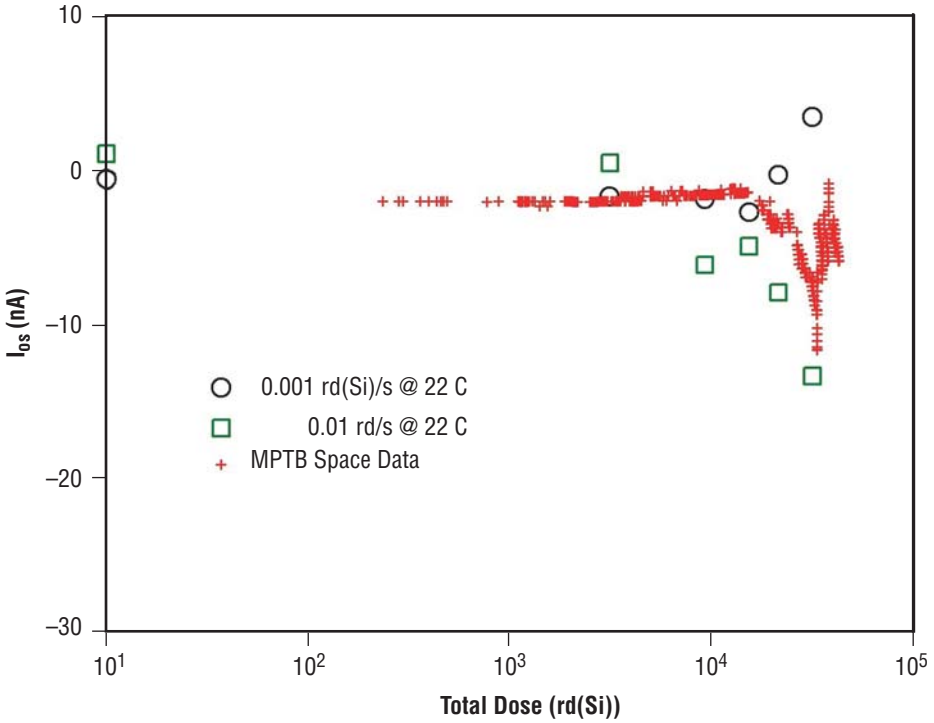

Figure 36. Comparison of MPTB space data to ground test data input I_{os} for LM139 COTS quad comparator (DC9530).

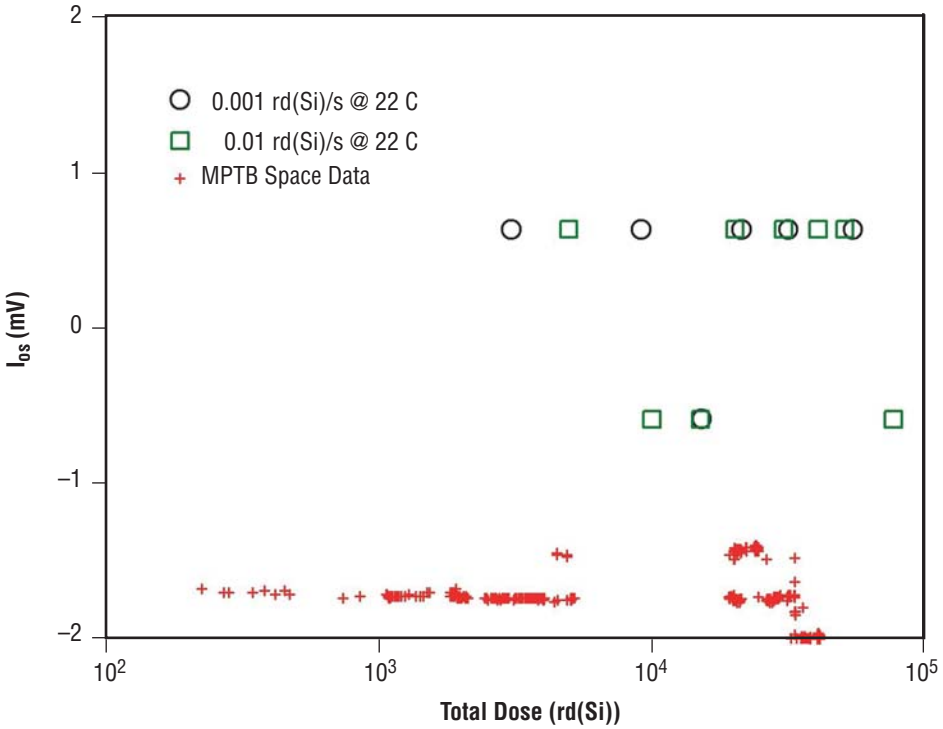

Figure 37. Comparison of MPTB space data to ground test data input I_{os} for PM139 quad comparator (DC9530).

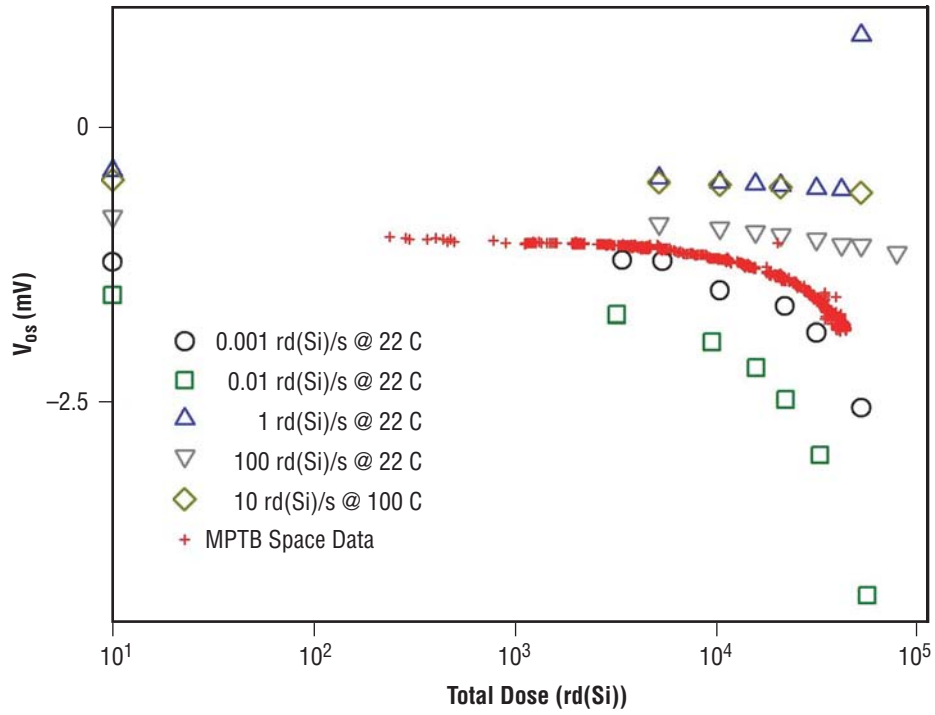

Figure 38. Comparison of MPTB space data to ground test data input V_{os} for LM124 quad op amp (DC9524).

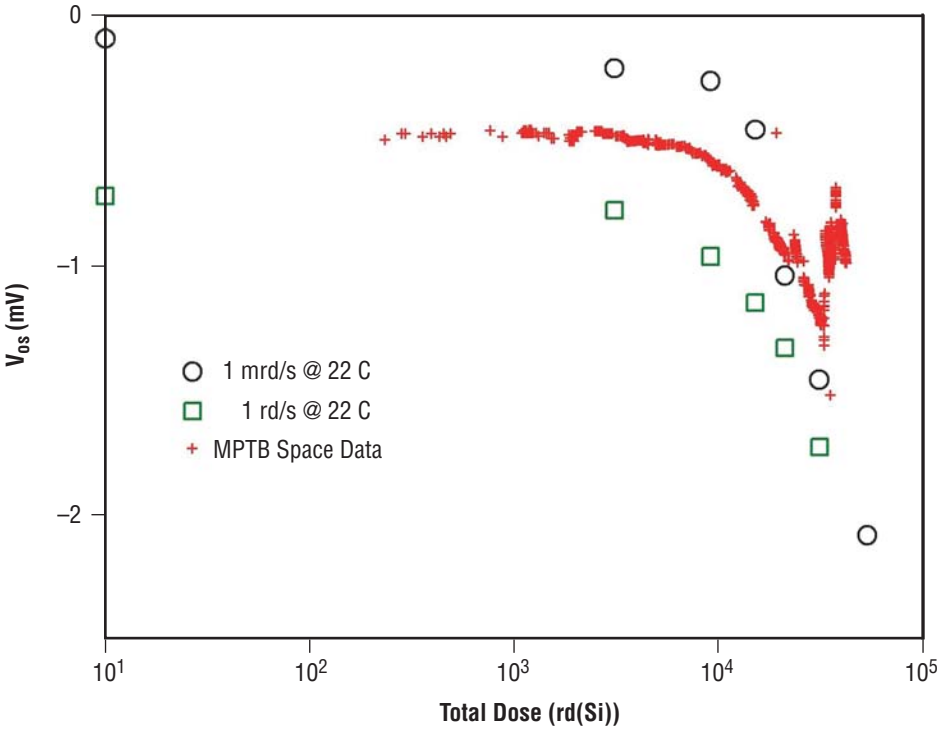

Figure 39. Comparison of MPTB space data to ground test data input V_{os} for LM139 quad comparator (DC9530).

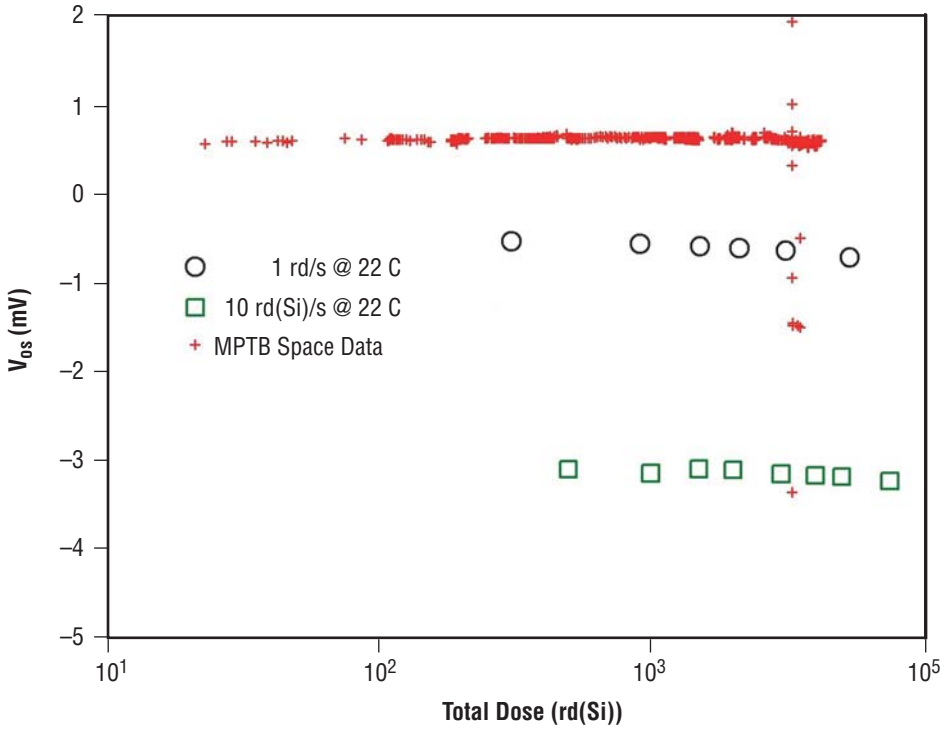

Figure 40. Comparison of MPTB space data to ground test data input V_{os} for PM139 quad comparator (DC9530).

5. SPACE EXPERIMENT INTERFERENCES

Prior to this experiment's launch in 1997, all ELDRS data were ground based. These ground-based data are taken predominately in Co60 or Cesium–137 cells. As such, the parts are exposed at a constant dose rate with uniform photon energies and constant temperature—when the experiment is designed properly. This is a significantly different environment than for a spacecraft. During this study, quantifying the primary interferences caused by performing an extended low dose rate ELDRS experiment in the space environment has been attempted. This experiment is particularly sensitive to external interferences, as the main data collected are low-level (nanoamp) current measurements that must be compared to ground-based data to fully realize the potential of the experiment.

The MPTB flies in a highly elliptical orbit that transitions the proton belts in each orbit. Thus, one experimental interference is that the dose rate varies by orders of magnitude within the orbit. Another experimental interference is that the radiation source is primarily a mix of electrons, protons, and heavy ions, with limited photons, mostly from secondary reactions of spacecraft materials with the particles. One reason the bipolar experiment on the MPTB was flown is to verify that the ELDRS effect would also be observed in the space environment, as some had suggested that ELDRS was merely a laboratory curiosity. Another experimental interference is the temperature of the experiment board, which varies significantly during the orbit, depending on the relative position of the Sun and Earth to the experiment. Finally, since the experiment can be turned off to save power for the primary payload, or when MPTB problems arise, an experimental interference is the variation in irradiation bias conditions. A significant benefit to this reexamination of the data from board A4 is to be able to better assess the impact of these various interferences that occur when flying a total dose experiment in Earth orbit as a guest on board a satellite with a separate prime mission.

5.1 Orbit

The MPTB orbit was described in section 3.1. The transit through the proton belts is observed clearly in figure 41, which shows the proton flux from the DSU instrument for three different proton energies for part of one orbit in April 2002. The great majority of the dose absorbed in each orbit occurs during the two belt transitions. The descending and ascending transits are not exactly symmetrical, with the ascending transition ≈6 min longer than the descending transition. In addition, an asymmetry between even and odd orbits can be observed. This even/odd asymmetry can be observed in figure 42, which shows the same DSU data displayed in figure 41, but over a period of about seven orbits. The peak proton flux is clearly higher every other orbit. Neither of these asymmetries is significant to the basic ELDRS experiment, but the even/odd orbit asymmetry did cause problems when attempting to utilize periods of relatively constant dose rate to examine dose rate effects, as will be discussed in section 7. These basic facts were known prior to launch, but this analysis better quantifies the difference between this space experiment and ground testing. All low dose rate ground testing has been done in Co60 cells at a constant dose rate, usually either 1 mrd(Si)/s or 10 mrd(Si)/s. As will be shown in more detail in section 7, for the MPTB, the average dose rate per 12-hr orbit usually varies between 0.1 mrd(Si)/s and 5 mrd(Si)/s, with brief

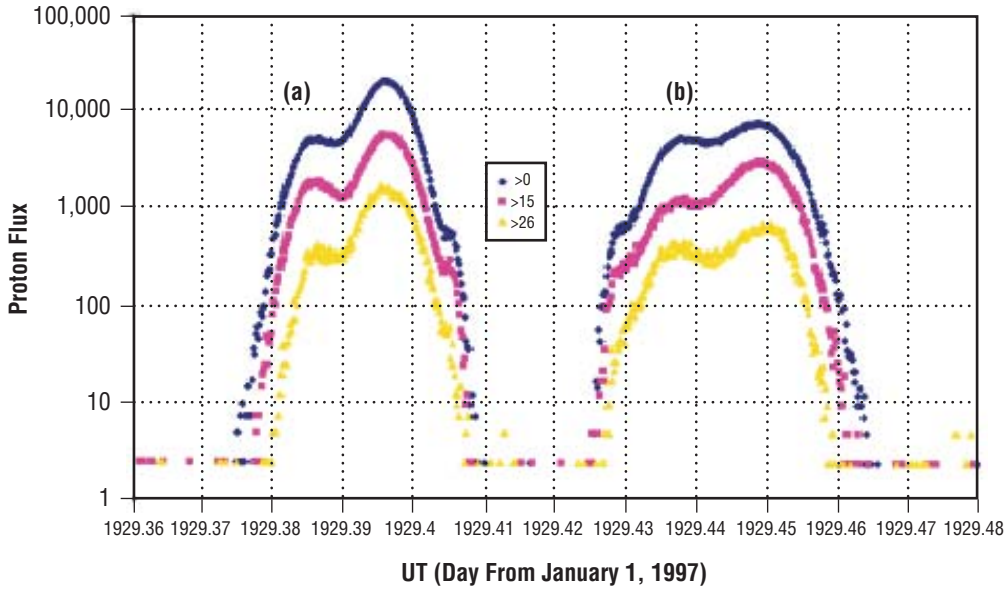

Figure 41. Aerospace DSU proton flux at three energies for a portion of one orbit (April 14, 2002): (a) descending belt transit and (b) ascending belt transit.

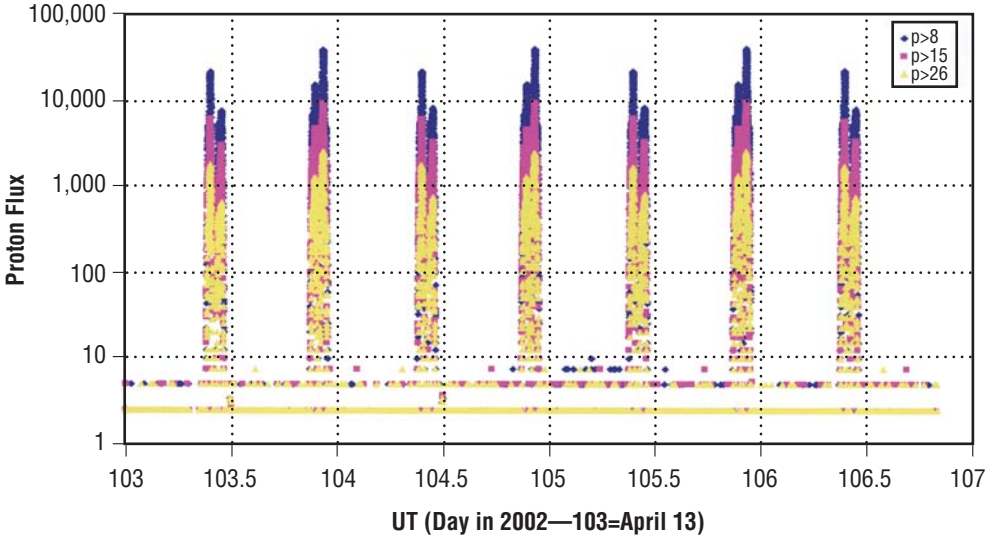

Figure 42. Aerospace DSU proton flux at three energies over approximately seven orbits. Even orbits reach higher peak flux, demonstrating even/odd orbit asymmetry.

excursions to higher average levels during solar events. However, if most of the dose accumulates within the belt transitions, the average dose rate during the belt transitions would average from 1.2 mrd(Si)/s to 60 mrd(Si)/s. Published data has shown that dose rates >50 mrd(Si)/s do not simulate low dose rate test data well, with major inconsistencies often reported with 100 mrd(Si)/s data. In either scenario, during much of the experiment's life, the average dose rate has been within bounds of established ground data, but there have been significant excursions outside the 1–10 mrd(Si)/s window predominately used in ground test. During the high dose rate periods, the rate of damage should slow. Extremely limited ground data taken at dose rates <1 mrd(Si)/s indicate that the rate of damage should probably increase, though the required lower bound to this increase in damage rate has not been established. A prime purpose of the dose rate analysis done in section 7 is to quantify these effects in support of suitable test method development.

5.2 System Outages

As stated earlier, the MPTB is a guest on a host satellite, which has a prime mission unrelated to the MPTB. Our role as guest does not permit interference with the prime mission. One particular problem relates to details of the GTO flown. During some periods, the satellite spends the majority of its time in the Earth's shadow. During these periods, available system power is greatly reduced. In some cases, no data were read (this activity increases power consumption significantly), and in other cases, power was turned off completely. Gaps in the data were known about since downloading started, but it was thought that they were interruptions in test sequencing, not power cycling. Only during this study was verification made that experiment bias was removed in some instances. Since experiment bias is carefully maintained during ground test, it is not easy to quantify what effect this power cycling may have on the data. However, most ELDRS ground tests are done in a step-stress manner, with power cycled during the test sequence, with no noted ill effect. In addition, the comparison to ground test data demonstrates a lack of effect on the experiment. This is a result of the fact that, for some parameters, such as I_{ib}, there is little difference between degradation for the biased and the all-leads grounded bias conditions. Significant differences are likely to occur for biased and unbiased irradiation for offset parameters such as V_{os}.

5.3 Temperature

Figure 43 shows the maximum temperature recorded on board A2 as a function of orbit. The temperature sensor on board A4 is not functional. While these readings are not necessarily synchronized with the data recording made on board A4, the error should be relatively small. The 40 °C range shown is significant to the parametric data of this experiment. I_{ib} is a function of chip temperature, with I_{ib} increasing with temperature. In addition, the measurement system was not characterized over this temperature range and could be an additional error source. Much of the measurement circuit is on board A4, but the analog-to-digital converter is a system function, and may be in a more temperature-sheltered location. A lesson learned for future space experiments is to characterize both the device under test and the measurement system as a function of temperature prior to launch. To visually correlate temperature effects to the data, this temperature curve is overlaid with device data in figures 44 through 49. As the temperature effects rise and fall in a somewhat cyclical manner, the net effect on overall shape of the total dose curve is probably minor. However, the impact during short time periods is of consequence, and did impact the attempts to look at dose rate effects. This impact is explained in section 7.

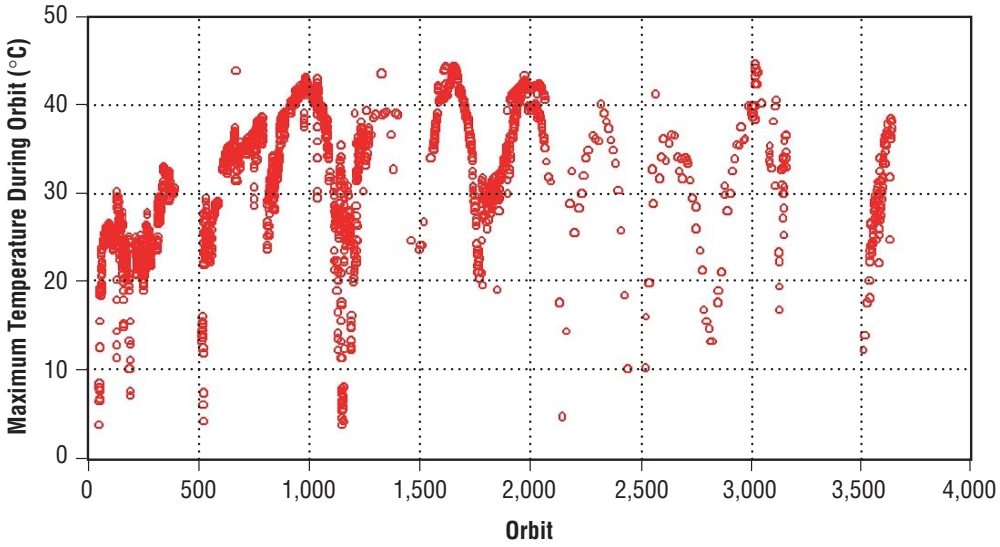

Figure 43. Maximum A2 board temperature recorded each orbit. While the lowest temperatures mostly represent times when the experiment was turned off, wide temperature variation does have impact on the experiment.

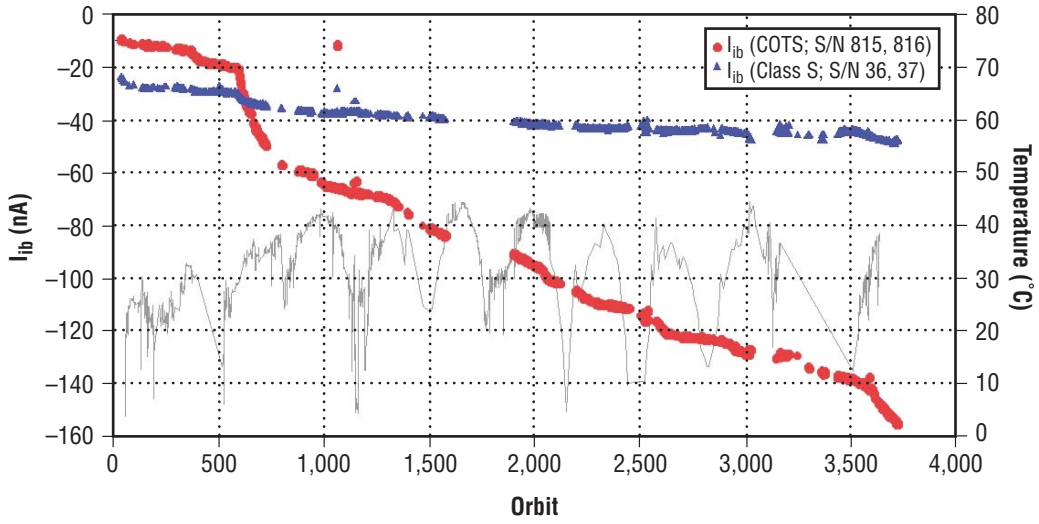

Figure 44. I_{ib} for the COTS and class S LM124 op amps versus satellite orbit. The curves show the average of all I_b data for each part type. The overlaid curve is the ambient temperature near the board where the parts were mounted.

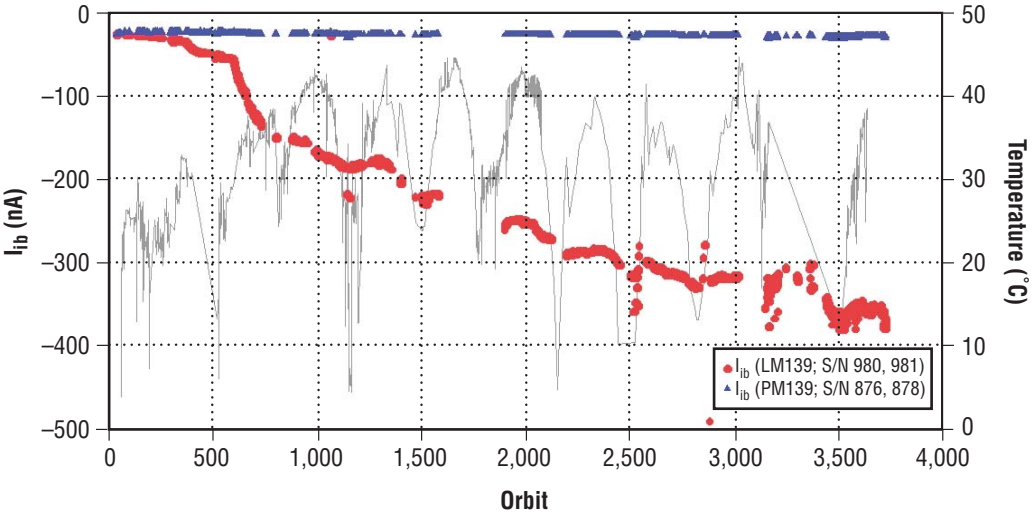

Figure 45. I_{ib} for the LM139 and PM139 comparators versus satellite orbit. The curves show the average of all I_b data for each part type. The overlaid curve is the ambient temperature near the board where the parts were mounted.

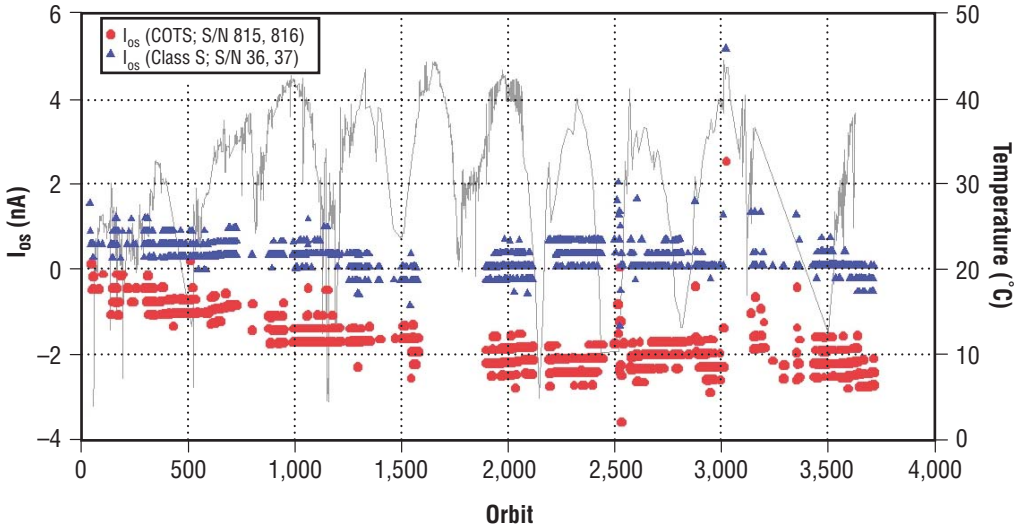

Figure 46. Input I_{os} for the COTS and class S LM124 op amps versus satellite orbit. The curves show the average of all I_b data for each part type. The overlaid curve is the ambient temperature near the board where the parts were mounted.

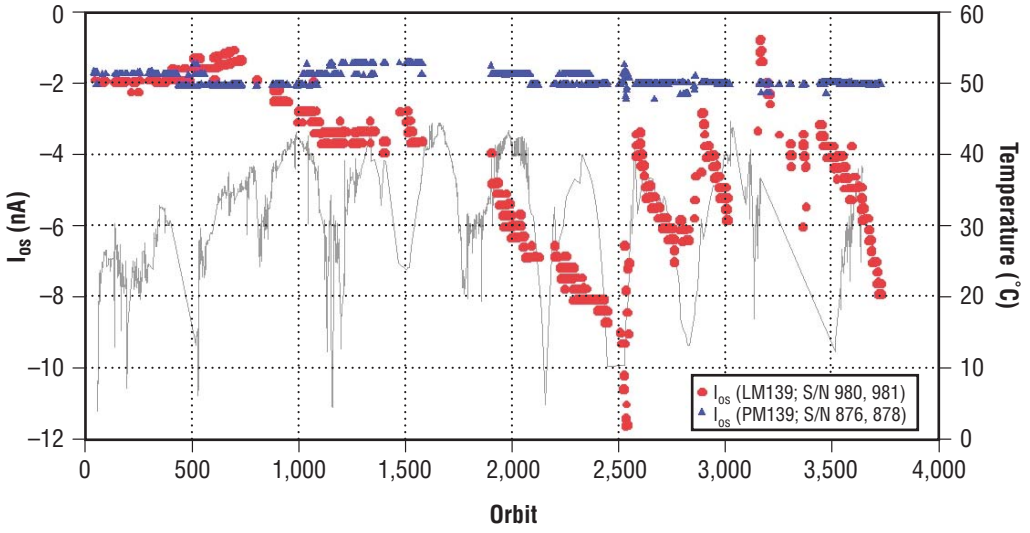

Figure 47. Input I_{os} for the LM139 and PM139 comparators versus satellite orbit. The curves show the average of all I_b data for each part type. The overlaid curve is the ambient temperature near the board where the parts were mounted.

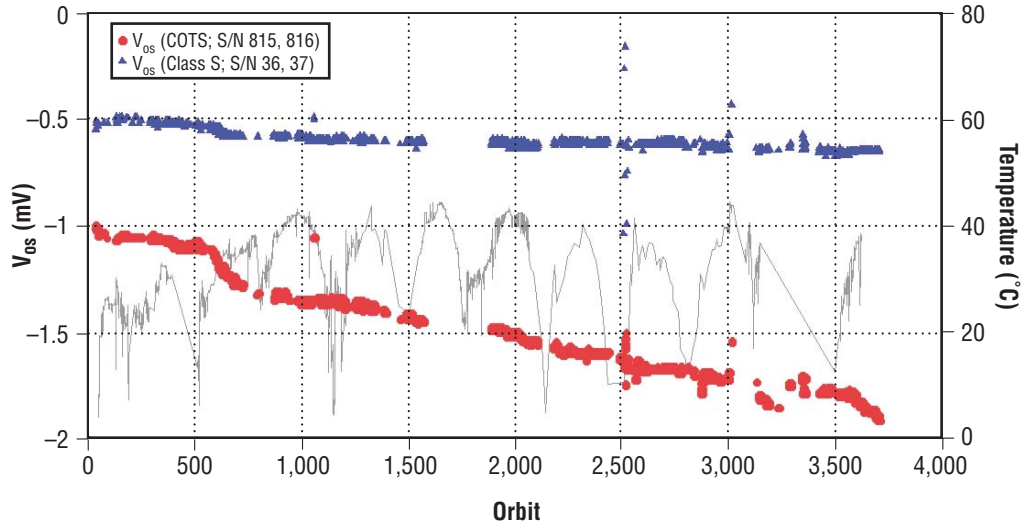

Figure 48. Input V_{os} for the COTS and class S LM124 op amps versus satellite orbit. The curves show the average of all I_b data for each part type. The overlaid curve is the ambient temperature near the board where the parts were mounted.

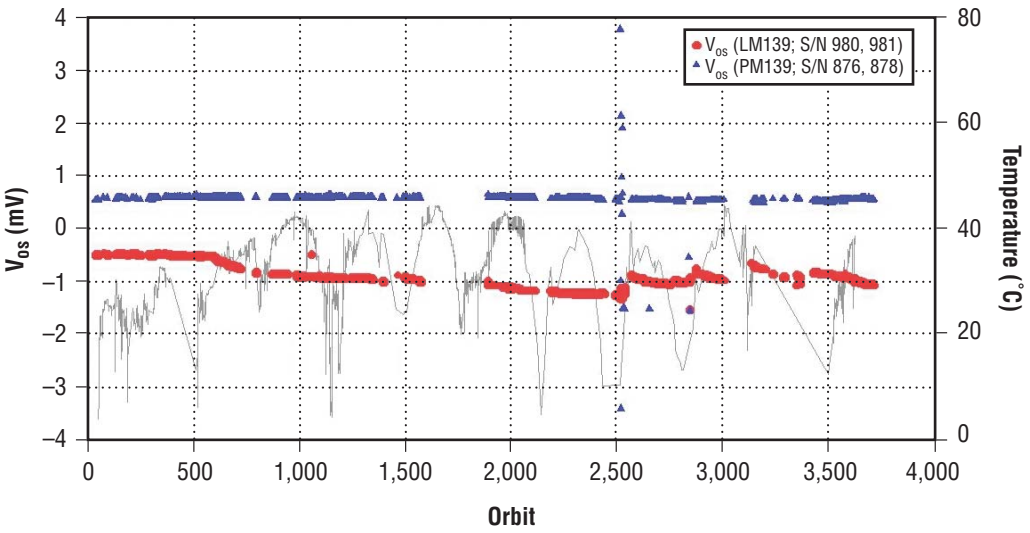

Figure 49. Input V_{os} for the LM139 and PM139 comparators versus satellite orbit. The curves show the average of all I_b data for each part type. The overlaid curve is the ambient temperature near the board where the parts were mounted.

6. PROTON DISPLACEMENT EFFECTS

In addition to total dose-induced degradation of the test devices, including the ELDRS, bipolar circuits are also susceptible to degradation by displacement effects, which reduce the minority carrier lifetime. Where photons and electrons will primarily deposit charge in the device, protons and neutrons also have sufficient mass to displace atoms in the crystal lattice of the semiconductor when a direct collision occurs. One question about this MPTB experiment that has not been previously addressed is the ratio of displacement damage to ionizing damage in the space data from the MPTB. In this section, the equivalence of the space environment proton fluence to a 1-MeV neutron fluence and the damage expected to occur in a 1-MeV equivalent neutron exposure using ground data will be estimated and compared with the MPTB data.

6.1 Proton Fluence and 1-MeV Neutron Equivalence

The proton flux per orbit and integral proton fluence was compiled for the location of board A4 on the MPTB experiment as part of the dosimetry study performed by the NRL. These data have been reported in section 3. The integral proton fluence curve is repeated in figure 50. To compare these data to ground neutron data requires an estimate of damage equivalence between the two environments. This is done using nonionizing energy loss (NIEL) for the various particles. The CREDO instrument has been calibrated in the coincidence mode to respond only to protons >38 MeV. In the singles (noncoincidence) mode, it is also sensitive to high-energy electrons during solar events.[19,20] To develop an integral proton fluence curve for analysis of the ELDRS data, it was determined that the penetration depth of protons >38 MeV have sufficient penetration depth that assures they will fully interact with the MPTB bipolar devices on board A4. This makes the coincident CREDO data the best available source of proton fluence. Table 1 lists NIEL factors for several relevant particles.

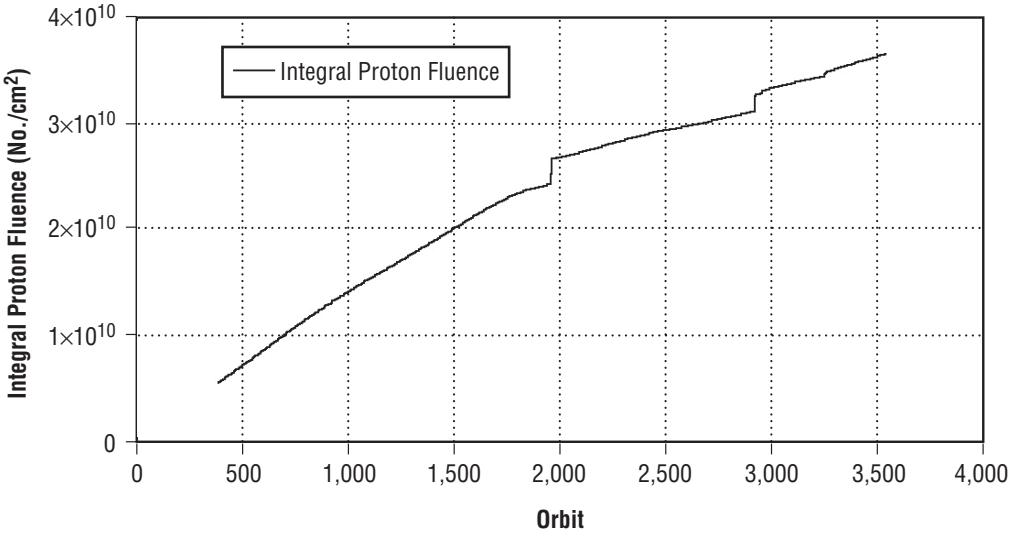

Figure 50. Integral proton fluence at board A4 as determined primarily by the CREDO instrument.

Table 1. NIEL factors for several relevant particles.

Energy and Particle	Nonionizing Energy Loss
1-MeV neutron	2.04×10^{-3} (MeV-cm^2/g)
30-MeV proton	4.78×10^{-3} (MeV-cm^2/g)
50-MeV proton	3.88×10^{-3} (MeV-cm^2/g)

The space proton environment is comprised of a wide spectrum of proton energies. Thus, the NIEL factor is an estimate that can represent a given spectrum. The 30- to 50-MeV range is considered a good estimate of the protons that cause the majority of damage to the MPTB boards. On this basis, the NIEL for the space protons is approximately 2× that of 1-MeV neutrons. To compare the MPTB data to ground neutron data, the proton fluence is reduced by a factor of 2.

6.2 Ground Neutron Test Data

The Naval Surface Warfare Center performed a limited neutron characterization of the MPTB devices in 1996. These data, along with Co60 and proton data, have not been previously published, and are included in appendix C.

The average neutron responses of these devices are plotted in figure 51. The LM139, PM139, and COTS LM124 consisted of four test packages for each part type. Each package contains four circuits and each circuit has two inputs. Therefore, the average given for these device types represents a total of 32 measurements at each neutron level. The class S LM124 consisted of three test packages for a total of 24 measurements averaged.

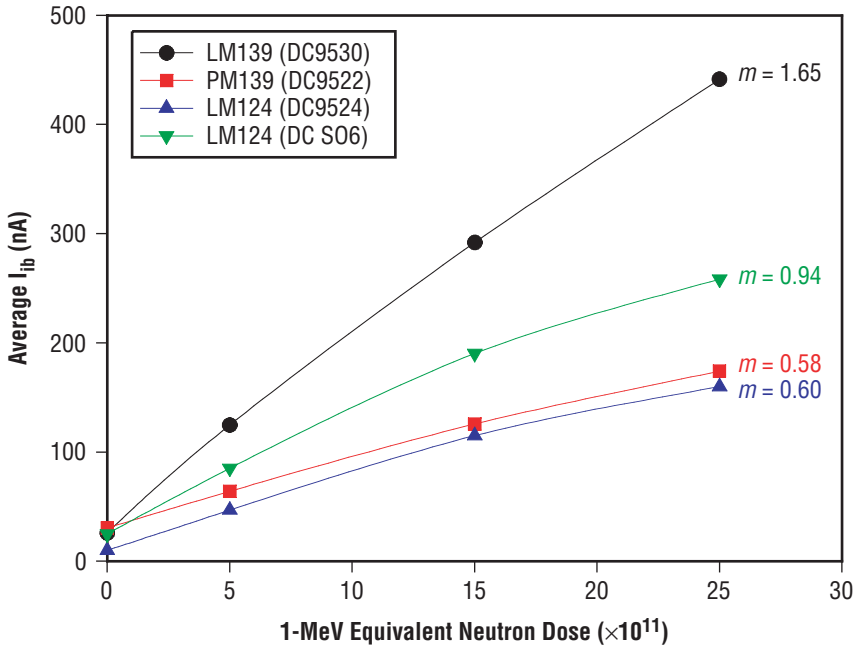

Figure 51. Ground-test neutron data, taken in 1996. Slope (m) values determined by linear regression fit.

Figure 51 shows that the displacement damage on the LM139 is the most severe, followed by the class S LM124, PM139, and COTS LM124. If a linear regressive fit is performed, a first-order approximation of the displacement damage slope for each of these devices can be determined. The LM139 exhibits 1.65 nA of change per 10^{10} neutrons. Class S LM124 exhibits 0.94 nA per 10^{10} neutrons, the PM139 exhibits 0.58 nA per 10^{10} neutrons, and the COTS LM124 exhibits 0.6 nA per 10^{10} neutrons.

6.3 Comparing Space Data to Expected 1-MeV Neutron Displacement Damage

I_{ib} is the most sensitive parameter for the four MPTB part types and will be used to examine the ratio of displacement damage to ionizing degradation. Using the NIEL factor as described above, the MPTB space data for the four part types can be plotted as an approximate function of 1-MeV neutron equivalence. These curves assume that 100 percent of the damage is caused by displacement, and must only be used for comparison purposes. The estimate for neutron damage is overlaid on the space data. These curves are calculated based on the slope of the neutron data, as described above.

6.4 Discussion and Analysis

By determining an approximate 1-MeV neutron equivalence for the space proton spectrum, and extracting a linear rate of damage from ground neutron test, direct comparison of the two data sets has been made in figures 52 and 53.

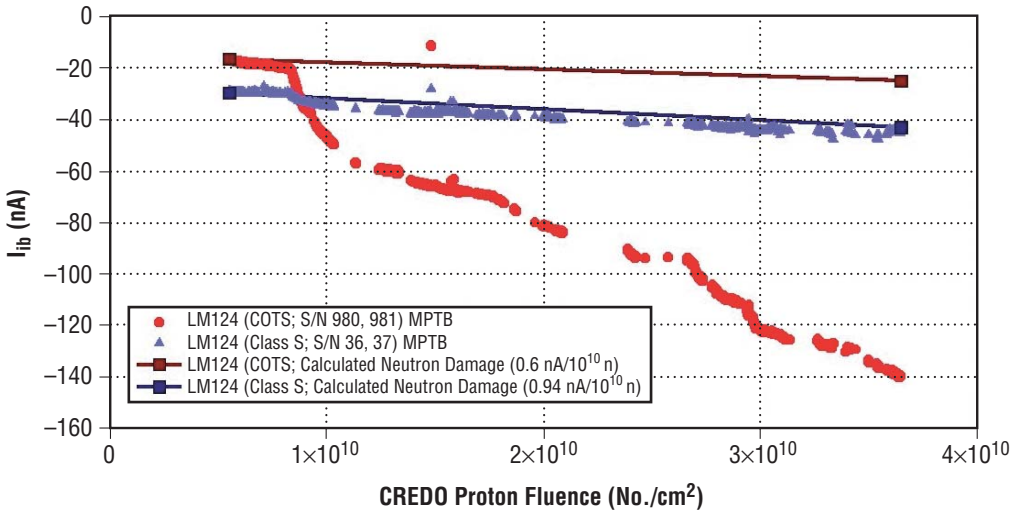

Figure 52. COTS and class S LM124 MPTB data and calculated 1-MeV equivalent neutron damage. Note: This plot is only valid for comparison of expected displacement damage. It does not imply the space damage is only from protons.

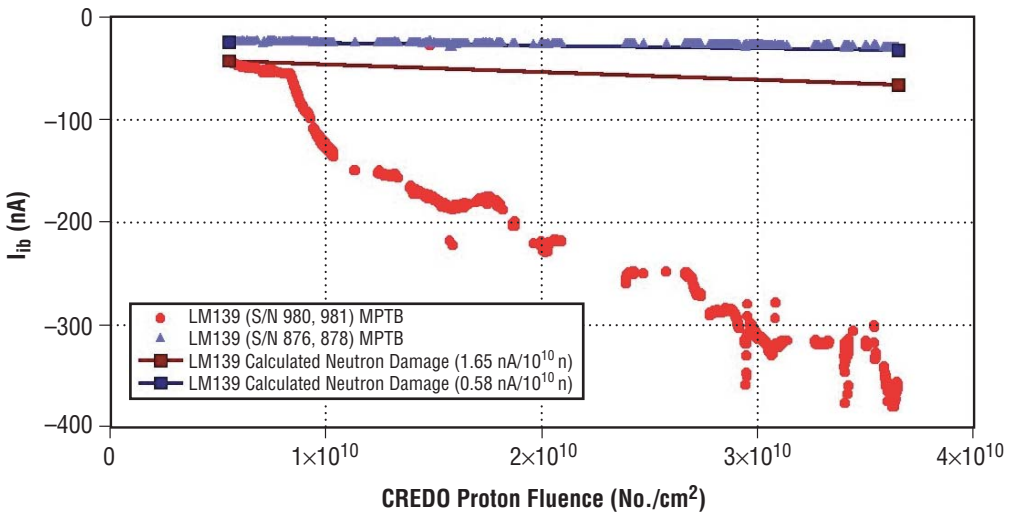

Figure 53. LM139 and PM139 MPTB data and calculated 1-MeV equivalent neutron damage. Note: This plot is only valid for comparison of expected displacement damage. It does not imply the space damage is only from protons.

It is clear for three of the device types—COTS LM124, class S LM124, and LM139—that the space damage significantly exceeds the damage that would be expected from displacement damage alone. For these devices, the majority of the recorded degradation can be attributed to ionization, not displacement damage.

The PM139 has shown little effect from its 5-yr exposure, with a total degradation of 1–2 nA in this period. This compares favorably with the expected damage from displacement, but the magnitude of change is negligible. If any ionization damage has occurred, it appears to have annealed within the interval of measurements (12 hr). These PM139 data do provide an indication of very good stability in the board A4 test circuitry over a 5-yr period in space, which is significant in itself.

From this analysis, ionization appears to be the dominant damage mechanism for this experiment.

7. ANALYSIS OF DOSE RATE EFFECTS

Two of the most pressing questions in the continuing study of the ELDRS effect are the best dose rate at which to perform low dose rate ground tests, and an accelerated test method to avoid the distress and cost of low dose rate testing. The MPTB space experiment cannot address the accelerated test method issue, but has already made a significant impact on the effectiveness of low dose rate testing. As shown in figures 32–40, independent of all interferences encountered in the space environment, the low dose rate ground data (both 1 and 10 mrd(Si)/s) provide an excellent representation of the damage encountered in space for these device types.

As observed in these plots, the 1 mrd(Si)/s data usually show slightly more degradation than the 10 mrd(Si)/s data. Research has also shown that the ELDRS effect is greatly diminished between 50 and 100 mrd(Si)/s, and usually not observed by 1 rd(Si)/s. Finally, it has been suggested that some part types degrade even more when the dose rate is reduced significantly below 1 mrd(Si)/s.

These results imply that a generalized ELDRS response curve exists. In this curve, the rate of degradation is lowest—and hopefully nearly constant—above 1 rd(Si)/s. The rate of degradation increases as the dose rate is reduced, with a rapid increase between 100 and 10 mrd(Si)/s, and then a very slow increase to somewhere below 1 mrd(Si)/s. At some dose rate, evidently well below 1 mrd(Si)/s, the rate of degradation must level and then reverse, or in the limit of increasing damage for lower and lower dose rates, a single photon would cause infinite damage, which is not the case. The dose rate curve of figure 7(a) demonstrates that on a 12-hr orbit average, the dose rate observed in the MPTB has varied from $<$0.1 mrd(Si)/s to $\approx$10 mrd(Si)/s. If intervals of time exist where the dose rate is relatively constant, and sufficient dose is accumulated so the test circuitry can resolve the damage to the parts consistently, it should be possible to analyze the impact of dose rate on these parts in a manner that is not practical with ground data.

A significant portion of this study has been devoted to analysis of dose rate effects within the MPTB data set. This section gives these results with the data from board A4 of the MPTB.

7.1 Data Mining and Filtering Techniques

Data mining techniques were used to analyze the MPTB experimental data for the LM139 and PM139 comparators and the COTS and class S LM124 op amps. The study was limited to the I_{ib} parameter, which exhibits the largest parametric change, and concentrates on the COTS LM124 and LM139. The non-ELDRS sensitive class S LM124 and PM139 are also examined, but in less detail, as the degradation is limited.

The first goal was to identify consecutive orbit intervals that received a relatively constant dose and then use those orbits within each interval to calculate the change in the device parametric values between orbits with respect to the total dose. The calculated values for ΔI_{ib}/dose of each interval were plotted versus the interval dose rate. Also shown in the various graphs are the effects of temperature, interval size, and interval dose.

There were three different sets of data used for the analyses: (1) Dose per orbit data that had been interpolated for the A4 test board on which the op amp and comparator parts were mounted, (2) device parametric measurements taken once per orbit, and (3) the part's ambient temperature per orbit. Data were missing for many orbits throughout the test period and the missing data for each data set did not always occur at the same orbit numbers. The data were stored in Microsoft® Excel spreadsheets and analyzed with routines written in Microsoft® Visual Basic® for Applications.

7.2 Analyses Method

The first step was to search the dose per orbit data to identify consecutive orbit intervals where the dose rate was relatively constant. As described in section 5, a space experiment has several interferences when compared to ground tests. It was demonstrated that these interferences have only a small impact on the accumulated dose data. However, when looking for relatively small intervals, the impact of the orbit, the even/odd asymmetry, temperature, and missing data make data selection quite difficult. Criteria were established to qualify the constant dose orbit intervals. Many trial orbit screenings were run with multiple sets of different criteria limit values in order to come up with the best compromise between finding the largest constant dose intervals and having a sufficient number of qualifying intervals for meaningful plots. In the end, the following criteria and limits were identified as the best possible and used for this analysis:

(1) The maximum deviation of the dose rate for any orbit within an interval must be within 20 percent of the median of all interval orbit dose rates. The program went through an iterative process of recalculating the interval median and orbit deviation with the addition of each new orbit.

(2) Because missing orbit data would disqualify many sections of otherwise usable data, the following criteria were used for allowing orbit gaps: dose rates of <20 rd per orbit were allowed five orbit gaps, 20–50 rd per orbit were allowed three orbit gaps, and dose rates >50 rds per orbit were not allowed any gaps. The allowable orbit gap sizes were scaled with respect to the calculated dose rate of the interval. Lower dose rate intervals were allowed larger orbit gaps.

(3) The interval must meet a minimum orbit count. It was desirable to maximize the size of the intervals to improve the confidence in the calculated value of ΔI_{ib}/dose. The best value for this criterion was determined to be seven orbits.

The next step was to match the qualifying orbits to the corresponding orbits for the parametric data of each device type; parametric data are missing for some orbits where dose data exist. A criterion was established that a minimum of six orbits of parametric data had to exist within the seven-orbit (minimum) dose interval in order for the interval to qualify. Again, the idea was to assure a reasonable number of orbits in the interval to calculate ΔI_{ib}/dose. The ΔI_{ib}/dose for each interval was determined by using the Excel linear regression function for calculating the slope of a set of x and y data points, where x was the total dose for a given orbit and y was the corresponding I_{ib} of the device.

7.3 Analysis of Results

The filtering techniques described above led to encouraging results, but there was more scatter in the results than desired, and there were no dose rate intervals identified greater than ≈3.5 mrd(Si)/s. To

avoid data overload, only the COTS LM124 and LM139 devices will be discussed at first, followed by the class S LM124 and PM139.

The results of the data mining process are presented in several stages to best explain the data and their value:

(1) In the first graphs, the calculated values of ΔI_{ib} per dose are plotted versus the interval dose rate. This is the result of the filter criteria discussed above. The unit of dose per orbit was converted to millirads per second, and the ordinate is ΔI_{ib} in units of picoamperes per rd(Si).

(2) The ΔI_{ib}/dose was plotted versus the accumulated interval dose. This is a quasi-second derivative done to look at the average absorbed dose needed to achieve consistent results from the test circuitry of the MPTB. To further reduce scatter, the next set of graphs show the effects of filtering the resultant data by first eliminating any data where the ambient board temperature was outside the range of 23 to 35 °C and then eliminating data where the accumulated interval dose is too low for consistent tester resolution.

(3) Finally, in an attempt to extend the range of observed dose rates, even if confidence in the data is lower, data were hand extracted from the one or two orbit intervals that occurred during the largest solar flares.

7.3.1 COTS LM124 I_{ib} Versus Interval Dose Rate

A very different method for representing the data set is used in this section. For short orbital intervals, the first derivative of the degradation curve of the I_{ib} for each part is taken, and the rate of degradation of the parameter as a function of the average dose rate of the space environment during that interval is plotted. Thus, while earlier analysis looked at the data set in the context of the entire mission, this analysis looks at short time intervals, and must consider short time effects that have been shown to average out in the long time interval. The purpose is to see if there is information available within the data set that can aid in development of a test methodology for ground testing ELDRS parts. If the concept of a generalized ELDRS response curve in the low dose rate regime of 1–10 mrd(Si)/s is considered, one would expect a fairly constant rate of degradation. Perhaps the rate will increase slowly as the dose rate decreases, as has been observed in many ground tests. From the extremely rare ground data that exist at dose rates <1 mrd(Si)/s, it appears the rate of degradation will continue to increase as the dose rate is reduced. At some dose rate, this trend must reverse, but this has never been observed in any ground test.

In this data mining process, the goal was to isolate intervals of relatively constant dose rate and attempt to observe (1) a relatively constant rate of degradation in the 1–10 mrd(Si)/s regime, (2) the increased rate of degradation for some range of lower dose rates, and (3) if lucky, a reduction in the rate of degradation at some higher dose rate. It was hoped that, for some short intervals, there might be data in the 50 mrd(Si)/s region, but such data does not exist in this data set over the 12-hr orbit collection interval.

When the filter rules described above were applied, the data shown in figures 54 and 55 for the COTS LM124 and LM139 devices, respectively, result. From about 1 to 3.5 mrd(Si)/s, the data are indeed fairly constant, as hoped. While there are many intervals in the low dose rate region, there is also a large

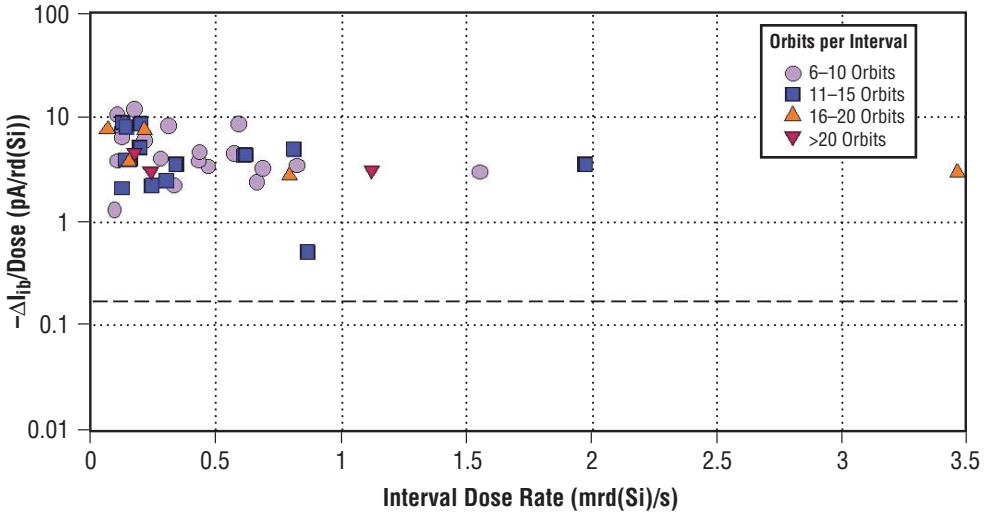

Figure 54. Change in I_{ib} with respect to dose for COTS LM124 op amp versus average interval dose rate for relatively constant dose rate orbit intervals. The symbols used to show the data points represent the interval size as a range of orbits.

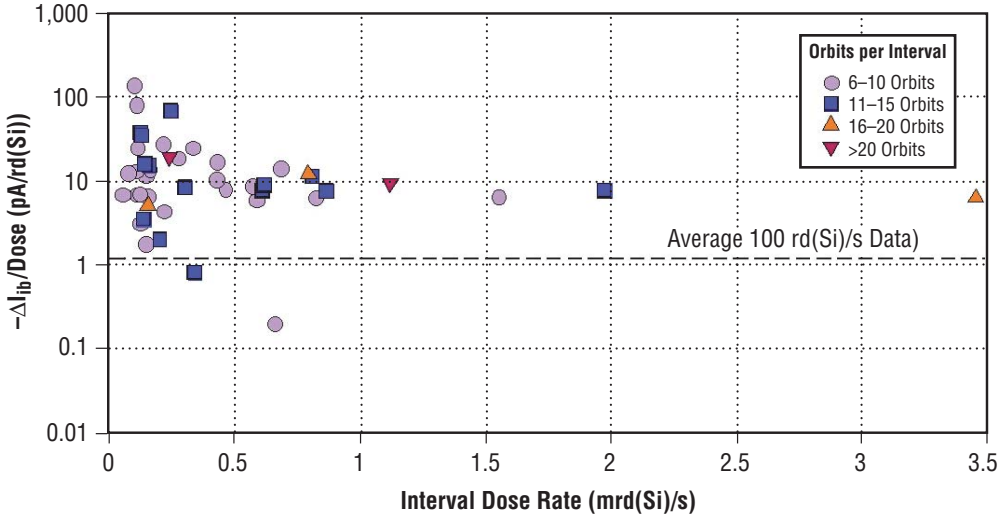

Figure 55. Change in I_{ib} with respect to dose for LM139 comparator versus average interval dose rate for relatively constant dose rate orbit intervals. The symbols used to show the data points represent the interval size as a range of orbits.

scatter in this range of the data. Some indication of an upturn in the rate of degradation is observed, but there are also points to counter this possible result. If the source(s) of this scatter are not isolated, no conclusions about the low dose rate region could be extracted. Additional filtering criteria were required.

7.3.2 Parameter Versus Interval Dose

Any test circuit has a limit of its resolution. When collecting data over a long time interval, such as is done on board A4, the long-term average pattern is very good. However, in small intervals, many variations in the data are observed. This has little impact in the long term, but can have significant impact when looking at the short interval. Some readings had a positive slope and had been eliminated. The immediate question was, in how small an accumulated dose interval could the test circuit reliably resolve degradation in the part.

To investigate this, the same data intervals shown in figures 54 and 55 were plotted against the dose accumulated in the interval. This represents a quasi-second derivative, where the rate of degradation is compared to the accumulated dose, not the average dose rate of any given interval.

The results, shown in figures 56 and 57, are encouraging. When the interval was at least 300 rd(Si), the rate was quite consistent, with few outliers. At intervals down to 200 rd(Si), minor scatter is observed, but the trend is still good. For intervals with <200 rd(Si), the scatter is significant. It is worth reminding the reader that while figures 56 and 57 look very similar to the earlier graphs, the graphs serve an entirely different purpose.

The result of this experiment is that any interval where <200 rd(Si) was accumulated is now considered to be below the limit of the test circuit resolution.

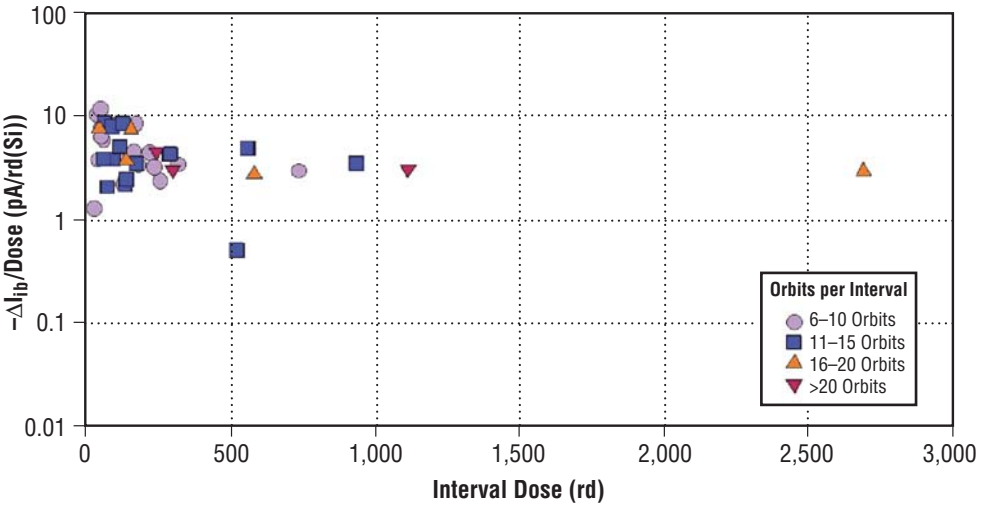

Figure 56. Change in I_{ib} with respect to dose for COTS LM124 op amp versus average interval dose for relatively constant dose rate orbit intervals. The symbols used to show the data points represent the interval size as a range of orbits.

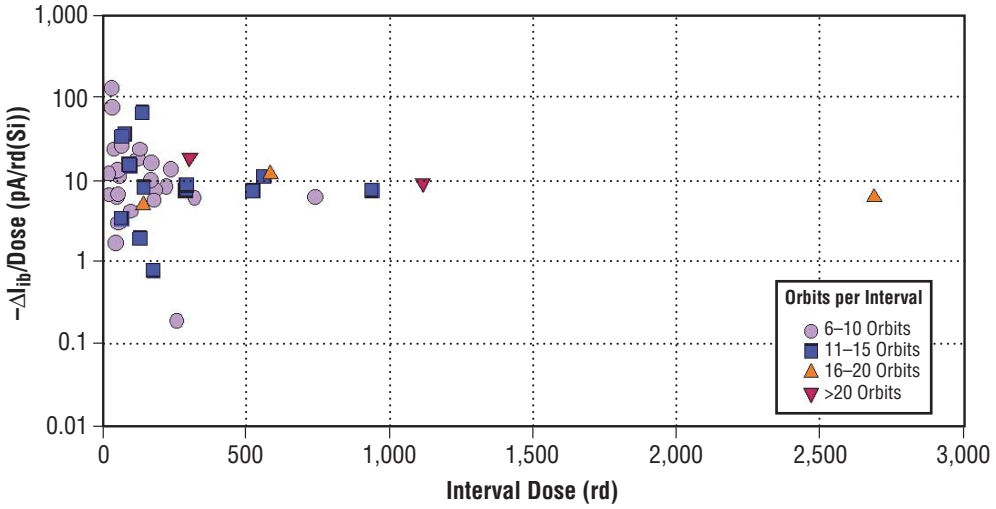

Figure 57. Change in I_{ib} with respect to dose for LM139 comparator versus average interval dose for relatively constant dose rate orbit intervals. The symbols used to show the data points represent the interval size as a range of orbits.

7.3.3 Parameter Versus Interval Dose Rate (for Internal Total Dose >200 rd and Limited Temperature)

The goal remains to see if this experiment can yield further clues about the shape of the response curve for these parts, and potentially impact ground test methodology. The 200 rd(Si) minimum dose per interval rule just established reduced scatter significantly, but some remained. A parameter that had not been considered prior to this project was the board temperature. As described in section 5, a temperature curve for the boards was recovered. There is significant variation—approximately 0 °C to over 40 °C. Temperature is a known factor in the measurement of I_{ib}, but to the best of our knowledge, neither the test devices nor the test board were temperature characterized prior to launch. Given this fact, the only plausible course was to further limit the data by the recorded temperature during the interval. Experimentation resulted in a usable temperature range of 23 to 35 °C, and this filter was also applied to the data. With no prior temperature data available, this range gave the most reasonable results.

The final results are shown in figures 58 and 59. While there are, unfortunately, few intervals left within the rules developed, those do still produce interesting results. The COTS LM124 does indeed show a slight increase in rate of degradation as the dose rate is reduced. All data points indicate a rate greater than the average observed at 100 rd(Si)/s. This trend—with one outlier—continues below 1 mrd(Si)/s to the minimum dose rate of ≈0.6 mrd(Si)/s. There is insufficient data to estimate if the rate of degradation has reached a maximum, but there is not a reversal in the rate of degradation noted at the 0.6-mrd(Si)/s point. The LM139 data show a very consistent rate of degradation—between 8 and 9 pA/rd—with one outlier over the entire dose rate range. Again, this is well elevated over the 100 rd(Si)/s average rate.

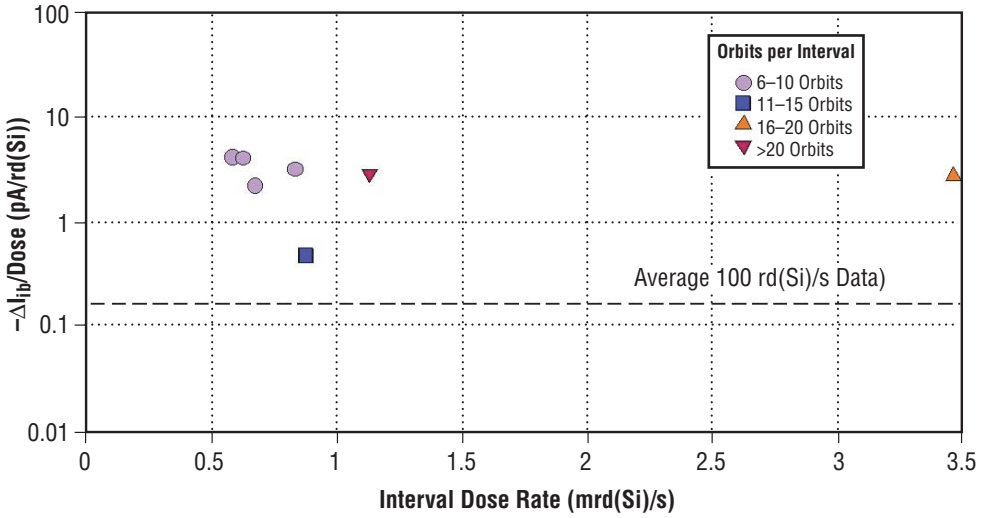

Figure 58. Change in I_{ib} with respect to dose for COTS LM124 op amp versus average interval dose rate for relatively constant dose rate orbit intervals. The graph only used data from orbits where the ambient temperature was between 23 and 35 °C and the interval accumulated dose was >200 rd. The symbols used to show the data points represent the interval size as a range of orbits.

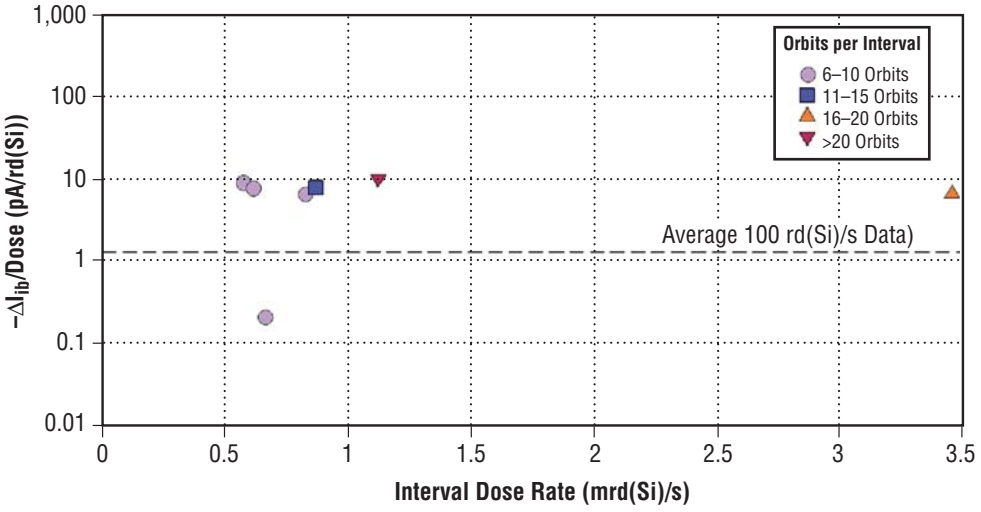

Figure 59. Change in I_{ib} with respect to dose for LM139 comparator versus average interval dose rate for relatively constant dose rate orbit intervals. The graph only used data from orbits where the ambient temperature was between 23 and 35 °C and the interval accumulated dose was >200 rd. The symbols used to show the data points represent the interval size as a range of orbits.

7.3.4 Parameter Versus Interval Dose Rate With High Dose Rate Data Added

From a viewpoint of helping define ground test methodology for low dose rate test, the fact that no interval was found with an average dose rate >3.5 mrd(Si)/s was disappointing. When one looks at the average dose rate per orbit, first shown in figure 7(a), there are four periods in the flight where the average dose rate approached 10 mrd(Si)/s. However, these occurred for only one or two orbit intervals. Since the time the measurement was made with the onset of the flare event that caused this could not be equated, it is difficult to consistently extract data in the same manner used for the longer intervals. However, the importance of 10 mrd(Si)/s ground test data is sufficiently high to attempt hand extraction of data for these few high dose rate intervals. The orbits were isolated, but there was only one interval where both dose rate and parametric data were available. These data were fit, and the results are shown in figures 60 and 61. Even though this extraction technique is considered less reliable than for the larger intervals, for the new data point (≈9 mrd(Si)/s) for both part types, it does fit with the other data very well. This provides a strong reinforcement to the validity of using 10 mrd(Si)/s ground data to estimate space degradation.

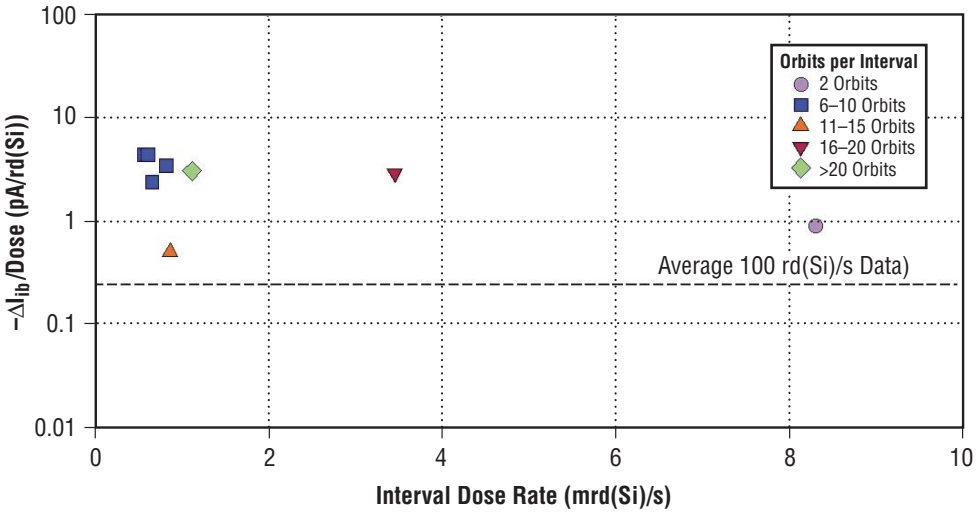

Figure 60. Change in I_{ib} with respect to dose for COTS LM124 op amp versus average interval dose rate for relatively constant dose rate orbit intervals. The symbols used to show the data points represent the interval size as a range of orbits.

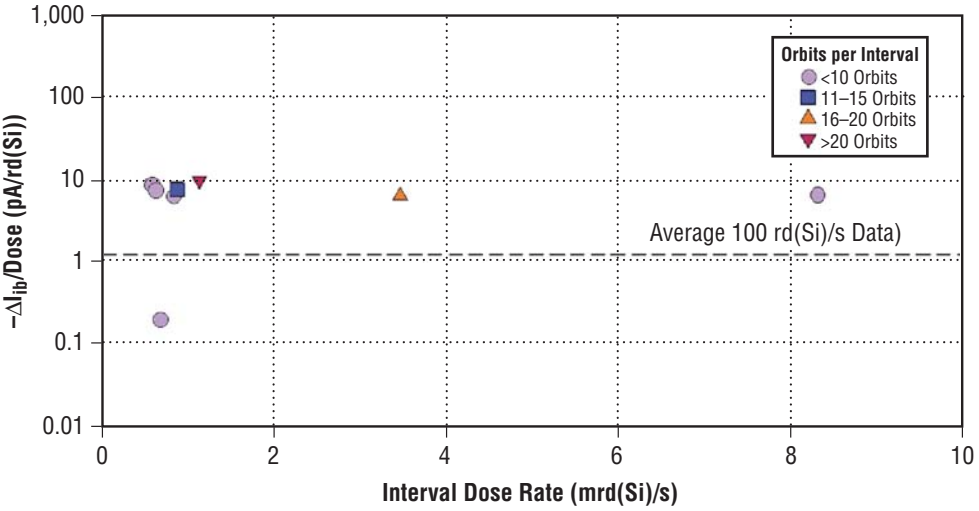

Figure 61. Change in I_{ib} with respect to dose for LM139 comparator versus average interval dose rate for relatively constant dose rate orbit intervals. The symbols used to show the data points represent the interval size as a range of orbits.

7.3.5 Class S LM124 and PM139 Data

Figures 62–67 duplicate the results shown above for the class S LM124 and PM139 for these part types.

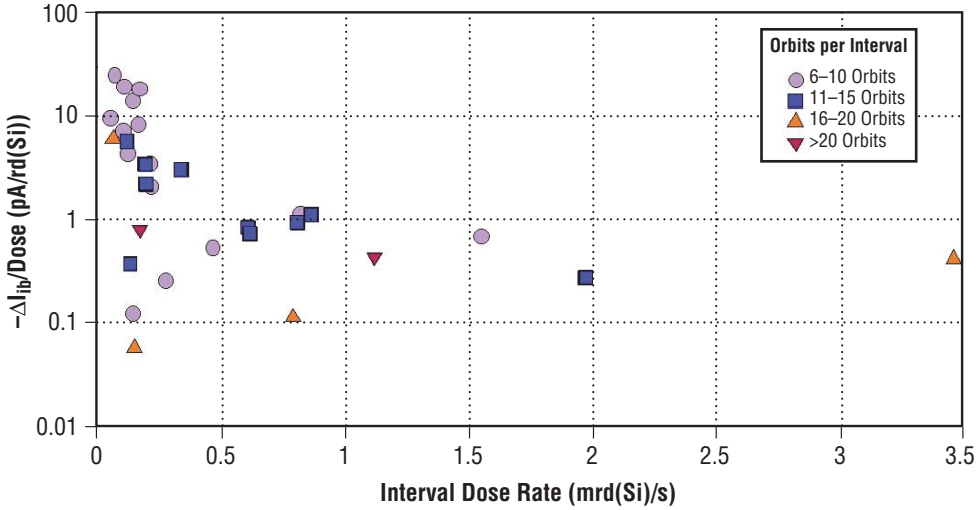

Figure 62. Change in I_{ib} with respect to dose for class S LM124 op amp versus average interval dose rate for relatively constant dose rate orbit intervals. The symbols used to show the data points represent the interval size as a range of orbits.

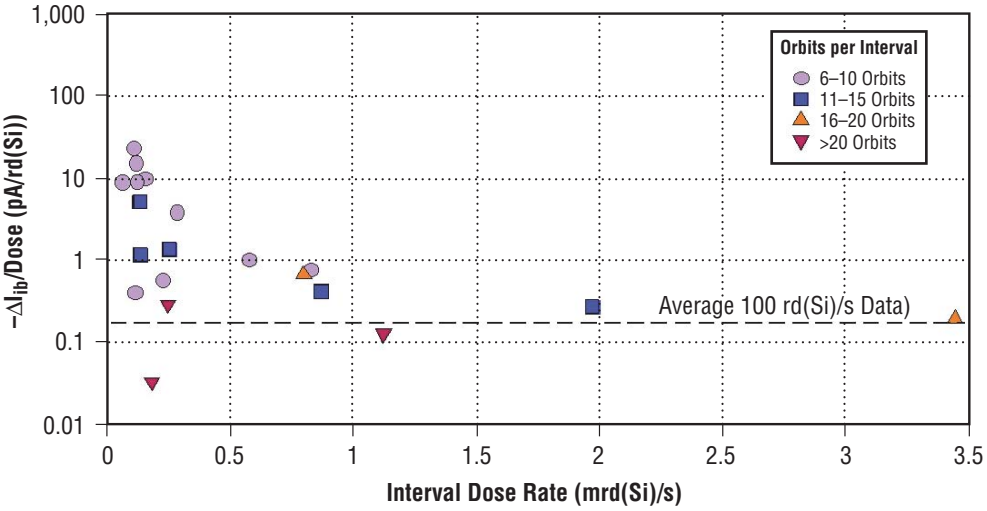

Figure 63. Change in I_{ib} with respect to dose for PM139 comparator versus average interval dose rate for relatively constant dose rate orbit intervals. The symbols used to show the data points represent the interval size as a range of orbits.

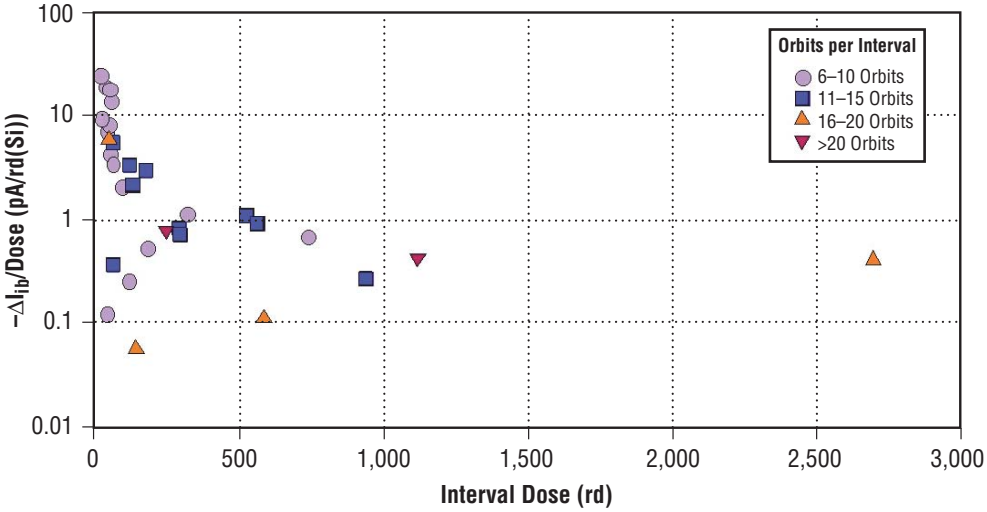

Figure 64. Change in I_{ib} with respect to dose for class S LM124 op amp versus average interval dose for relatively constant dose rate orbit intervals. The symbols used to show the data points represent the interval size as a range of orbits.

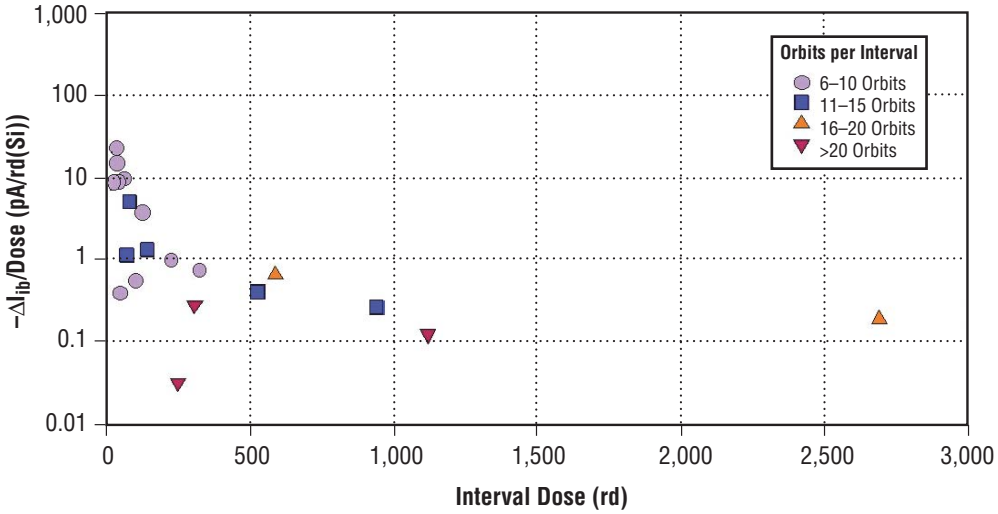

Figure 65. Change in I_{ib} with respect to dose for PM139 comparator versus average interval dose for relatively constant dose rate orbit intervals. The symbols used to show the data points represent the interval size as a range of orbits.

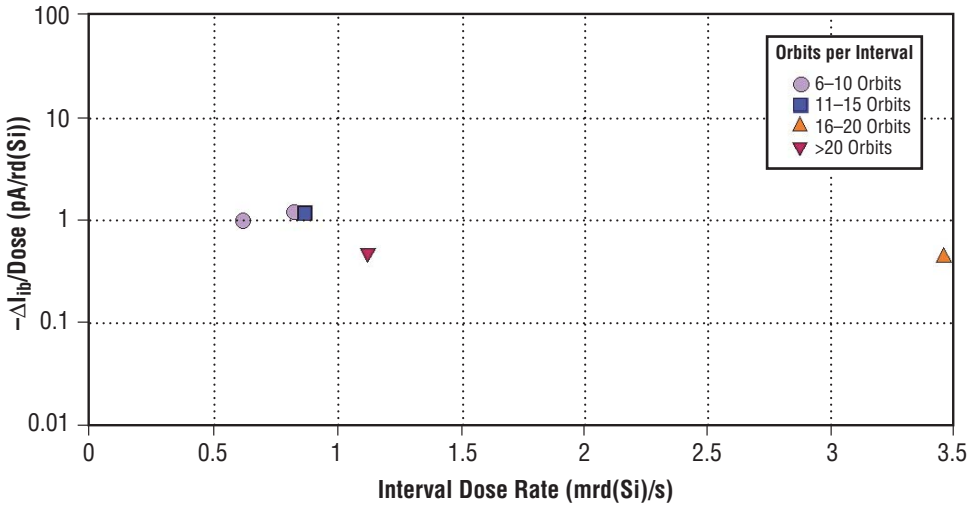

Figure 66. Change in I_{ib} with respect to dose for class S LM124 op amp versus average interval dose rate for relatively constant dose rate orbit intervals. The graph only used data from orbits where the ambient temperature was between 23 and 35 °C and the interval accumulated dose was >200 rd. The symbols used to show the data points represent the interval size as a range of orbits.

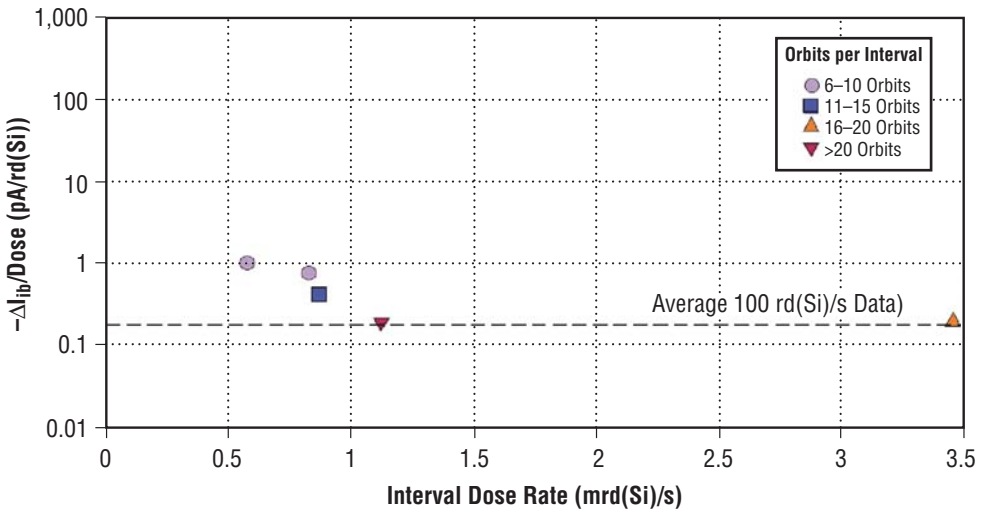

Figure 67. Change in I_{ib} with respect to dose for PM139 comparator versus average interval dose rate for relatively constant dose rate orbit intervals. The graph only used data from orbits where the ambient temperature was between 23 and 35 °C and the interval accumulated dose was >200 rd. The symbols used to show the data points represent the interval size as a range of orbits.

8. CONCLUSIONS

This study of the ELDRS data set from board A4 of the MPTB space experiment has proven to be significant, both as a compilation of the latest data and for the opportunity to revisit outstanding issues and attempt new analyses. Once significant PMOS dosimeter fade was observed in the space dosimetry data, the confidence in the comparison of space data with ground data was reduced, which interfered with published updates past the 1999 paper (app. B). Resolving the best dosimetry fit and understanding the impact of the space environment on this particular experiment proved to be a more significant task than initially thought, but has greatly increased confidence in the data. Perhaps the most important findings from this study of board A4 on the MPTB are the lessons learned, as might be applied to future ELDRS space experiments.

Both boards A4 and B1 were constructed and integrated into the MPTB experiment under the DTRA ELDRS program. Basic data downloading and the extensive analysis that resulted in the 1998 and 1999 papers (apps. A and B, respectively) were also funded by the DTRA program. The fact that the hardware, which was designed for a nominal 2-yr mission, continues to function well after 5 yr in space is a testament to the design of these boards and the MPTB experiment overall. This study, under the NASA Living With a Star program, has allowed confidence in the mission dosimetry to be restored through use of additional instruments on the MPTB, a compilation of the 5-yr data set, and new analyses which may aid in the design of improved ground test protocols for the ELDRS effect.

Significant conclusions include the following:

(1) By utilizing all available data, including that from The Aerospace Corporation's DSU unit and the QinetiQ CREDO instrument, as well as early data from the PMOS dosimeter (prior to fade), a best-fit dose curve was compiled. While the net changes were fairly small, removal of fade and uncertainty has resulted in high confidence in the comparison of space data to ground data.

(2) Prior to this study, it had been assumed by the experimenters that when solar activity was low, nearly all the dose was accumulated during the brief proton belt transits. This study has shown that there is significant dose accumulation from electrons in the outer belts as well. Furthermore, the amount of nonionizing energy loss from the protons has been shown to be low, with little displacement damage in the bipolar test circuits noted. Future ELDRS space experiments would be better suited for a more circular orbit with a more consistent dose rate during the orbit. It is quite significant that MPTB and ground data compare as well as they do, given the radiation environment of the MPTB. While this study does not attempt to explain why this occurred, it raises confidence in use of ground test to predict space behavior of enhanced low dose rate-sensitive parts.

(3) The impact of card temperature variations was not considered when this hardware was built. In ground test, the temperature of the test part is controlled to remove known temperature effects from the data. It was shown that both the test parts and the measurement circuits vary widely, from approximately 0 °C to nearly 45 °C. While this variation had minimal impact on the basic experiment, its impact over short

intervals was significant and limited the ability to analyze the data over short intervals. Future experiments should perform temperature evaluations of both the test devices and the measurement circuitry to allow for corrections that will result in better comparison with ground data.

(4) The lingering question on the impact of displacement damage on this data set has been settled. When the proton fluence was made equivalent to 1-MeV neutron damage, using NIEL and compared to ground data, it was clearly demonstrated that the great majority of the damage observed on board A4 was due to ionization, not displacement.

(5) Finally, there was limited success in analysis of the rate of damage during periods of relatively constant dose rate. The major problems encountered were the various interferences described in section 5, particularly board temperature and the even/odd orbit variance. In spite of these difficulties, a relatively constant rate of degradation was demonstrated over a range of dose rates from <0.5 mrd(Si)/s to > 8 mrd(Si)/s. These results raise the confidence that 10 mrd(Si)/s ground data is a good predictor of space degradation.

These results will assist future ELDRS space experiments, and impact development of ground test methodology for enhanced low dose rate-sensitive parts.

APPENDIX A—1998 PAPER ENTITLED "FIRST OBSERVATIONS OF ENHANCED LOW DOSE RATE SENSITIVITY (ELDRS) IN SPACE: ONE PART OF THE MPTB EXPERIMENT"

Appendix A is the paper presented at the 1998 NSREC and published in *IEEE Trans. Nucl. Sci*, December 1998.

First Observations of Enhanced Low Dose Rate Sensitivity (ELDRS) in Space: One Part of the MPTB Experiment [1]

J. L. Titus [2], *Member, IEEE*, W. E. Combs [2], T. L. Turflinger [2], *Member, IEEE*, J. F. Krieg [2], H. J. Tausch [3], *Member, IEEE*, D. B. Brown [4], *Senior Member, IEEE*, R.L. Pease [5], *Senior Member, IEEE*, and A. B. Campbell [4], *Senior Member, IEEE*

[2] Naval Surface Warfare Center, 300 Hwy 361, Crane, Indiana 47522
[3] Mission Research Corp., 1720 Randolph Rd. S. E., Albuquerque, New Mexico, 87106
[4] Naval Research Laboratory, Code 6610, Washington, DC 20375
[5] RLP Research, 1718 Quail Run Ct. N. E., Albuquerque, New Mexico, 87122

Abstract

Bipolar devices, most notably circuits fabricated with lateral PNP transistors (LPNP) and substrate PNP transistors (SPNP), have been observed to exhibit an enhanced low dose rate sensitivity when exposed to ionizing radiation. These dose rate sensitive bipolar devices exhibited enhanced degradation of base current in transistors and of input bias current, offset current, and/or offset voltage in linear circuits at dose rates less than 0.1 rd(Si)/s) compared to devices irradiated at dose rates greater than 1 rd(Si)/s). The total dose responses of several bipolar transistors and linear circuits in a space environment are demonstrated to exhibit enhanced degradation comparable, in magnitude, to ground-based data irradiated at a dose rate of 10 mrd(Si)/s indicating that enhanced low dose rate sensitivities (ELDRS) do indeed exist in space.

I. Introduction

Over the past several years, extensive total dose irradiations (hereafter, referred to as ground-based testing) of bipolar devices have demonstrated that many of these devices exhibited an enhanced low dose rate sensitivity (ELDRS) [1-9]. In sensitive bipolar transistors, ELDRS produced enhanced degradation of base current (resulting in enhanced gain degradation) at dose rates below 0.1 rd(Si)/s compared to similar transistors irradiated at dose rates above 1 rd(Si)/s. In 1994 [3-5], several bipolar linear integrated circuits were demonstrated to exhibit enhanced degradation of input bias current (I_{IB}), offset current (I_{OS}), and/or offset voltage (V_{OS}) when irradiated at dose rates below 0.1 rd(Si)/s compared to similar circuits irradiated at dose rates above 1 rd(Si)/s.

Until now, ELDRS research has been limited to ground-based testing. The applicability of ground-based observations to space environments has been questioned because of the complex nature of these environments and the lack of known system failures attributed to ELDRS. Now, space-based measurements are being taken allowing a comparison to ground-based data.

To that end, an experiment was designed to characterize the total dose response of several bipolar devices in space. Three types of bipolar transistors (RF25) and three types of bipolar linear integrated circuits (LM124A, LM139J, and PM139Y) were selected as test vehicles. Two test boards were designed and built to allow parametric measurements on devices while being flown in a highly elliptical orbit in space as part of the Microelectronics and Photonics Test Bed (MPTB) satellite experiment which was launched in November of 1997.

This paper provides details about the test devices, the in-flight experiment, flight-based observations, and ground-based observations. Flight data are presented for the first seven months of the mission. These data are compared to ground-based data taken on devices from the same date code lots. Comparisons of the flight data to ground-based data irradiated at a dose rate of 10 mrd(Si)/s clearly demonstrate that ELDRS effects do indeed occur in space and produce enhanced degradation.

[1] Work sponsored, in part, by the Defense Special Weapons Agency.

II. Experimental Details

A. Orbital Information

The satellite carrying the MPTB payload was launched in November, 1997 and placed in a highly elliptical orbit with an orbital period of approximately 12 hours. Most of the accumulated dose per orbit occurs when the spacecraft traverses the proton and electron belts. These belt traversals last approximately 70 minutes per orbit or about 10% of the time.

The MPTB experiment uses silicon MOS dosimeters, Harris/RCA 4007s, that are read once every orbit for dosimetry. The average accumulated dose produces a linear change in the gate-to-source voltage (V_{GS}) at a rate of 90 mV/krd(Si) when measured at a constant drain-to-source current (I_{DS}) of 24 μA. Measurements are temperature and bias compensated. The calibration of the dosimeters is within ±5%. The dosimeters have a fade rate of approximately 10% per year. The test boards are mounted behind an equivalent of 55 mils of aluminum. A more detailed description of the MPTB dosimetry system will be published by others at a future date.

Using dosimetry data, the average measured dose between orbits 0 and 363 was approximately 4.8 rd(Si) per 12-hour orbit. In April, 1998, significant solar flare activity increased the average measured dose for orbits above 363 to approximately 48 rd(Si) per 12-hour orbit. A dosimetry plot (average accumulated dose as a function of orbit) from one of the MPTB experiments is shown in Figure 1 (reported up to orbit number 410).

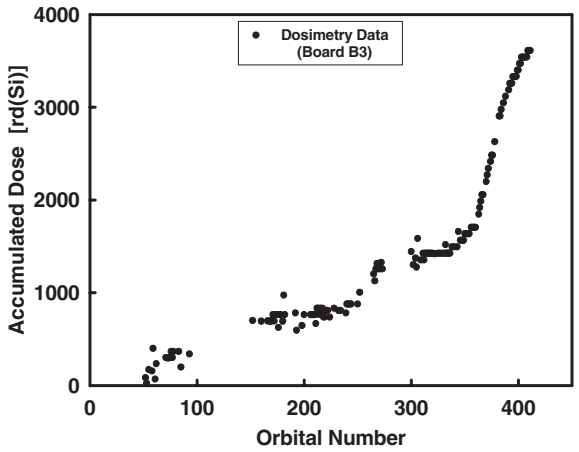

Figure 1: Average accumulated dose from Board B3 dosimeter.

B. RF25 Transistor Board Description

One of the two test boards was designed to characterize the bipolar transistors. A digital-to-analog output on the motherboard provides the base-to-emitter voltage (V_{BE}). On-board resistors allow direct measurements of the base (I_B) and collector (I_C) current which are then processed by the motherboard for subsequent downloading. V_{BE} is swept from 0.1 to 0.9 volts in 0.02-volt increments. I_B and I_C are measured at each voltage increment. This board is designated as B1 on the MPTB experiment. Figure 2 shows a photograph of board B1, which clearly highlights the spatial location of the six RF-25 transistor packages mounted along the edge of board B1.

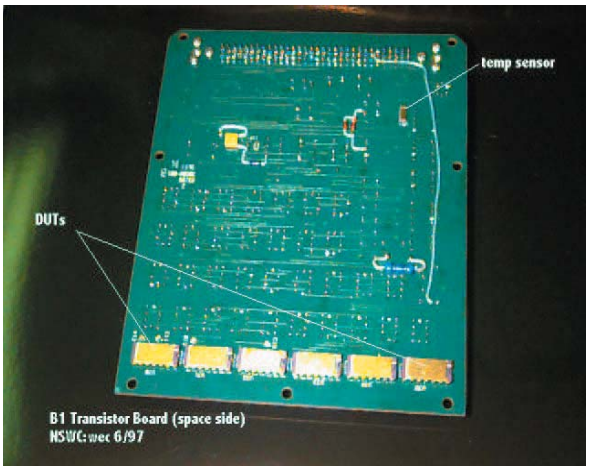

Figure 2: Photograph of the transistor flight board (back side).

C. RF25 Process/Transistor Description

The RF25 process is manufactured by Analog Devices and was developed for low noise amplifiers, power amplifiers, mixers, and RF switches which are used in many communication applications [10]. Test die from wafer fab lot #350569.1 contain a large lateral PNP (LPNP), a small LPNP, a substrate PNP (SPNP), and a vertical NPN. Die were mounted in a 14-pin dual-in-line ceramic package and date coded, DC94. The small LPNP and SPNP use a square geometry with an emitter area of 1.2 μm x 1.2 μm. The large LPNP uses a square geometry with five parallel emitter areas of 1.2 μm x 1.2 μm each.

D. RF25 Transistor Biasing Description

Figure 3 shows the insitu bias configuration for the RF25 transistor package during flight. The substrate is always at ground. The emitters of the PNP transistors have an insitu bias of 2.5 volts while the base and collector are floating. The collector of the NPN transistor has an insitu bias of 2.5 volts while the base and emitter are floating. The bias conditions were determined, in part, by constraints imposed by test board and satellite system such as size and power requirements.

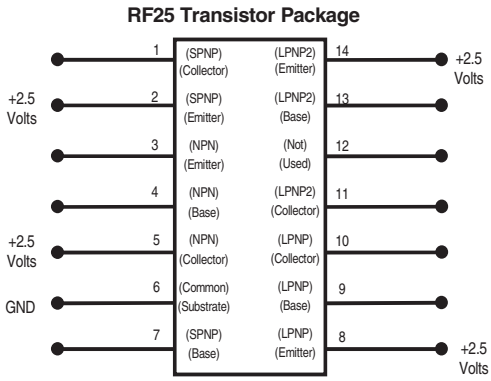

Figure 3: Representative bias configuration for the RF25 package.

E. Linear Integrated Circuit Board Description

The other test board was designed to characterize the linear integrated circuits, specifically the LM124A, LM139J, and PM139Y. The on-board op-amp and comparator circuitry allowed measurements of three parameters which are then processed by the motherboard for subsequent downloading. These three measurements are used to determine V_{OS}, I_{OS}, and I_{IB}. This board is designated as A4 on the MPTB experiment. Figure 4 shows a photograph of board A4, which clearly highlights the spatial location of the eight linear integrated circuit packages consisting of four op-amp packages and four comparator packages mounted along both sides of the board.

F. Linear Integrated Circuit Description

The four LM124A op-amps are manufactured by National Semiconductor. Two packages have a date code of 9524. The other two packages have a date code of 9520 and are class-S type devices. Each LM124A package consists of four independent op-amp circuits. I_{IB} is temperature compensated in these devices.

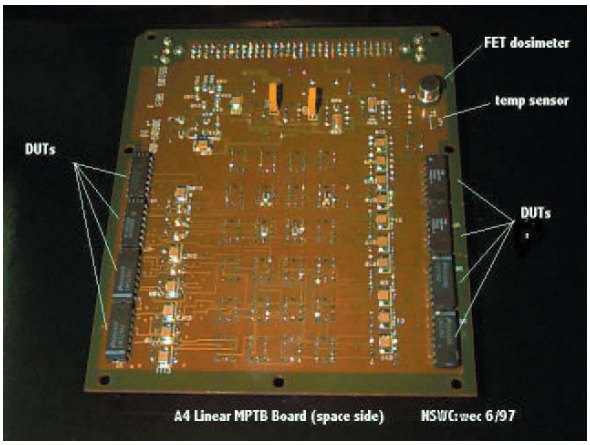

Figure 4: Photograph of the linear flight board (back side).

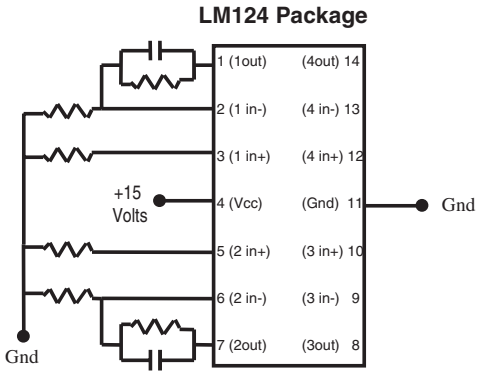

Figure 5: Representative bias configuration for the LM124 package.

The two LM139 comparators are also manufactured by National Semiconductor and have a date code of 9530. The two PM139 comparators are manufactured by PMI and have a date code of 9522. Each LM139 and PM139 package consist of four independent comparators. The input structures of the National LM124 and LM139 are fabricated using a SPNP and LPNP hybrid structure.

G. Linear Integrated Circuit Biasing Description

Figure 5 is a representative insitu bias configuration for the LM124 (voltage follower with gain of 1) and Figure 6 is a representative insitu bias configuration for the LM139s and PM139s (basic comparator with inputs at ground potential). These configurations were selected because of certain test system constraints and to define the input bias state. The inputs were identified as containing the sensitive structures to be controlled during the experiment.

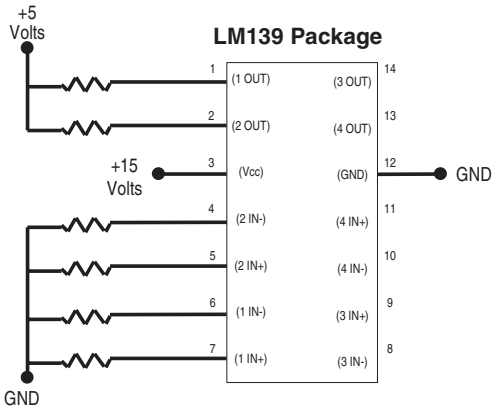

Figure 6: Representative bias configuration for LM139 and PM139.

III. Flight- and Ground-based Comparison

Orbital flight data were converted to average accumulated dose using a conversion factor of 4.8 rd(Si) per orbit for orbits up to 364. For orbits between 364 to 410, the orbital flight data were converted using a conversion factor of 48 rd(Si) per orbit which corresponds to the solar flare activity that occurred in April, 1998 (see Figure 1).

The transistor flight data are only qualitatively compared to existing ground-based data [11] because insitu bias conditions are different. Previous experiments on RF25 transistors using different bias conditions have indicated no appreciable differences [8]. At this time, these data provide quantitative measurements of temperatures during flight adding valuable insight into the insitu conditions of the transistors and linear circuits as well as lending support to the linear circuit data.

Ground-based data were taken on the linear circuits (same date code) and irradiated with a Co60 source using dose rates of 100, 1, and 0.01 rd(Si)/s. The linear circuits used insitu bias configurations similar to the flight boards. These data clearly demonstrate enhanced degradation during flight.

A. RF25 Transistor Response

A representative set of the transistor flight data is provided in Appendix B, Figures B1 - B6 showing I_B and I_C curves of the small LPNP, large LPNP, and SPNP for transistor package designated U30. Ionization induces shifts in I_B, but does not induce shifts in I_C. Temperature induces shifts in both the I_B and I_C characteristic. Shifts in I_C as shown in Figures B2, B4, and B6 imply that the transistor temperature is varying from orbit to orbit. Since I_B is a strong function of temperature, the flight data have to be corrected for orbital temperature variations, before analyzing any potential ionization effects.

One method to remove temperature variations in the flight data is to apply parameter extraction techniques using the I_C characteristic of each orbit. First, the saturation current (I_S) is extrapolated using the ideal portion of the I_C curve. The extrapolated values of I_S are then used to determine the transistor temperature for that orbit using Equation (1), where E_G is the energy gap in eV, T_1 is the baseline temperature in Kelvin, T_2 is the extracted temperature in Kelvin, and $V_T(T)$ is the thermal voltage at T_1 or T_2 in volts. The transistor temperature of the

large LPNP was found to vary from approximately 298 to 340 K, which corresponds to recorded temperature variations of other flight boards on MPTB.

$$I_S(T_2) = I_S(T_1) e^{\frac{E_G}{V_T(T_1)} - \frac{E_G}{V_T(T_2)} \cdot 1.11 Ln\left(\frac{T_2}{T_1}\right)} \quad (1)$$

Once the transistor temperature is determined, an ideal I_C and I_B characteristic can be calculated using Equations (2), where q is elementary charge, k is Boltzmann constant, T is temperature, and H_{FE} is pre-radiation gain. Normalizing the flight data using the ideal base characteristic of a given orbit, the temperature variation is removed. Any subsequent changes in the normalized data are attributed to ionization.

$$I_C(T) = I_S(T) e^{\frac{qV_{BE}}{kT}} \quad ; \quad I_B(T) = \frac{I_C(T)}{H_{FE}} \quad (2)$$

Another method to remove temperature variations from the flight data is to interpolate I_B at a fixed I_C current. Before applying this technique, the I_B and I_C curves of each orbit are smoothed using a regressive fitting program. Curve smoothing is performed to remove certain aberrations (nonlinearities, self-heating, etc.) and discontinuities (autoranging) caused by the test circuitry and test methodology. By interpolating I_B at a fixed I_C, temperature variations are removed and the total dose response of the transistor can be determined. Both methods were used to remove temperature variations in the large PNP and were found to be in good agreement. The initial SPNP response (pre-flight) exhibited excessive collector current leakage and a qualitative comparison to ground-based data is not performed.

Figure 7 shows a representative plot of normalized base currents at three values of base-to-emitter voltages (V_{BE}) of the large LPNP transistor for package U30 based on the parameter extraction technique. The base current is observed to increase approximately 75% after accumulating approximately 1.7 krd(Si) of dose. A similar degradation was noted on the small LPNP. These data indicate that the LPNP transistors appear to be exhibiting enhanced degradation when qualitatively compared to existing ground-based data [11]. Additional ground-based experiments using transistors under similar bias conditions are needed to verify this observation before any quantitative comparisons can be made. However, the transistor data provide quantitative measurements of actual device temperatures for each orbit providing valuable information about the insitu conditions of the transistors and linear circuits during flight.

B. Linear Integrated Circuit Response

A representative set of orbital flight data for the linear circuits is provided in Appendix A, Figures A1 - A6. These figures demonstrate that I_{OS} and V_{OS} are not exhibiting any notable changes through orbit number 410. Figures A1 and A4 show that the LM124 and LM139 are both exhibiting an increase in I_{IB}, which was expected to be the sensitive parameter. All the measured parameters are within maximum operating limits.

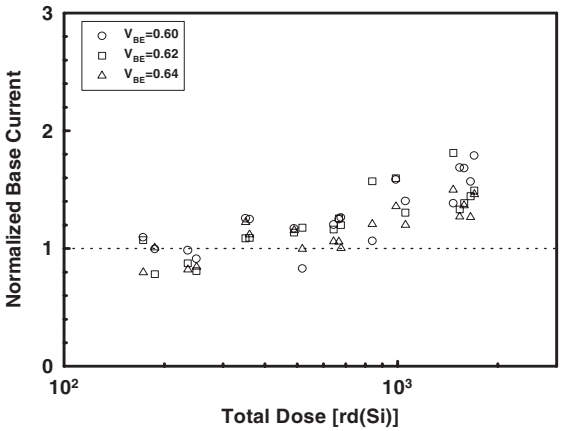

Figure 7: Normalized base current of large LPNP to total dose.

Figures 8, 9, and 10 show LM124, LM139, and PM139 flight data for a seven month period superimposed upon ground-based data on similar devices (same date code) using similar insitu bias conditions. Certainly, insitu flight conditions are more complex than the ground-based conditions due to power interruptions, temperature variations, dose rate variations (belt traversal, flare activity, etc.), and other variables associated with actual satellite operation. Figures 8 and 9 show enhanced degradation in I_{IB} of the LM124 and LM139 flight data when compared to the 100 rd(Si)/s and 1 rd(Si)/s ground data. The degradation in I_{IB} of the LM124 flight data is bounded by ground data taken at 10 mrd(Si)/s, and the degradation in I_{IB} of the LM139 flight data is in good agreement with the 10 mrd(Si)/s ground data. Upon closer examination, the solar flare event (April 1998) appears to have decreased the rate of degradation in I_{IB} of the LM139 as can be readily seen in Figure 11. This is consistent with enhanced low dose rate effects not yet in saturation.

Bipolar linear circuits are known to be susceptible to displacement damage from both protons and electrons [12]. Since the ratio of ionizing energy loss to non-ionizing energy loss (NIEL) is orders of magnitude higher for electrons than for protons in the earth radiation belts, we may assume that only the protons are of concern for displacement damage. To determine the relative displacement damage of the MPTB bipolar circuits, neutron irradiations were conducted using White Sands Missile Range Fast-Burst Reactor to 1 MeV equivalent fluences of 5, 15, and 25 x 10^{11} n/cm^2. Five samples of each device type using samples with the same date code were exposed and degradation in I_{IB} recorded. The degradation in I_{IB} was linear with neutron fluence, as expected. The measured rates of degradation were 2 nA per 10^{10} n/cm^2 for the LM139s and 1 nA per 10^{10} n/cm^2 for the LM124s and PM139s. Since the displacement damage rate of the PM139s is comparable to the other device types, that response can be used as a measure of the displacement damage at a dose of 4.1 krd(Si) acquired through orbit 410 of the MPTB experiment. Figure 10 shows that I_{IB} of the PM139s is not degrading. Therefore, it is reasonable to assume that degradation in I_{IB} of the LM124s and LM139s are a direct result of ionization and not displacement damage.

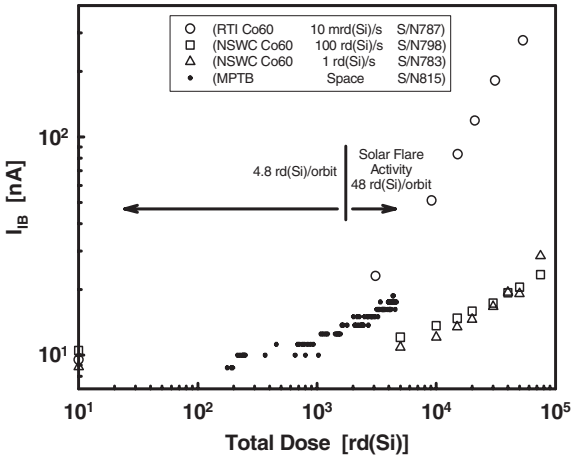

Figure 8: Comparison of flight and ground-based data of LM124.

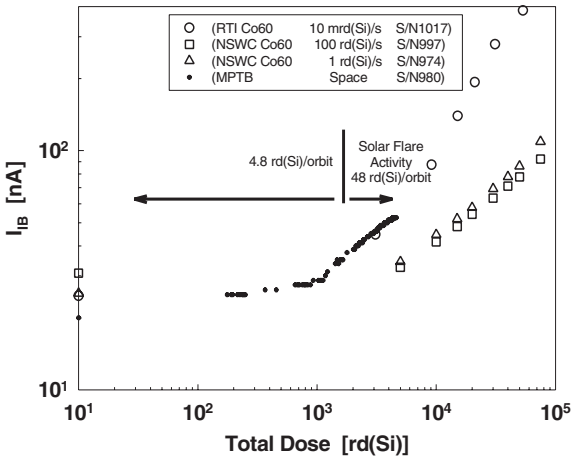

Figure 9: Comparison of flight and ground-based data of LM139.

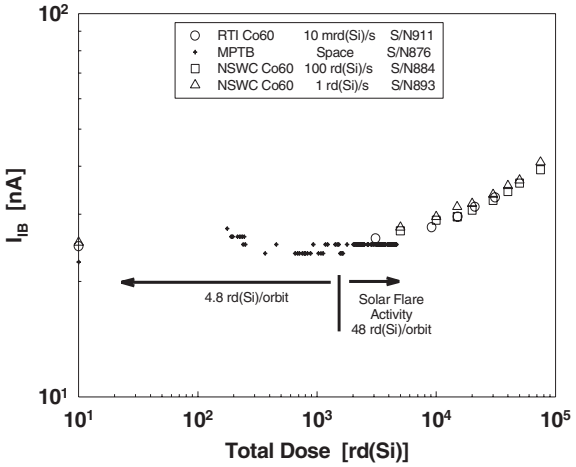

Figure 10: Comparison of flight and ground-based data of PM139.

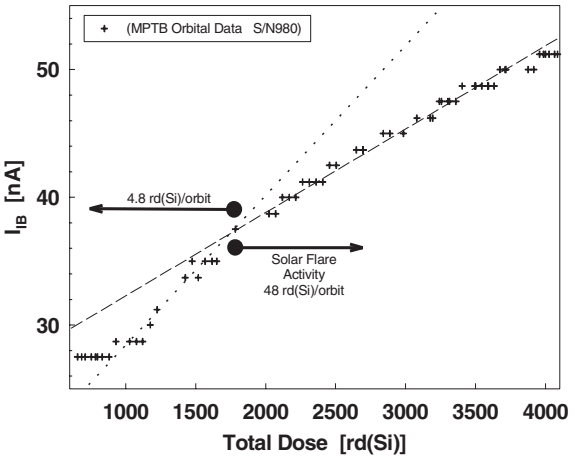

Figure 11: Expanded data set from Figure 8 showing flare event.

IV. Discussions and Implications

The flight-based data appear to be responding to the space environment comparable to ground-based testing at dose rates below 0.1 rd(Si)/s. The transistor data demonstrate that the devices are varying in temperature from 298 to 340 K. Ground-based observations have indicated that elevated temperatures may actually enhance the ELDRS effect. However, the rates of degradation in the observed I_{IB} (See Figure 8 and 9) of the LM124s and LM139s are comparable to the ground-based observations at 10 mrd(Si)/s and definitely worse than the observations at 1 or 100 rd(Si)/s. The LM139 response during the solar flare event in April implies that the dose rate sensitivity of these devices are not in saturation. The PM139 response (see Figure 10) strongly suggests that the degradation in I_{IB} of the LM124s and LM139s are induced by ionization and not displacement damage based on degradation induced by neutrons.

These results demonstrate that these bipolar devices are responding to a complex time-variant space environment in a manner comparable to ground-based testing at dose rates on the order of 10 mrd(Si)/s. The data show that an enhanced low dose rate sensitivity is observed when operated in a space environment comprised mainly of protons and electrons where the instantaneous dose rate varies by orders of magnitude (<<1 mrd(Si)/s to 50 mrd(Si)/s). It has been suggested that either the radiation source (protons and electrons rather than photons) or the time-varying nature of a space environment may induce a significantly different response. These data demonstrate otherwise.

System performance could be significantly impacted if an ELDRS prone device were selected for a space mission. Such a selection could result in premature system failure if insufficient design margins are incorporated. Therefore, selections of space-based devices require adequate test methods to be used to identify dose rate sensitive devices (qualification testing). Test method 1019 does not address bipolar linear circuits with ELDRS, since that portion which applies to space radiation only

covers CMOS circuits. However, a new unreleased revision of ASTM-F867 (renumbered F1892 - Guide for Ionizing Radiation Effects Testing of Semiconductor Devices) has included an entire Appendix devoted to ELDRS in bipolar linear circuits. In addition, development of hardness assurance test methods for ELDRS continues [13,14].

The MPTB mission is on-going and parametric data will continue to be accumulated providing even better insights into the total dose response of bipolar devices operating in a space environment.

V. CONCLUSIONS

For the first time, an experiment is being conducted in an actual space environment to investigate the effects of ELDRS on selected bipolar device (RF25 transistors, LM124s, LM139s, and PM139s). The results from the first seven months demonstrate that bipolar devices (transistors and linear integrated circuits) flown in a highly elliptical orbit in space exhibit enhanced parametric degradation which is comparable to ground-based data taken at a dose rate of 10 mrd(Si)/s. These data clearly demonstrate that an enhanced low dose rate effect (ELDRS effect) exists in a space environment and is comparable to the ground-based observations for each part type. Finally, flight data are responding to the space environment as predicted by ground-based data.

ACKNOWLEDGMENTS

The authors would like to recognize and acknowledge the efforts of all those researchers, manufacturers, and sponsors who have contributed to this project. We are particularly grateful to Lew Cohn (DSWA) for his continuing technical and funding support; to Jim Ritter, Jeff Cleveland, Ralph Freitag, Sharon Mozersky, and others at NRL who have technically supported this work; to Denny Adamson, Hugh Barnaby, and others at MRC who assisted in the design, layout, and programming of the flight boards; and to Mike Keeton and others at Orbital Sciences who helped to fabricate the flight boards.

REFERENCES

[1] R. N. Nowlin, E. N. Enlow, R. D. Schrimpf, and W. E. Combs, " Trends in the Total-Dose Response of Modern Bipolar Transistors," *IEEE Trans. Nucl. Sci.*, NS-39, No. 6, pp. 2026-2032, Dec. 1992.

[2] S. McClure, R. L. Pease, E. Will, and G. Perry, "Dependence of Total Dose Response of Bipolar Linear Microcircuits on Applied Dose Rate," *IEEE Trans. Nucl. Sci.*, NS-41, No. 6, pp. 2544-2549, Dec. 1994.

[3] J. T. Beaucour, T. Carriere, A. Gach, D. Laxague and P. Poirot, "Total Dose Effects on Negative Voltage Regulator," *IEEE Trans. Nucl. Sci.*, NS-41, No. 6, pp. 2420-2426, Dec. 1994.

[4] A. H. Johnston, G. M. Swift, and B.G. Rax, "Total Dose Effects in Conventional Bipolar Transistors and Linear Integrated Circuits," *IEEE Trans. Nucl. Sci.*, NS-42, No. 6, pp. 1650-1656, Dec. 1995.

[5] D. M. Fleetwood, L. C. Riewe, J. R. Schwank, S. C. Witczak, and R. D. Schrimpf, "Radiation Effects at Low Electric Fields in Thermal, SIMOX, and Bipolar Base Oxides," *IEEE Trans. Nucl. Sci.*, NS-43, No. 6, pp 2537-2543, Dec 1996.

[6] R. L. Pease, L. M. Cohn, D. M. Fleetwood, M. A. Gehlhausen, T. L. Turflinger, D. B. Brown, and A. H. Johnston, "A Proposed Hardness Assurance Test Methodology for Bipolar Linear Circuits and Devices in a Space Ionizing Radiation Environment," *IEEE Trans. Nucl. Sci.*, NS-44, No. 6, pp. 1981-1987, Dec. 1997.

[7] X. Montagner, R. Briand, P. Fouillat, R. D. Schrimpf, A. Touboul, K.F. Galloway, M.C. Calvet, and P. Calvel, "Dose-Rate and Irradiation Temperature Dependence of BJT SPICE Model Rad-Parameters," *IEEE Trans. Nucl. Sci.*, NS-45, No. 3, pp. 1431-1437, Jun 1998.

[8] D. M. Schmidt, D. M. Fleetwood, R. D. Schrimpf, R. L. Pease, R. J. Graves, G. H. Johnson, K. F. Galloway, and W. E. Combs, "Comparison of Ionizing-Radiation-Induced Gain Degradation in Lateral, Substrate, and Vertical PNP BJTs," *IEEE Trans. Nucl. Sci.*, NS- 42, No. 6, pp. 1541-1549, Dec 1995.

[9] A. H. Johnson, B. G. Rax, and C. I. Lee, "Enhanced Damage in Linear Bipolar ICs at Low Dose Rates," *IEEE Trans. Nucl. Sci.*, NS-42, No. 6, pp. 1650-1659, Dec 1995.

[10] K. O, P. Garone, C. Tsai, B. Scharf, M. Higgins, D. Mai, C. Kermarrec, and J. Yasaitis, "A Double-Polysilicon Self-Aligned NPN Bipolar Process (ADRF) with Optional NMOS Transistors for RF and Microwave Applications," *IEEE BCTM Proc.*, pp. 221-224, 1994.

[11] S. C. Witczak, R. D. Schrimpf, K. F. Galloway, D. M. Fleetwood, R. L.Pease, J. M. Puhl, D. M. Schmidt, W. E. Combs, and J. S. Suehle, "Accelerated Tests for Simulating Low Dose Rate Gain Degradation of Lateral and Substrate PNP Bipolar Juntion Transistors," *IEEE Trans. Nucl. Sci.*, NS-43, No. 6, pp. 3151-3160, Dec 1996.

[12] A. H. Johnston and R. E. Plaag, "Models for Total Dose Degradation in Linear Integrated Circuits," *IEEE Trans. Nucl. Sci.*, NS-34, pp. 1474-1480, Dec. 1987.

[13] R. K. Freitag and D. B. Brown, "Study of Low-Dose-Rate Radiation Effects on a Commercial Linear Bipolar IC," *IEEE Trans. Nucl. Sci.*, NS-45, No. 6, Dec. 1998.

[14] R. L. Pease, M. Gehlhausen, J. F. Krieg, J. L. Titus, T. Turflinger, D. Emily, and L. Cohn, "Evaluation of Proposed Hardness Assurance Method for Bipolar Linear Circuits with Enhanced Low Dose Rate Sensitivity (ELDRS)," *IEEE Trans. Nucl. Sci.*, NS-45, No. 6, Dec. 1998.

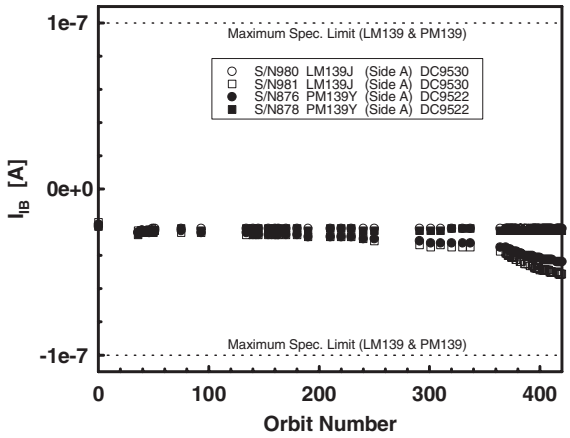

Figure A1: Total dose response (I_{IB}) of the LM139 and PM139.

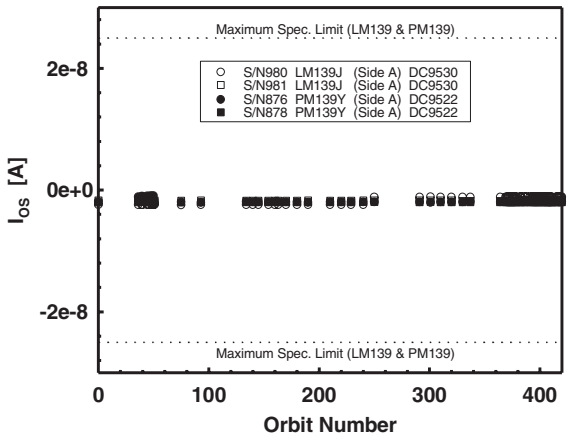

Figure A2: Total dose response (I_{OS}) of the LM139 and PM139

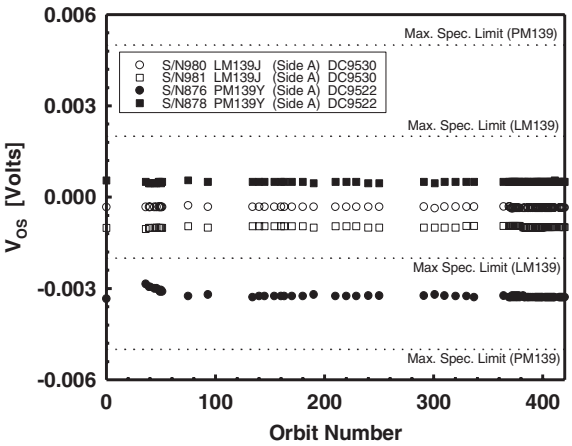

Figure A3. Total dose response (V_{OS}) of the LM139 and PM139

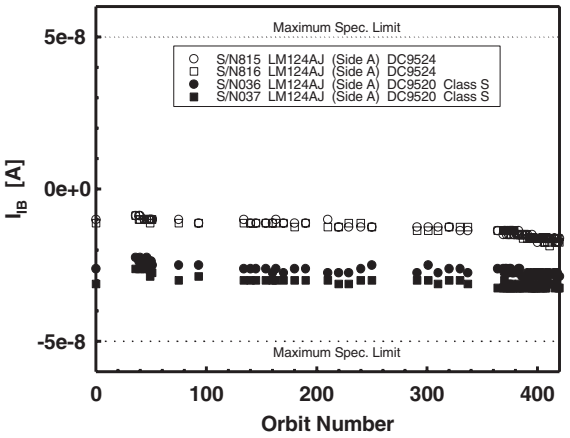

Figure A4: Total dose response (I_{IB}) of the LM124s

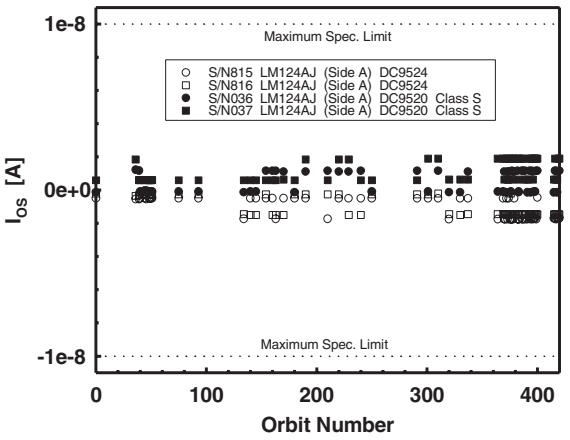

Figure A5: Total dose response (I_{OS}) of the LM124s

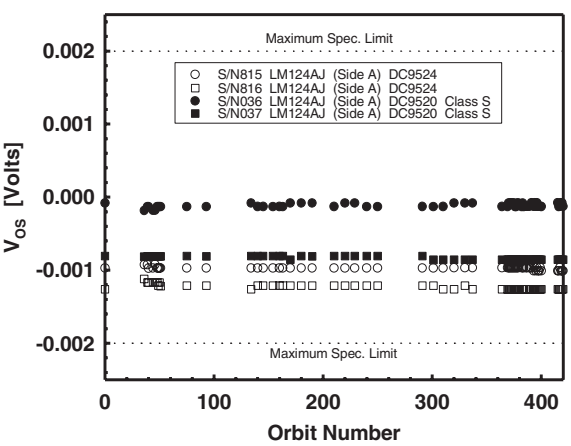

Figure A6: Total dose response (V_{OS}) of the LM124s

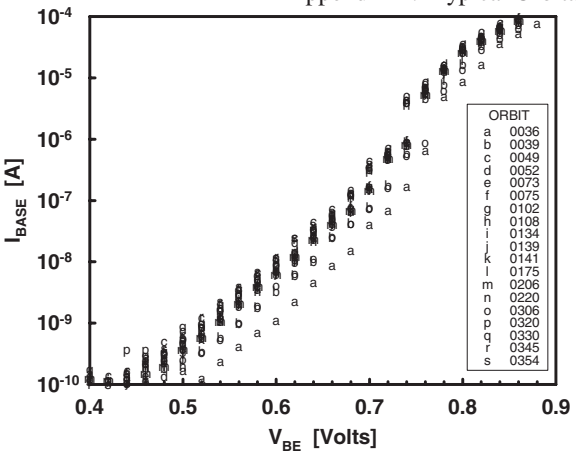

Figure B1: Orbital response (I_B) of small LPNP (U30).

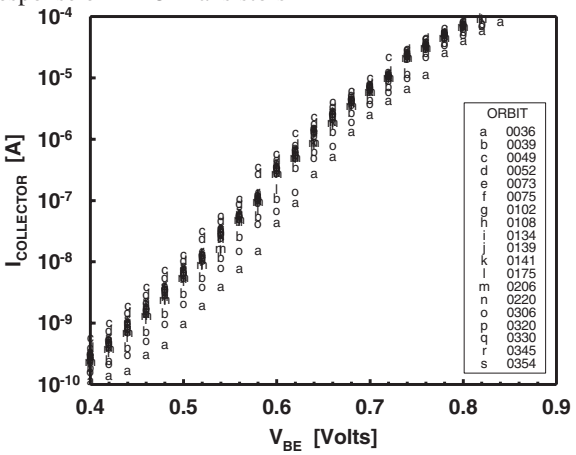

Figure B2: Orbital response (I_C) of small LPNP (U30).

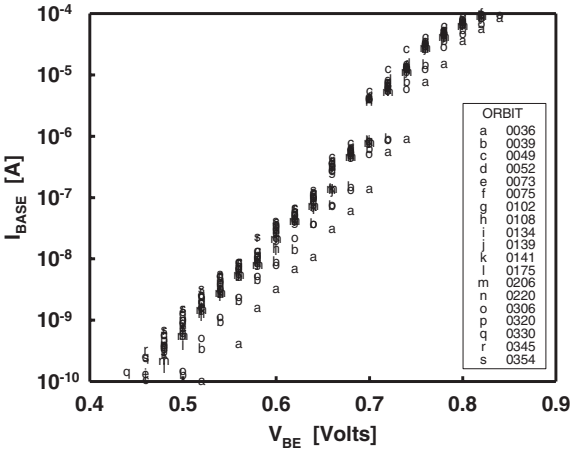

Figure B3: Orbital response (I_B) of large LPNP (U30).

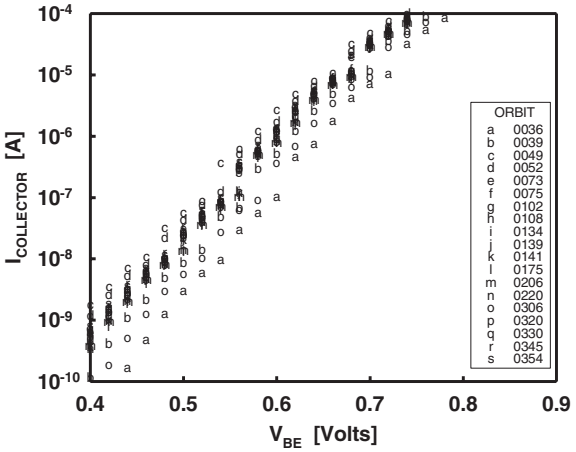

Figure B4: Orbital response (I_C) of large LPNP (U30).

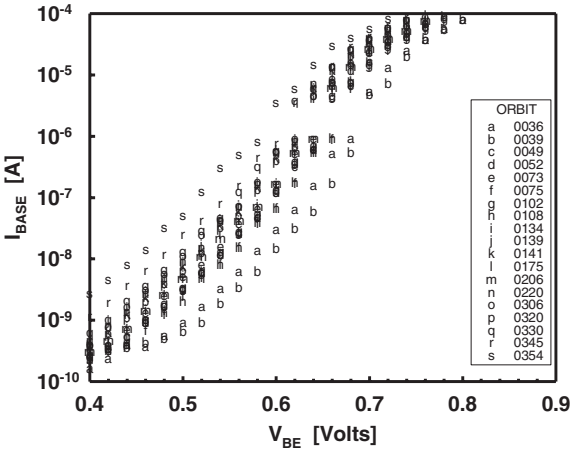

Figure B5: Orbital response (I_B) of SPNP (U30).

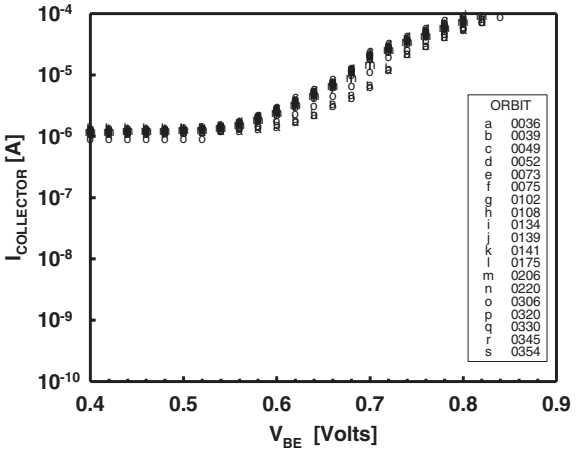

Figure B6: Orbital response (I_C) of SPNP (U30).

APPENDIX B—1999 PAPER ENTITLED "ENHANCED LOW DOSE RATE SENSITIVITY (ELDRS) OF LINEAR CIRCUITS IN A SPACE ENVIRONMENT"

Appendix B is the paper presented at the 1999 NSREC and published in *IEEE Trans. Nucl. Sci.*, December 1999.

Enhanced Low Dose Rate Sensitivity (ELDRS) of Linear Circuits in a Space Environment [1]

J. L. Titus [2], *Associate Member, IEEE*; D. Emily [2], *Member, IEEE*; J. F. Krieg [2];
T. Turflinger [2], *Member, IEEE*; R. L. Pease [3], *Senior Member, IEEE*; and
A. Campbell [4], *Senior Member, IEEE*

[2] Naval Surface Warfare Center, 300 Hwy 361, Crane, Indiana 47522
[3] RLP Research, 1718 Quail Run Court NE, Albuquerque, NM 87122
[4] Naval Research Laboratory, Code 6610, Washington, DC 20375

Abstract

To investigate the ELDRS effect in a real space environment, an experiment was designed, launched, and placed in a highly elliptical orbit in November 1997. After its deployment, the electrical responses of several bipolar transistors and linear circuits have been and continue to be recorded once during every 12-hour orbit. System dosimeters are monitored to establish an average accumulated dose per orbit. With this information, the electrical parameter data are correlated with the dosimetry data to determine the total dose response of each device. This paper updates information on the ELDRS experiment through May 14, 1999. As of this date, the experiment has been in flight for a period of 18 months and has accumulated an approximate dose of 18 krd(Si). For comparison, devices, specifically linear circuits with the same date code, were irradiated using Co-60 sources, herein defined as ground-based tests. The ground-based tests are used to evaluate two hardness assurance tests, a room temperature irradiation at 10 mrd(Si)/s and an elevated temperature irradiation at 100°C and 10 rd(Si)/s and to evaluate the ELDRS response. To that end, irradiations were performed at room temperature, approximately 22°C, at fixed dose rates of 100, 1, and 0.01 rd(Si)/s and at elevated temperature, approximately 100°C, at a fixed dose rate of 10 rd(Si)/s. Currently, irradiations are being performed at room temperature at a fixed dose rate of 0.001 rd(Si)/s. Comparing the ground-based data to the flight data clearly demonstrates that enhanced parametric degradation has occurred in the flight parts. The two hardness assurance screens predicted ELDRS but the design margin for the elevated temperature test may not be adequate.

I. Introduction

In commercial or military space systems, electronic components are subjected to radiation stresses that include cosmic rays, protons, electrons, and other particles. However, most of the dose is deposited from the interaction with protons and electrons trapped in the inner and outer belts. A complete description of the actual environment would require extensive knowledge of each particle type as well as its energy, direction, and position at any given moment in time. To complicate matters, space particles can be influenced by many factors including spacecraft and packaging shielding. Further complications can arise because the particle spectra can change due to random events such as solar activity and magnetic storms. As a whole, space environments are extremely complex when compared to typical ground-based Co-60 experiment which are performed under controlled laboratory conditions at fixed dose rates. Therefore, the total dose response of devices which exhibit ELDRS, when placed in a space environment, was uncertain due to those and other uncontrolled conditions that exists in space.

Over the past several years, extensive ground-based Co-60 irradiations have demonstrated that many bipolar devices, most notably lateral PNP transistors, exhibit ELDRS [1-4]. In dose-rate sensitive bipolar transistors, enhanced gain degradation due to increased base current at a given dose occurs when exposed to lower dose rates (e.g., dose rates below 100 mrd(Si)/s) relative to traditional dose rates (e.g. dose rates between 50-300 rd(Si)/s as specified by Test Method 1019). In 1994, several bipolar linear integrated circuits were observed to exhibit an enhanced degradation of certain electrical parameters when subjected to ionizing dose rates below 1 rd(Si)/s when compared to similar devices subjected to higher dose rates between 50 and 100 rd(Si)/s [2-4]. This enhanced degradation was observed as a significant increase in the input bias current (I_{IB}), input offset voltage (V_{OS}), and input offset current (I_{OS}).

The experiment described herein is the first verification/demonstration of ELDRS in space, as all previous experiments were ground-based experiments where the environmental conditions are controlled. Last year, we reported upon the total dose responses of these linear circuits in the same experiment after six months of flight and an accumulated dose of 4 krd(Si) [5]. The linear circuits consist of operational amplifier (op-amps) and comparator type circuits. The LM124s are op-amps manufactured by National Semiconductor, the LM139s are comparators manufactured by National Semiconductor, and the PM139s are comparators manufactured by Analog Devices. The flight board was designed and built to allow limited in-flight characterization of the linear circuits. This ELDRS study is a small part of a larger project known as the Microelectronics and Photonics Test Bed (MPTB) which was launched in November 1997.

This paper updates the linear circuit results reported upon last year (see reference 5). The total dose responses of these same devices are updated from a 6-month period to an 18-month

[1] Material presented at 1999 IEEE NSREC. Work sponsored, in part, by Defense Threat Reduction Agency (DTRA).

period and from an accumulated dose of 4 krd(Si) to an accumulated dose of 18 krd(Si). During this eighteen-month period, several solar events have occurred producing significant increases in the accumulated dose over short periods of time (e.g., a few days to a few weeks). In addition to the flight data, irradiations of linear circuits with the same date code have been performed using ground-based Co-60 sources. Ground-based irradiations were performed at room temperature, approximately 22°C, with fixed dose rates of 100, 1, and 0.01 rd(Si)/s and at elevated temperature, approximately 100°C, with a fixed dose rate of 10 rd(Si)/s. The 10 mrd(Si)/s, room temperature test and the 10 rd(Si)/s, elevated temperature test are two hardness assurance screens for ELDRS [6,7]. In addition to these tests, ground-based irradiations at room temperature are in progress with a fixed dose rate of 0.001 rd(Si)/s. Ground-based irradiations using even lower dose rates may be necessary to identify the worse-case ELDRS response. However, lower dose rates require longer exposure times (e.g., months to years) to evaluate the total dose response making it undesirable. Assuming that the ELDRS effect saturates at low dose rates (see Figures 1 and 2 of reference 8), the 0.01 and 0.001 rd(Si)/s tests should provide an upper boundary for the flight and other ground-based data.

II. Orbital Description

The satellite carrying the MPTB payload was launched in November 1997 and placed in an elliptical orbit with an orbital period of approximately 12 hours. Data have now been collected and analyzed for the first 1,108 orbits which corresponds to approximately 18 months of flight.

Since ground-based experiments are readily quantified by a fixed dose rate, it would be useful to quantify a fixed dose rate for the space-based experiment. However, assignment of a fixed dose rate is unrealistic because of the highly elliptical orbit. The instantaneous dose rate varies significantly within an orbit as the satellite traverses the proton and electron belts in its path. Orbit-to-orbit variations occur from random solar events and magnetic storms. During quiet periods (periods of little or no solar and/or magnetic storm activity), a typical 12-hour orbit accumulates a dose of 4.5 rd(Si). The majority of this dose is deposited during several smaller periods of time having a total duration of about 70 minutes. The smaller periods of time correspond to those times when the spacecraft traverses the proton and electron belts in its orbital path. During solar events and/or magnetic storms, a 12-hour orbit may accumulate a dose of 100 rd(Si) or more, increasing the average dose by a factor of 20 or more.

For the first 18 months (1108 orbits), in-flight devices have accumulated a ionizing dose of approximately 18 krd(Si). For comparison purposes only, an average dose rate of approximately 16.25 rd(Si)/orbit or 0.00038 rd(Si)/s may be implied. However, nearly 13 krd(Si) of that dose occurred after three significant solar events. Prior to and after the solar events, the average dose rate was approximately 4.5 rd(Si)/orbit or 0.0001 rd(Si)/s; but during and for a period of time after the solar events, the average dose rate increased anywhere from 40 to 100 rd(Si)/orbit. These enhanced periods lasted for several orbits before slowly decaying to background levels. A representative "average" dosimetry plot (accumulated dose as a function of orbit number) from a calibrated PMOS dosimeter on Board B3 of the MPTB experiment is shown in Figure 1. The effects of the three solar events, 20 April 1998 (orbit 364), 24 August 1998 (orbit 584), and 30 September 1998 (orbit 656) are clearly visible in this plot.

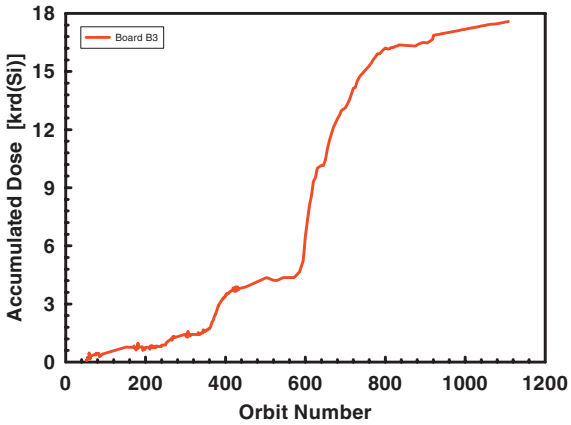

Figure 1: A representative plot of the average ionizing dose accumulated for each orbit (data obtained from a PMOS dosimeter on another MPTB board designated as Board B3) showing a background dose rate of 4.5 rd(Si)/s and periods of higher dose rates.

III. EXPERIMENTAL DESCRIPTION

The MPTB payload has three panels and each panel contains eight flight boards. The linear circuit flight board is part of Panel A and is designated as A4. All the devices for the flight and ground based tests were purchased in single date code lots of 100 devices for each device type except the Class-S LM124s which were provided separately as a lot of 20 devices. All packages were hermetically sealed 14-pin dual in-line packages (DIPs). Sensors on each panel indicate that operating temperatures have fluctuated between 30 and 55 °C.

A. Flight Tests

Board A4 has a total of eight linear circuit packages. Each package contains four linear test circuits, a quad package type. Four of the eight packages are LM124s, operational-amplifiers (op-amps) circuits, manufactured by National Semiconductor. Two of those four are standard COTS devices which were identified as radiation and ELDR sensitive. The other two are Class S devices which were identified as not radiation and ELDR sensitive. An explanation for this radiation difference is not known at this time, but it is believed to be related to the isolation oxide and/or passivation (see Section, Subsection E for additional details). The op-amp circuits were biased in a

unity-gain configuration with both inputs grounded during irradiation. Electrical measurements of V_{OS}, I_{OS}, and I_{IB} are taken once every orbit using a standard closed loop configuration unless system problems (e.g. MPTB power turned off, core required system reset, etc.) override a measurement. Loss of data has occurred approximately 11 times resulting in missing data for 101 of the 1108 orbits. Measurements are resumed when the system problems are resolved. A representative plot of I_{IB} for the standard COTS and Class-S LM124s is shown in Figure 2. Representative plots of V_{OS} and I_{OS} are not shown, since these parameters do not exhibit significant degradation for the selected bias conditions. This was expected.

The other four packages are comparator circuits. Two of these are LM139s manufactured by National Semiconductor which are known to be radiation and ELDR sensitive; and the PM139s manufactured by Analog Devices are known to be radiation and ELDR insensitive. An explanation for their radiation and ELDRS differences is not known at this time, but is probably related to differences in their design, layout, and processing. The comparators are biased with both inputs grounded through resistors and the output is pulled up through a resistor to 5 volts. As noted previously, electrical measurements of V_{OS}, I_{OS}, and I_{IB} are taken once every orbit using a standard closed loop configuration unless system problems prevent taking a measurement. This has resulted in a loss of data for 101 orbits. As before, measurements resume when the system problems are resolved. A representative plot of I_{IB} for the LM139s and PM139s is shown in Figure 3. Representative plots of V_{OS} and I_{OS} are not shown. Again, these two electrical parameters do not exhibit significant degradation for the selected bias conditions.

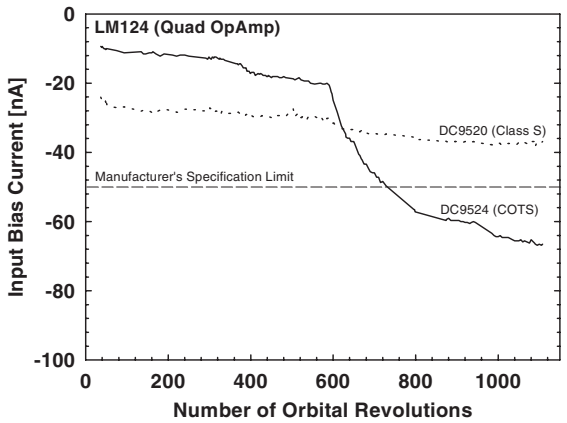

Figure 2: A representative plot of the input bias current response of the standard LM124 and the Class-S LM124 as a function of completed orbital revolutions.

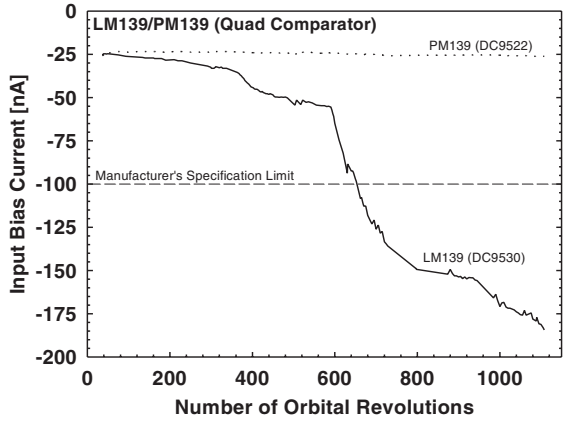

Figure 3: A representative plot of the input bias current response of the LM139 and PM139 as a function of the number of completed orbital revolutions.

B. Ground Tests

Ground tests were performed on circuits with the same date code as the orbital samples. However, the Class-S LM124 was only characterized at 1 and 100 rd(Si)/s due to the limited number of test samples available. Electrical tests on the operational amplifiers (LM124s) and comparators (LM139s and PM139s) were performed using an Eagle LSI-4, an automated linear test system. The Eagle LSI-4 provides measurements of power supply current, offset voltage, input offset current, input bias current, open loop gain, power supply rejection ratio, common mode rejection ratio, output voltage high and low, output current high and low, and propagation delay or slew rate.

Irradiations were performed using Co-60 sources at fixed dose rates using similar insitu bias conditions as the flight board. Irradiations were performed with fixed dose rates of 100, 1.0, 0.01, and 0.001 rd(Si)/s at room temperature (approximately 22°C). For dose rates of 100 and 1 rd(Si)/s, irradiations were performed using a Shepherd Model 484 Co-60 irradiator located at the Naval Surface Warfare Center (NSWC) in Crane IN. For dose rates of 0.01 and 0.001 mrd(Si)/s, irradiations were performed using a Gammabeam 150 Co-60 source located at Research Triangle Institute(RTI), NC. All devices were placed inside a Pb/Al box during irradiation and dosimetry was performed using CaF_2 TLDs to determine the initial dose rate for that test. Accumulated dose was calculated based upon the established dose rate and exposure times.

For the low dose rate tests, the dose rates were adjusted to account for the Co-60 decay by decreasing the initial dose rates based on the Co-60 half-life of 5.27 years. The low dose rate tests conducted at the RTI facility were interrupted at specific total dose levels, shipped overnight to NSWC, electrically characterized using the Eagle LSI-4, and then returned to RTI to continue the radiation exposures. The time between exposure levels for the low dose rate tests was typically two to three days. Annealing was not examined. For the ground based tests, a sample size of four devices for each part type was used. Results (an average of the four samples) of the Co-60 tests, performed at room temperature and shown as symbols for the LM124s, LM139s, and PM139s, are presented in Figures 4-6, respectively.

The individual responses of the tested samples were tightly clustered. In the majority of cases, the data spread is smaller than the symbol used to represent the averaged data points.

Irradiations were also performed using the NSWC Co-60 source with a fixed dose rate of 10 rd(Si)/s at elevated temperature, approximately 100°C. The temperature of the devices was elevated using a Thermionics system which uses pressurized air (heated and cooled) to raise and lower the temperature. Two thermocouples were mounted on the test board to monitor and control the air flow allowing the temperature during irradiation to be set at approximately 103°C ±5°C. The time between exposure levels for the elevated temperature tests was typically 40 to 60 minutes allowing sufficient time for the devices to cool, to electrically characterize all the devices, and to elevate the temperature for the next exposure. The averaged results of the elevated temperature tests, shown as a solid line, for the LM124s, LM139s, and PM139s are also presented in Figures 4-6, respectively.

Upon closer examination of the LM124 and LM139 devices (see Figures 4 and 5), the total dose response of these devices at fixed dose rates of 1 and 100 rd(Si)/s are essentially identical. Many ELDRS devices may demonstrate a marked enhancement at a dose rate of 1 rd(Si)/s. Obviously, these devices do not. However, the total dose response of the devices at a fixed dose rate of 10 mrd(Si)/s demonstrate a significant increase in parametric degradation, which is indicative that the devices are ELDRS. This observation demonstrates that hardness assurance screens performed with dose rates of 1 rd(Si)/s or higher may not be adequate to identify ELDRS.

Figure 6 clearly shows that the PM139 is neither radiation or ELDR sensitive. Even at an elevated temperature of 100 °C during irradiation, the total dose degradation of the PM139s are only minor. It even appears that the I_{IB} response at lower dose rates of 10 mrd(Si)/s and 1 mrd(Si)/s) may be exhibiting a smaller increase when compared to the higher dose rate data at 1 rd(Si)/s or 100 rd(Si)/s.

IV. Flight Data Comparison

To compare the flight data to the ground based data, flight data must be determined as a function of rd(Si). Using the dosimetry curve of Figure 1, the number of orbital revolutions are converted into an average accumulated dose. Using this technique, a total dose response curve is generated for each set of devices. These data are then compared to data obtained from two hardness assurance tests [6,7], 10 mrd/s at room temperature and 10 rd/s at elevated temperature, as shown in Figures 7-9 for the standard COTS LM124s, LM139s, and PM139s, respectively. This comparison provides insights into the validity of the two hardness assurance tests. However, one must also consider that space experiments are not a controlled environment, since temperature, dose rate, and bias variations do occur. For reference only, the average dose rate per orbit varied from approximately 4.5 rd(Si)/orbit during periods of little or no solar activity to nearly 100 rd(Si)/orbit during periods of high solar activity.

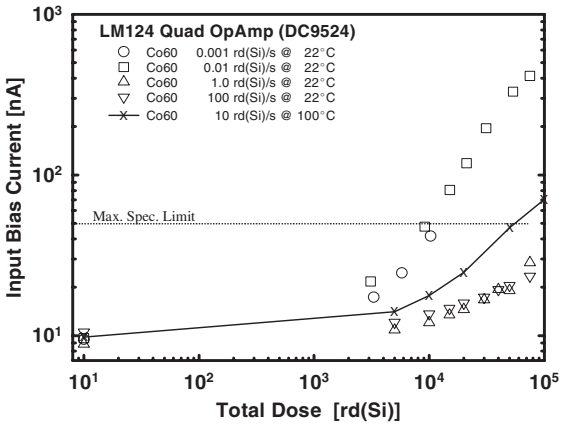

Figure 4: Total dose response of LM124 (standard COTS) at fixed dose rates of 0.001, 0.01, 1.0, and 100 rd(Si)/s at room temperature.

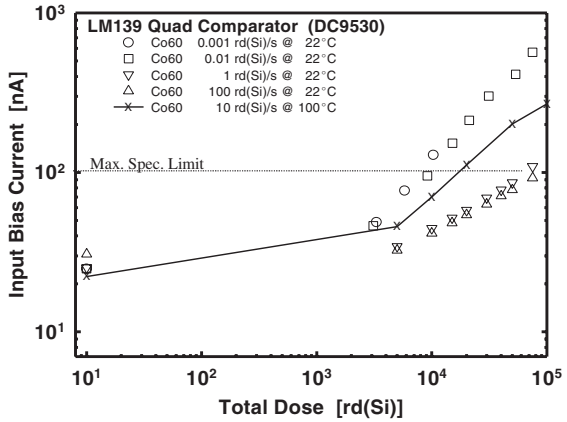

Figure 5: Total dose response of LM139 at fixed dose rates of 0.001, 0.01, 1.0, and 100 rd(Si)/s at room temperature.

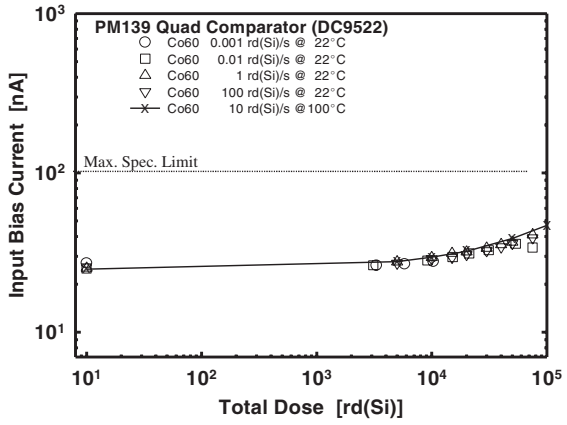

Figure 6: Total dose response of PM139 at fixed dose rates of 0.001, 0.01, 1, and 100 rd(Si)/s at room temperature.

Based upon the ground tests, I_{IB} was identified as the critical parameter. Figures 7-9 show orbital I_{IB} data converted to dose superimposed upon ground data taken on similar devices with the same date code under similar insitu bias conditions. In spite of the uncontrolled environmental conditions that existed during the space experiment, the flight data clearly exhibit enhanced degradation in the standard COTS LM124s and the LM139s devices. As with the ground data, the PM139s exhibit little or no enhance degradation.

A. Comparison of LM124

Figure 7 shows the LM124 response. The LM124 flight data are compared to data obtained from two hardness assurance tests [6,7] and data at 1 mrd(Si)/s. The flight data definitely fall below the upper boundary provided by the 1 and 10 mrd(Si)/s data. The 10 mrd(Si)/s ground data are conservative compared to the flight data whereas the flight data are approximately 2x greater than the elevated temperature data at a dose of 18 krd(Si). However, the hardness assurance test using elevated temperature allows for a design margin of 3x and the 10 mrd(Si)/s test allows for a design margin of 2x. Based upon the ground data at this dose, both tests predicted ELDRS and both had adequate design margins. However, when the ground data are compared at 75 krd(Si), the 10 mrd(Si)/s data are approximately 6x worse than the elevated temperature data. This strongly suggests the elevated temperature test may not always predict the low dose rate degradation within a factor of 3.

B. Comparison of LM139

Figure 8 shows the LM139 response. The LM139 flight data are in good agreement with the 10 mrd(Si)/s data. On the other hand, the flight data are approximately a factor of 2 worse than the elevated temperature test data at 18 krd(Si). Again, this is within the 3x design margin. For these devices, the elevated temperature test data are observed to be within a factor of 2 of the low dose rate response at 10 mrd(Si). The hardness assurance techniques produced a positive result for ELDRS and the design margins of 2x and 3x are adequate.

C. Comparison of PM139

Figure 9 shows the PM139 response. The flight data are in good agreement with the low dose rate tests and elevated temperature tests. Flight data show slightly less degradation than ground based data which may be a result of long term annealing, temperature variations, and bias variations in the flight data. Obviously, the PM139s are not ELDR sensitive. The devices tested negative for ELDRS and the low dose rate data support that result. This provides direct evidence that ground tests can be used to identify dose rate sensitive as well as insensitive devices. Since the PM139s are relatively hard to ionizing radiation (I_{IB} increased a factor of 2 at 100 rd(Si) from 24 nA to 48 nA) but sensitive to displacement effects, they can be used to monitor displacement damage in the LM124s and LM139s. If the flight parts exhibit more degradation than is expected for the

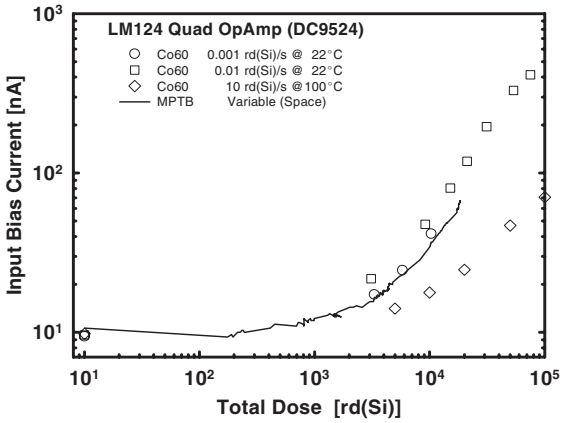

Figure 7: A graphical comparison of the ground-based data to the flight data for the LM124 (standard).

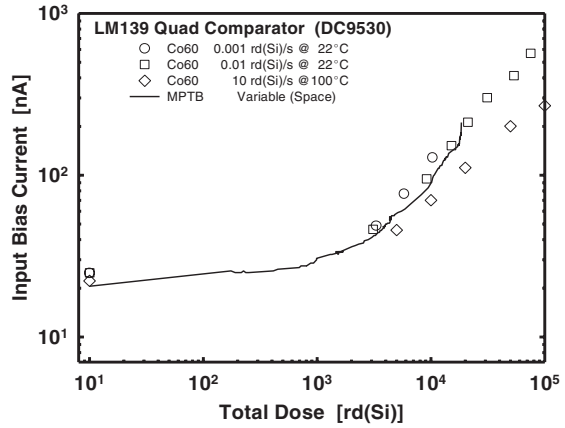

Figure 8: A graphical comparison of ground-based data to flight data for the LM139.

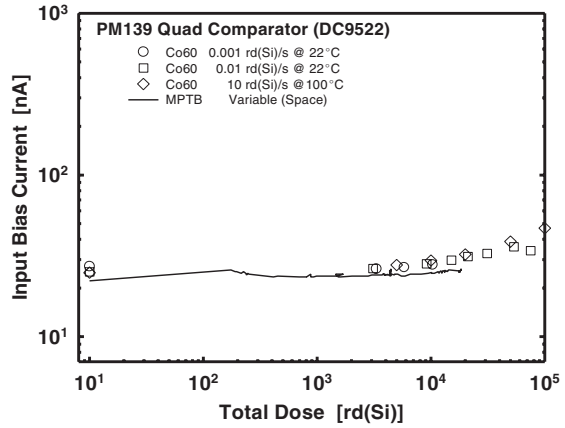

Figure 9: A graphical comparison of the ground-based data to flight data for the PM139.

deposited dose, the excess degradation must be due to displacement damage effects. This will be discussed further in Part V, Section C. Although not shown, the response of the Class-S LM124s are similar to PM139s in that they too appear to be radiation and ELDR insensitive which was expected based upon earlier data. The Class-S LM124 data are not discussed in detail or shown due to the limited number of devices available for ground-based tests.

V. DISCUSSIONS

A. Ground Correlation

The flight data are easily within a factor of 2 of the Co-60 results at 10 mrd(Si)/s. A factor of 2 is used by Pease et al. [6,7] as the design margin for the low dose rate hardness assurance technique. A lower dose rate test at 1.0 mrd(Si)/s tests is currently in progress at the RTI facility. The response at this lower dose rate based upon the last recorded radiation exposure of 10.3 krd(Si) appears to be saturating on the LM139s and the response of the LM124s even show less degradation when compared to the 10 mrd(Si)/s data. Given that the average dose rate per orbit varies from 0.1 mrd(Si)/s during periods of little or no solar activity to approximately 3 mrd(Si)/s during periods of high solar activity. Note that higher dose rates exist within an orbit as the belts are traversed. The flight data are in *good* agreement with ground test data with the possible exception of the LM124s. One possible explanation for the I_{IB} response of the LM124s is that the dose rate effect has saturated; and, at dose rates below 10 mrd(Si)/s, the degradation in the I_{IB} response is less and may even recover as a result of annealing which may occur during periods of negligible dose rate. If this is the case, the I_{IB} response of the LM124 may reflect less degradation in I_{IB} because the average space rate is 0.33 mrd(Si)/s over the 18 month period.

B. Dose Rate Variations

If enhanced degradation of I_{IB} occurs in a dose rate sensitive device and the devices are then subjected to an accumulated dose using different dose rates, then the total dose response of that device should reflect slope changes in the I_{IB} degradation curve. That is, the response at a lower dose rate should have a steeper slope until the dose rate effect begins to saturate. The LM139 and LM124 flight data are plotted in Figure 10 to show the I_{IB} characteristic more closely during periods of increased solar activity and periods of little or no activity, where the shaded areas represent the periods of little or no solar activity. The average dose rate during those periods was approximately 4.5 rd(Si)/orbit. Under closer examination, the LM139 curve clearly indicates that the I_{IB} characteristic is responding to periods of increased activity as well as those periods of little activity. During periods of increased solar activity, the average accumulated dose per orbit increases dramatically and the rate of change in I_{IB} decreases. During periods of solar inactivity, the rate of change in I_{IB} would be expected to increase. This response is evident in the six month period that occurred at approximately 18 krd(Si). During this six-month period, no measurable solar activity was noted and the rate of change in the I_{IB} degradation was observed to increase dramatically.

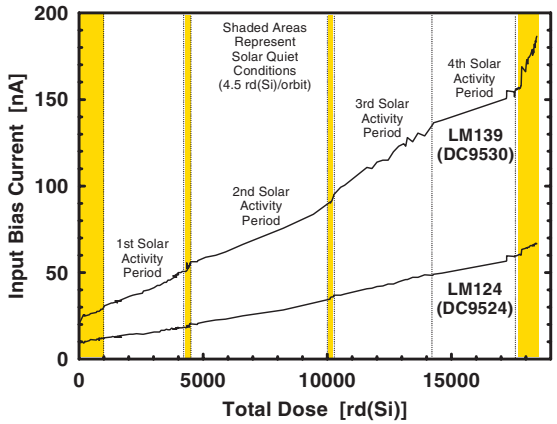

Figure 10: The LM139 and LM124 flight data are plotted to show periods of solar activity and inactivity (shaded areas) and its affect on the I_{IB} response due to variations in the average dose rate during these periods.

C. Displacement Damage Effects

As discussed earlier, the majority of the deposited dose (ionization damage) is from protons and electrons which are also known to produce displacement damage in bipolar linear circuits [9]. Since the ratio of ionizing energy loss to non-ionizing energy loss (NIEL) is orders of magnitude higher for electrons than protons in the earth radiation belts, we assume that only the protons are of immediate concern for displacement damage. Protons produce ionization and displacement damage which, in turn, cause an increase in the input bias current. Ionization and displacement damage must be qualitatively or quantitatively separated. We do this by examining the relative change in I_{IB} due to displacement damage in these device types when exposed to neutrons. Neutron irradiations were performed using White Sands Missile Range Fast-Burst Reactor to 1 MeV equivalent fluences of 5, 15, and 25×10^{11} n/cm^2. Five samples of each device type from the same date code lot were exposed and characterized with the Eagle LSI-4. The degradation in I_{IB} was linear with neutron fluence. This was expected. The measured rates of degradation were 2 nA per 10^{10} n/cm^2 for the LM139s and 1 nA per 10^{10} n/cm^2 for the LM124s and PM139s. Since the relative displacement damage of the PM139s are comparable to the other device types, the PM139 flight data can be used as a measure of displacement damage at a dose of 18 krd(Si) accumulated through orbit 1108. Figure 9 clearly shows that the PM139s have only degraded approximately 4 nA. Even if we assumed that all this degradation were produced by displacement damage, the subsequent impact on the LM124 and LM139 response would be negligible. Therefore, it is reasonable to assume that degradation in I_{IB} of the LM124s and LM139s are a direct result of ionization and not displacement damage.

D. Hardness Assurance Issues

These updated results continue to demonstrate that bipolar linear circuits in this study can respond to a complex time-variant environment (elliptical orbit in space) in a manner comparable to the responses obtained using fixed dose rates on the order of magnitude of 10 mrd(Si)/s in a controlled environment (radiation tests in the laboratory). The data clearly demonstrate that ELDRS exists in space as well as the laboratory. It has been suggested that the effect of protons and electrons encountered in space rather than the photons used in the laboratory or the time-varying nature of space could induce significantly different responses. Obviously, this is not the case in this study.

System performance could be compromised if ELDRS prone devices are used in space systems. Such a selection could result in premature failure rendering the system useless. Therefore, selection criteria must require adequate screens for ELDRS in bipolar devices. Test Method 1019 does not address requirements for ELDRS in bipolar devices, since that portion concerning space only applies to CMOS devices. However, an ASTM standard, ASTM-F1892-98 [*Guide for Ionizing Radiation (Total Dose) Effects Testing of Semiconductor Devices*], has included an entire Appendix devoted to ELDRS.

As was shown in Figure 7, the hardness assurance screens may not always provide adequate safety margins. The elevated temperature screen under predicted the MPTB response by a factor of 3 but under predicted the 10 mrd(Si)/s response by a factor of 6. The elevated temperature tests may not always bound the ELDRS response using a design margin of 3x. This supports a similar observation in a previous study where the elevated temperature design margin of 3x was not adequate in some cases [7].

We provide the following example to demonstrate why ELDRS could pose a serious risk to a deployed system. A satellite placed in a geostationary orbit (apogee = 35,790 km; perigee = 35,790 km, and inclination = 0°) may be expected to survive 10 years. Using Space Rad 4.0 [10], the expected dose without any shielding is approximately 10^9 rd(Si) per year which is reduced to approximately 10^6 rd(Si) when 40 mils of aluminum spherical shielding is assumed. Then, the dose is reduced to approximately 2.1 krd(Si) per year using a RAD PAK 1 package limiting the total accumulated dose on the system electronics to approximately 21 krd(Si) for a 10-year mission. The designer selects an LM139 comparator and determines that I_{IB} cannot exceed 100 nA in the specified application. Using high dose rate curves (as shown in Figure 5), the designer believes that he has ample design margin to ensure safe operation. I_{IB} equals 100 nA at 75 kr(Si) giving a design margin of 3.5x in dose. However, these devices are dose rate sensitive and exhibit ELDRS. Since this device will be subjected to low dose rates in this orbit, the high dose rate curve does not provide a valid assessment. If we examine the low dose rate curve (see Figure 5), I_{IB} degrades to 100 nA after accumulating a dose of 10 krd(Si), causing the system to fail after 4.75 years of operation. Remember, that this was a simple example to demonstrate the importance of identifying devices that exhibit ELDRS.

E. Process Analysis of LM124

As stated before, the Class-S LM124 is less sensitive to ionizing radiation than the standard LM124A. In light of this, some simple failure analysis techniques were performed on both devices. Microscopic examination of both die revealed that the layout and design were similar if not the same. However, the devices did use different mask sets and were fabricated at different facilities. This observation is based upon a code (1902F) stamped on the standard LM124 which used an underscored F whereas the code (1902F) stamped on the Class-S LM124 which used an F without an underscore [11]. Another notable difference between the Class S and standard devices was their metallization. The metallization of the standard LM124 was observed to have numerous hillocks; whereas, the metallization of the Class-S device was observed to be smooth with little or no hillocks. As stated earlier, the difference in radiation hardness between the Class-S and standard COTS was thought to be related to the passivation layer, based upon information supplied by the manufacturer. Based upon this information, it was suspected that one of the devices was fabricated with a nitride passivation layer and the other an oxide passivation layer. We examined the composition of both passivation layers and determined that neither device incorporated a nitride passivation layer. Both devices used a silicon oxide passivation layer. The difference in radiation hardness is still unclear, but we believe that it is related to the quality of the isolation oxide which is known to significantly influence the total dose response of bipolar transistors.

VI. Conclusions

An on-going space experiment has successfully monitored the total dose responses of several bipolar linear circuits for the past 18 months. These results were presented for the LM124, LM139, and PM139. The total dose responses of these devices obtained using a fixed dose rate in a controlled environment (the laboratory) correlate to the total dose response obtained using a variable dose rate in an uncontrolled environment (in space). The flight data clearly indicate that a low dose rate effect does exist in space validating the laboratory results. Comparison of two hardness assurance tests used to screen for ELDRS demonstrated that the low dose rate test (10 mrd(Si)/s) would have bounded the space data within the proposed 2x design margin. However, the elevated temperature test was marginal in bounding the space data within a design margin of 3x.

Acknowledgments

The authors would like to recognize and acknowledge the efforts of the researchers, manufacturers, and sponsors who have contributed to this project. We are particularly grateful to Lew Cohn (DTRA) for his continuing technical and funding support; to Jeff Cleveland, Ralph Freitag, Sharon Mozersky, and others at NRL who provided technical support; to Denny Adamson, Jake Tausch, and others at MRC who assisted in the board design and

software development; and finally to Mike Keeton and others at Orbital Sciences who assisted in the flight board fabrication.

REFERENCES

[1] R. N. Nowlin, E. N. Enlow, R. D. Schrimpf, and W. E. Combs, "Trends in the Total-Dose Response of Modern Bipolar Transistors," IEEE Trans. Nucl. Sci., NS-39, pp. 2026-2032, Dec 1992.

[2] S. McClure, R. L. Pease, E. Will, and G. Perry, "Dependence of Total Dose Response of Bipolar Linear Microcircuits on Applied Dose Rate," IEEE Trans. Nucl. Sci., NS-41, pp. 2544-2549, Dec 1994.

[3] A. H. Johnston, G. M. Swift, and B. G. Rax, "Total Dose Effects in Conventional Bipolar Transistors and Linear Integrated Circuits," IEEE Trans. Nucl. Sci., NS-42, pp. 2427-2436, Dec 1994.

[4] J. T. Beaucour, T. Carriere, A. Gach, D. Laxague and P. Poirot, "Total Dose Effects on Negative Voltage Regulator," IEEE Trans. Nucl. Sci., NS-41, pp. 2420-2426, Dec 1994.

[5] J. L. Titus, W. E. Combs, T. L. Turflinger, J. F. Krieg, H. J. Tausch, D. B. Brown, R. L. Pease, and A. B. Campbell, "First Observations of Enhanced Low Dose Rate Sensitivity (EDRS) in Space: One Part of the MPTB Experiment," IEEE Trans. Nucl. Sci., NS-45, pp. 2673-2680, Dec 1998.

[6] R. L. Pease, L. M. Cohn, D. M. Fleetwood, M. A. Gehlhausen, T. L. Turflinger, D. B. Brown and A. H. Johnston, "A Proposed Hardness Assurance Test Methodology for Bipolar Linear Circuits and Devices in a Space Ionizing Radiation Environment," IEEE Trans. Nucl. Sci., NS-44, pp. 1981-1987, Dec 1997.

[7] R. L. Pease, M. A. Gehlhausen, J. F. Krieg, J. L. Titus, T. L. Turflinger, D. W. Emily, and L. M. Cohn, "Evaluation of Proposed Hardness Assurance Method for Bipolar Linear Circuits with Enhanced Low Dose Rate Sensitivity (ELDRS)," IEEE Trans. Nucl. Sci., NS-45, pp. 2665-2672, Dec 1998.

[8] R. L. Pease, W. E. Combs, A. Johnston, T. Carriere, C. Poivey, A. Gach, and S. McClure, “A Compendium of Recent Total Dose Data on Bipolar Linear Microelectronics,” IEEE Radiation Effects Data Workshop, pp. 28-37, 1996.

[9] A. H. Johnston and R. E. Plaag, “Models for Total Dose Degradation in Linear Integrated Circuits,” IEEE Trans. Nucl. Sci., NS-34, pp. 1474-1480, Dec 1987.

[10] J. R. Letaw, Space Radiation 4.0 is a commercial code available from Space Radiation Associates.

[11] Mike Maher, National Semiconductor Corporation, South Portland ME, Private Communication, 1999.

APPENDIX C—MICROELECTRONICS AND PHOTONICS TEST BED GROUND TEST DATA

Appendix C is a compilation of previously unpublished ground test data taken in 1996 in support of the MPTB board A4.

NAVSEA CRANE Surface Warfare Center Division

MPTB Ground Test Data

- 1996 data on MPTB flight lot parts
  - Taken as Part of DTRA ELDRS Program
  - Cobalt-60 data at 1 rad(Si)/sec
  - 200 MeV Protons at 1 rad(Si)/sec
  - 1 MeV eq Neutrons
- Never previously published
- Data compiled by Jeff Titus, Dec. 2002
  - Co-60 and Proton data on individual devices
    - Each quad (op-amp/comparator) plotted separately
  - Neutron data average of the test lot

NAVSEA
CRANE
Surface Warfare Center Division

LM124 COTS and LM139

Co-60, 1 Rad(Si)/sec Data

NAVSEA CRANE Surface Warfare Center Division

LM124 – Pos. Input Leakage, Ibp (Co-60)

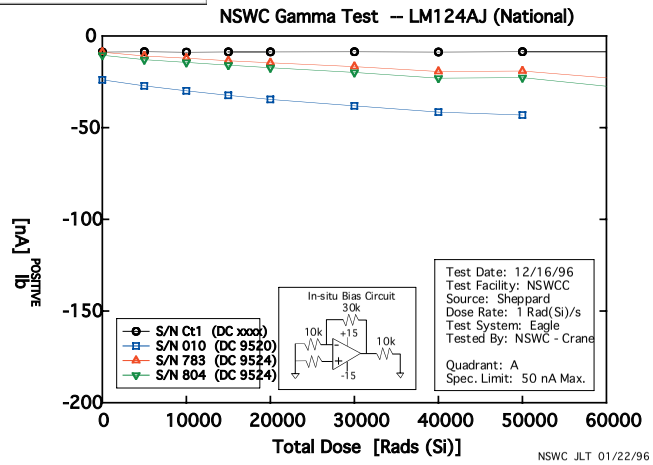

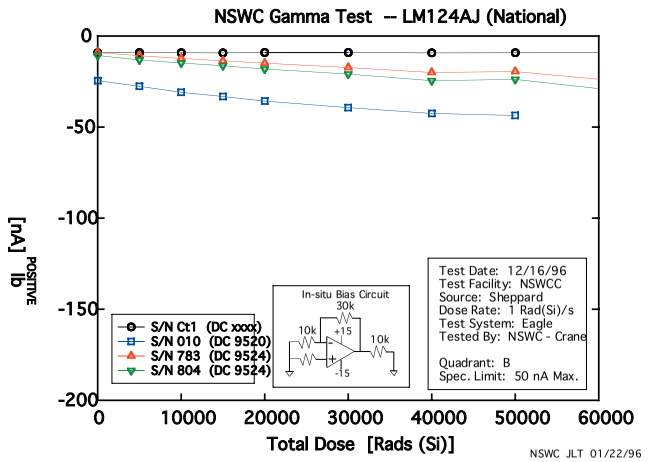

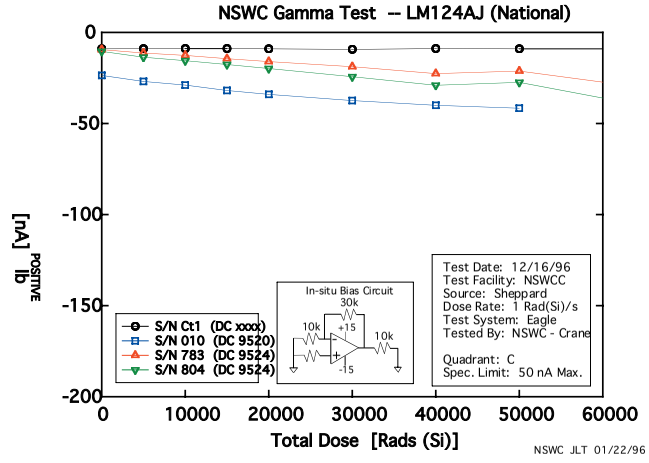

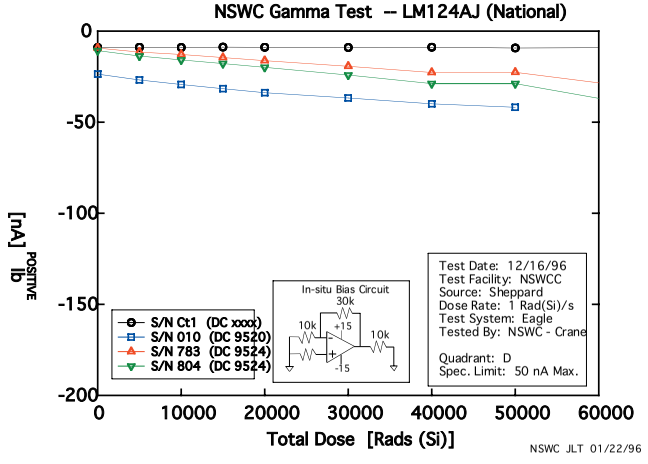

LM124 – Neg. Input Leakage, Ibn (Co-60)

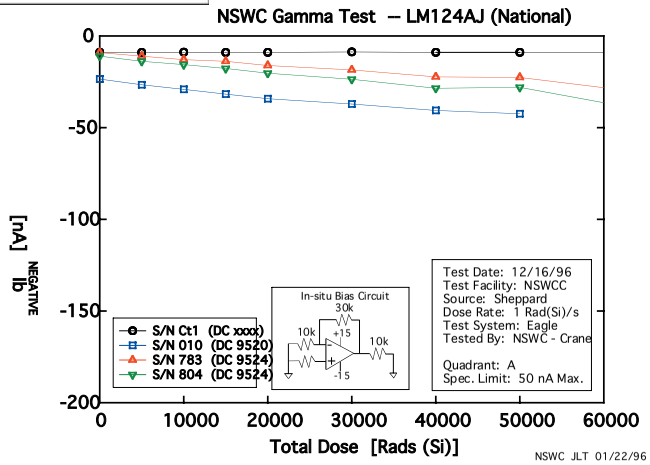

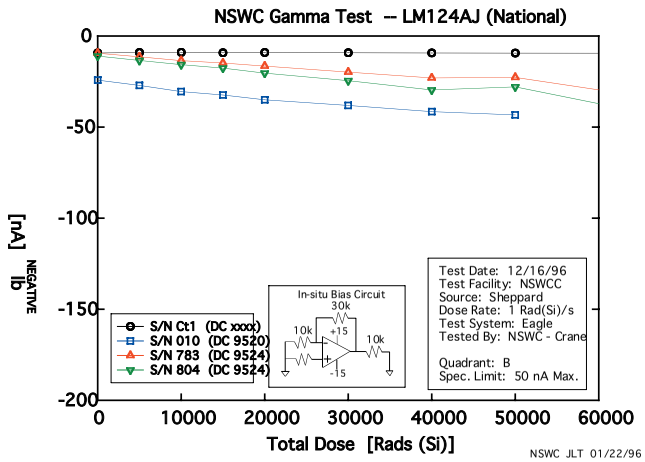

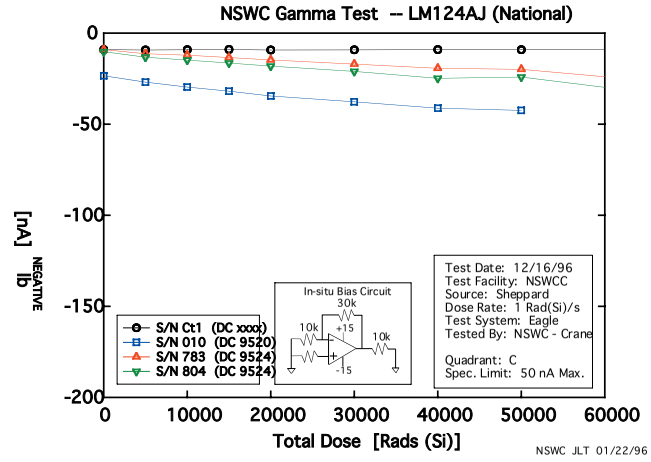

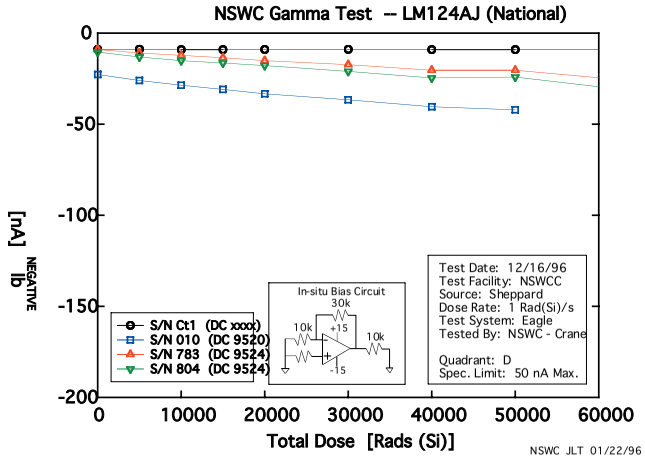

NAVSEA CRANE Surface Warfare Center Division

LM124 – Offset Current, Ios (Co-60)

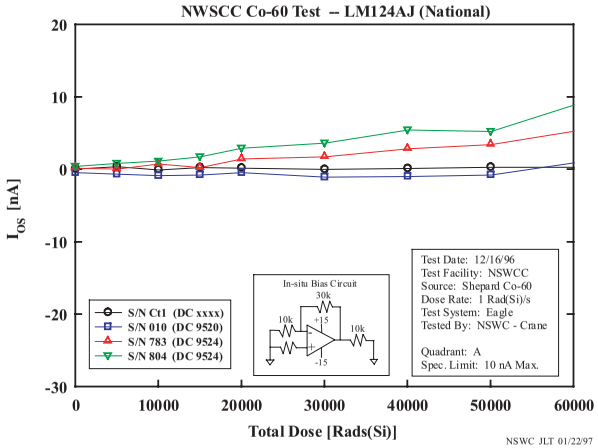

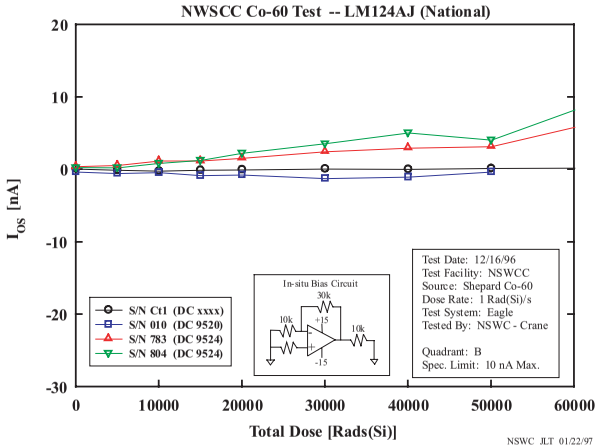

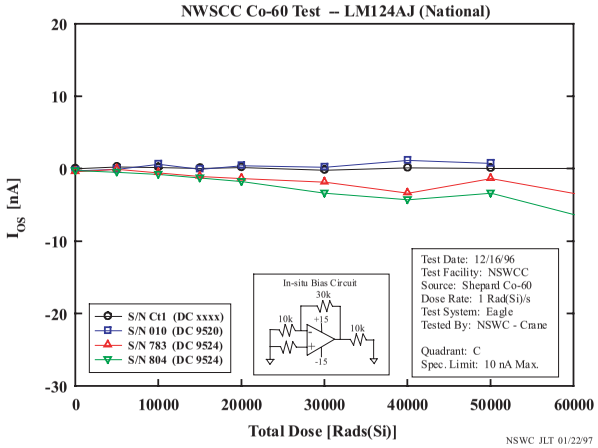

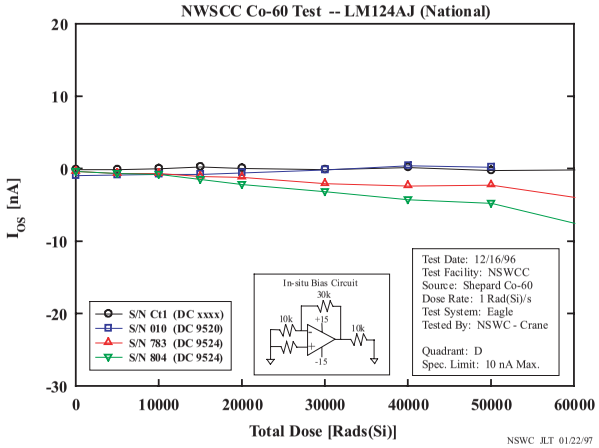

LM124 - Slew Rate (Co-60)

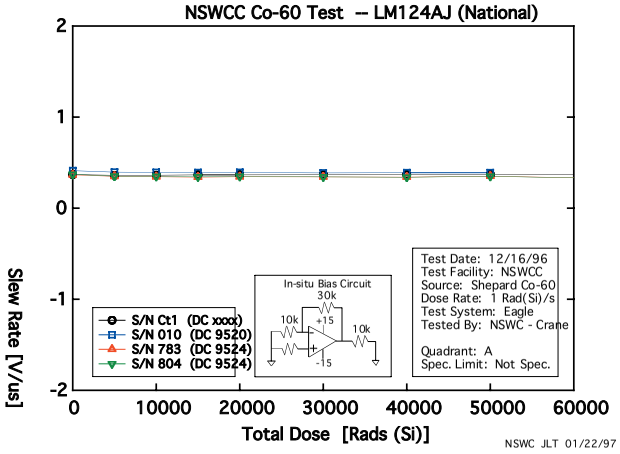

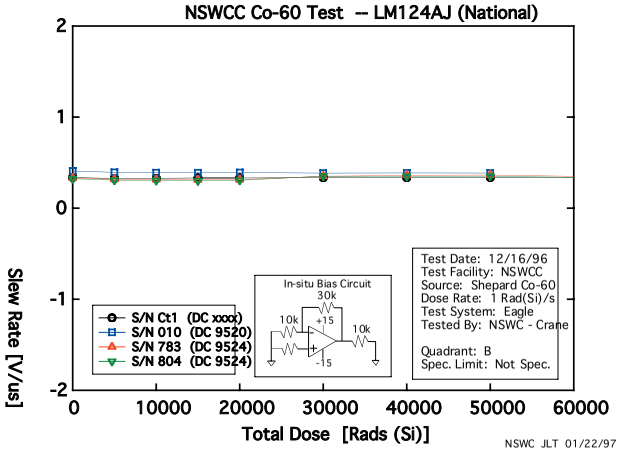

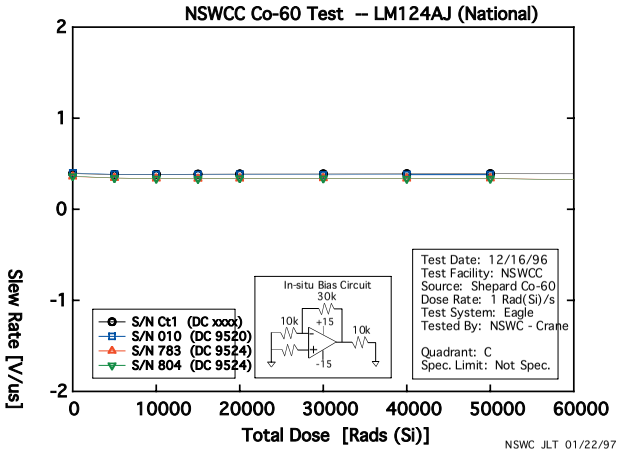

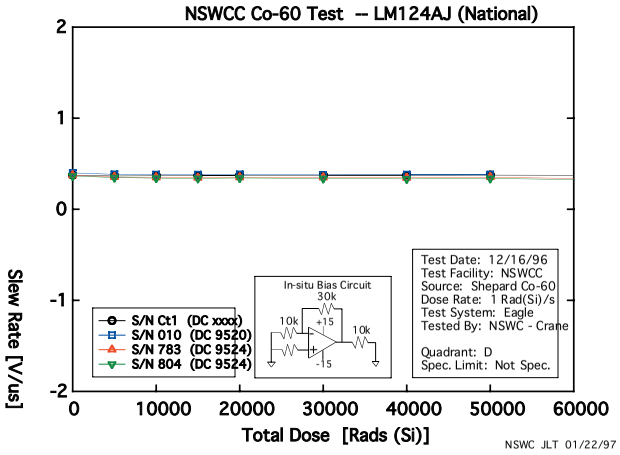

NAVSEA CRANE Surface Warfare Center Division

LM124 – Offset Voltage, Vos (Co-60)

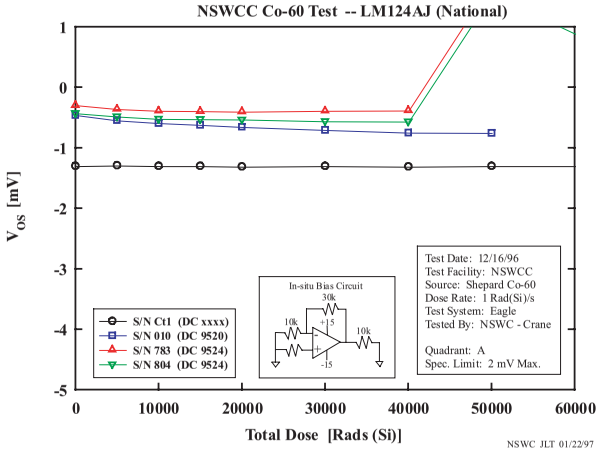

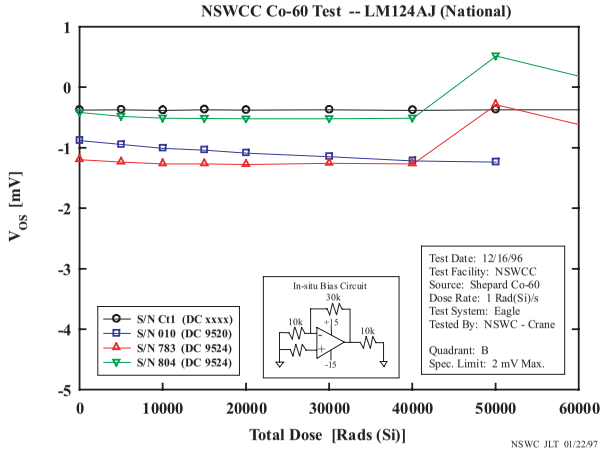

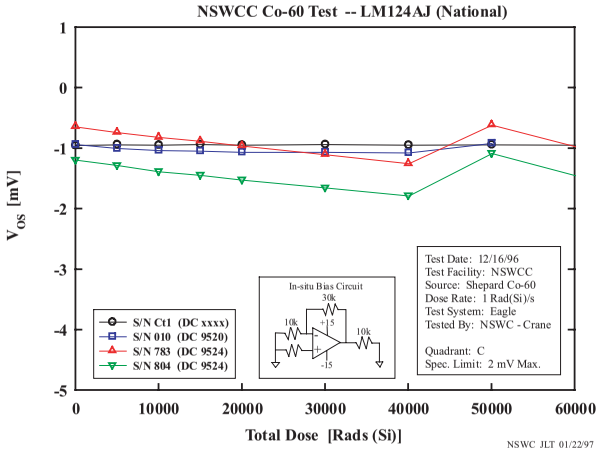

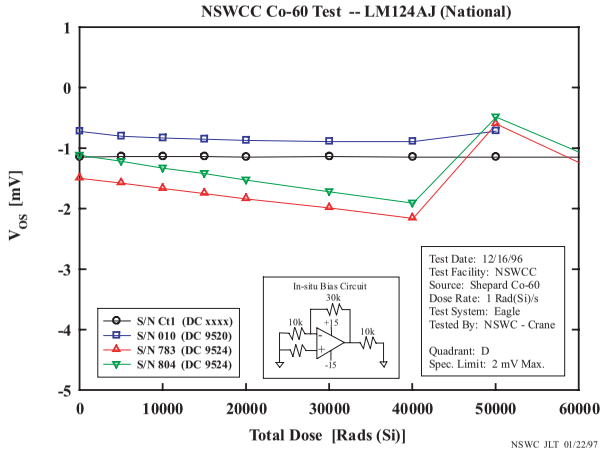

LM124 – Power Supply Current, Ips (Co-60)

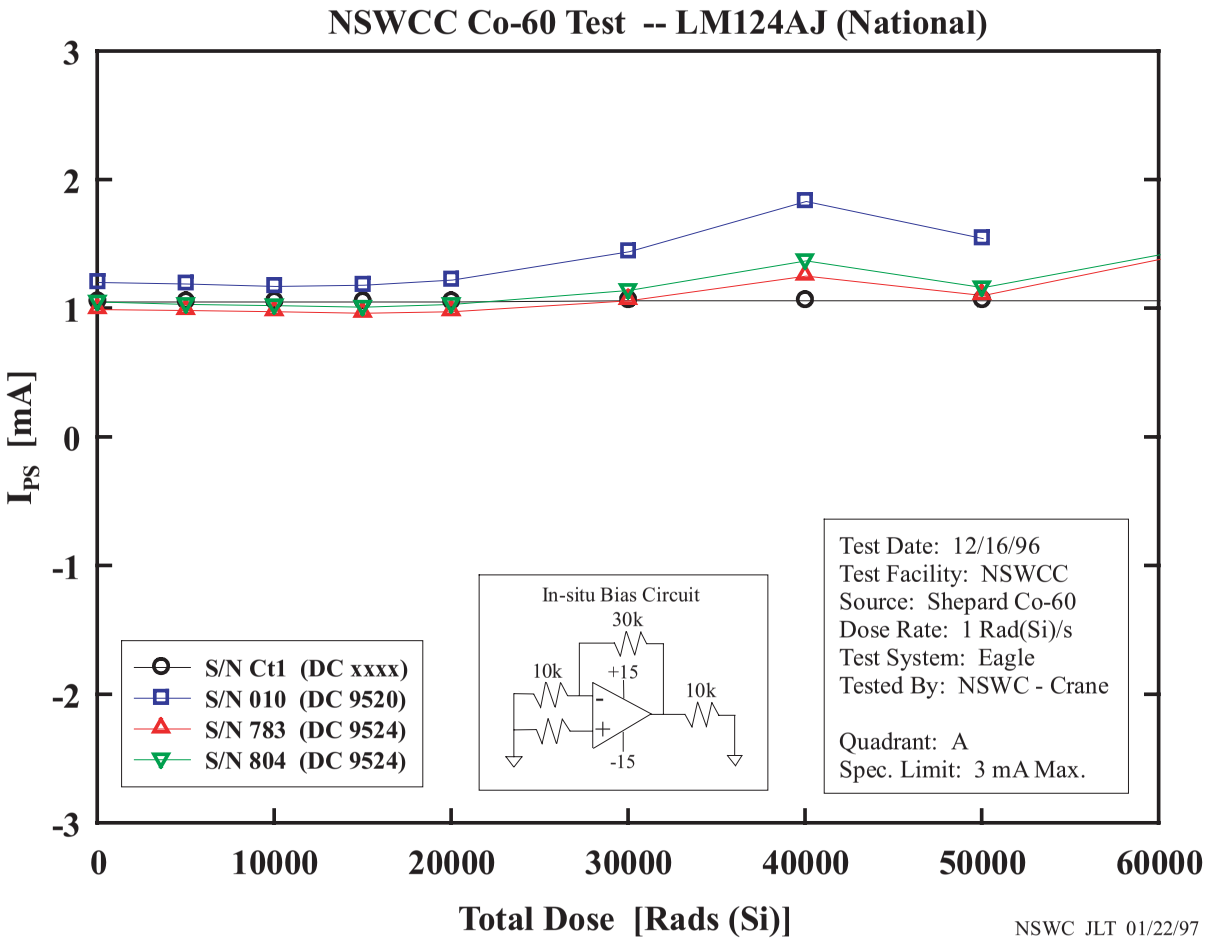

NSWC JLT 01/22/97

Harnessing the Power of Technology for the Warfighter

NAVSEA CRANE Surface Warfare Center Division

LM139 – Pos. Input Leakage, Ibp (Co-60)

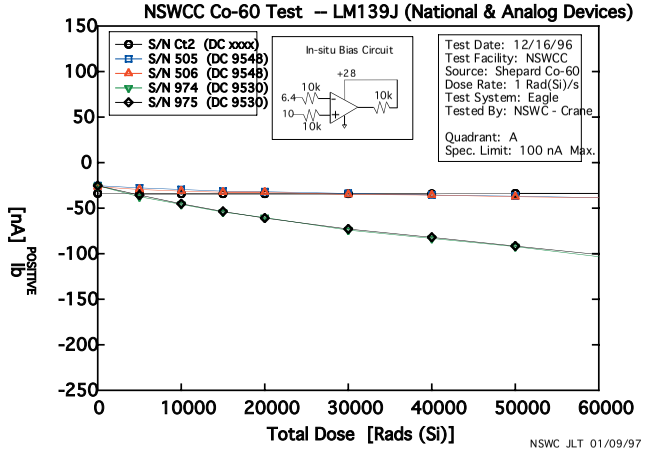

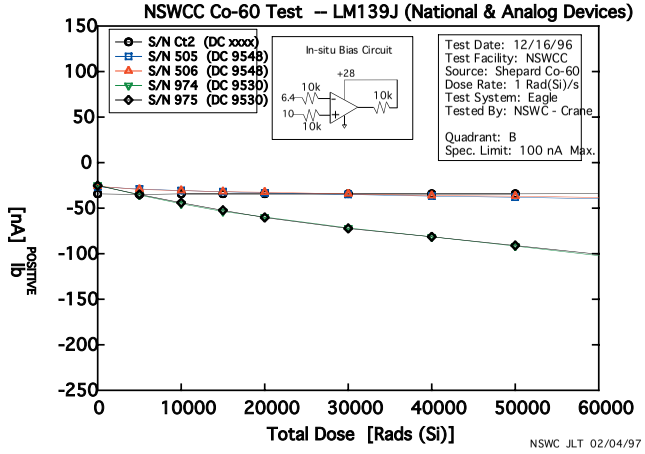

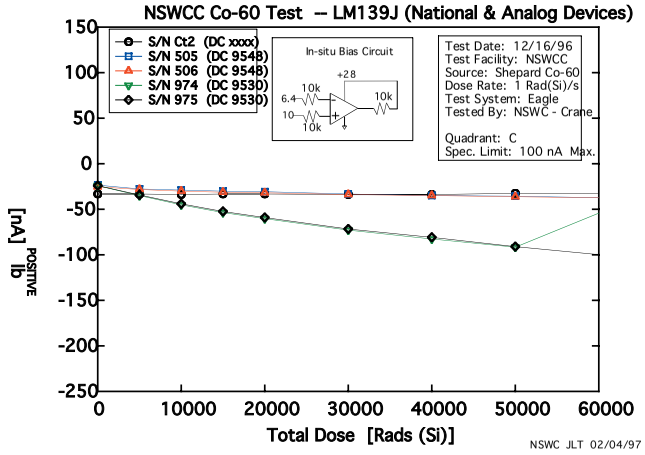

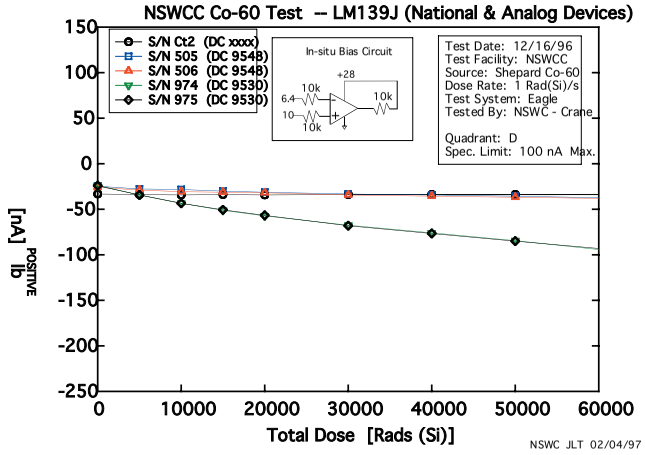

LM139 – Neg. Input Leakage, Ibn (Co-60)

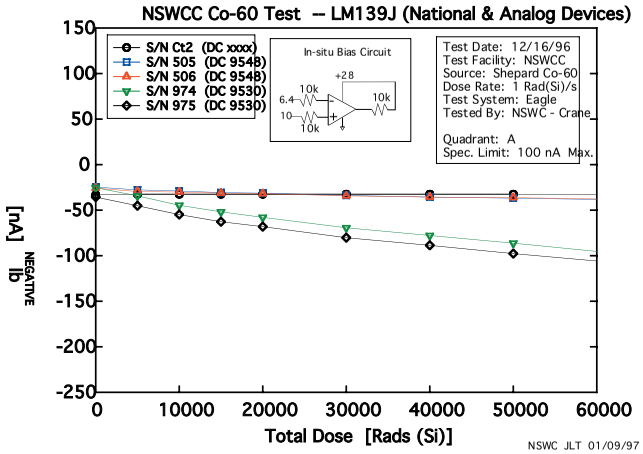

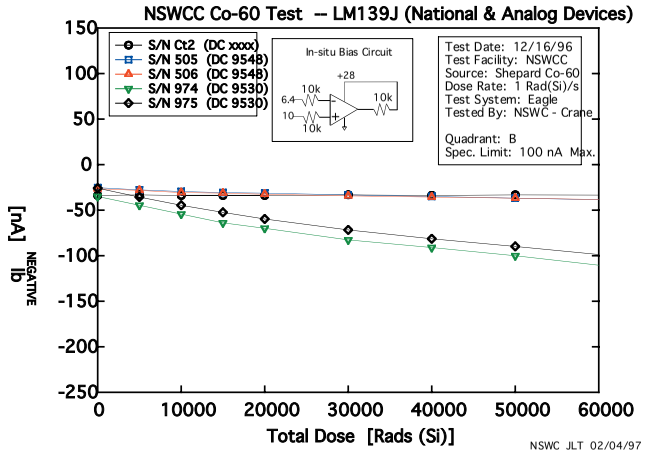

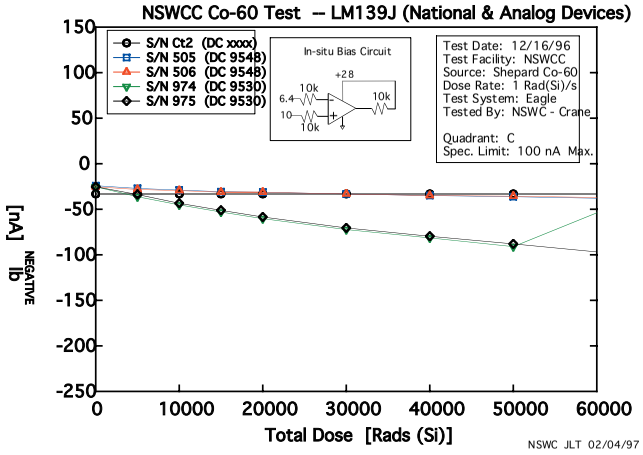

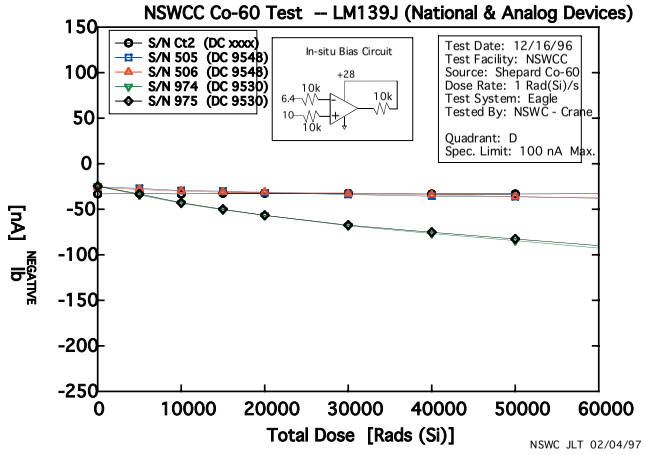

NAVSEA CRANE
Surface Warfare Center Division

LM139 – Offset Current, Ios (Co-60)

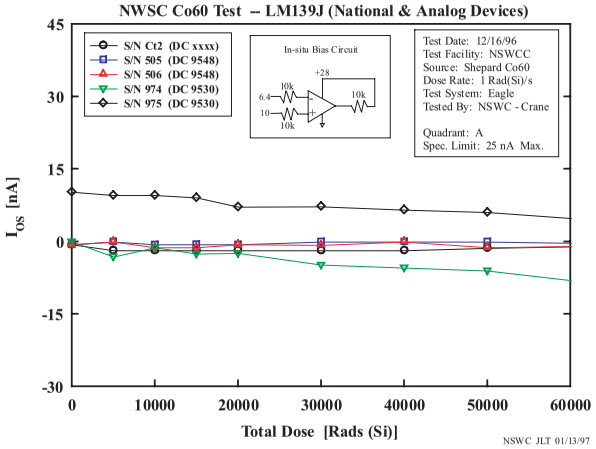

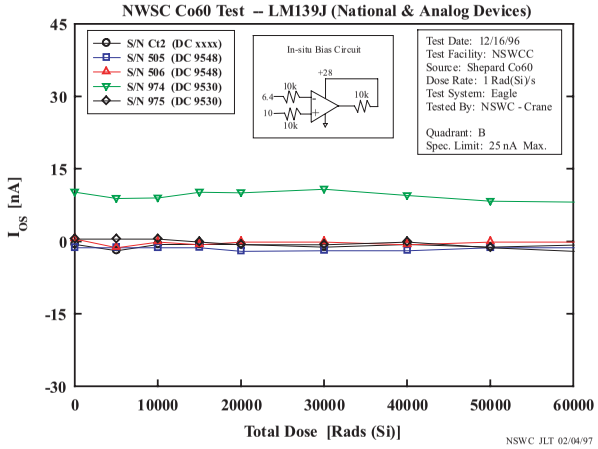

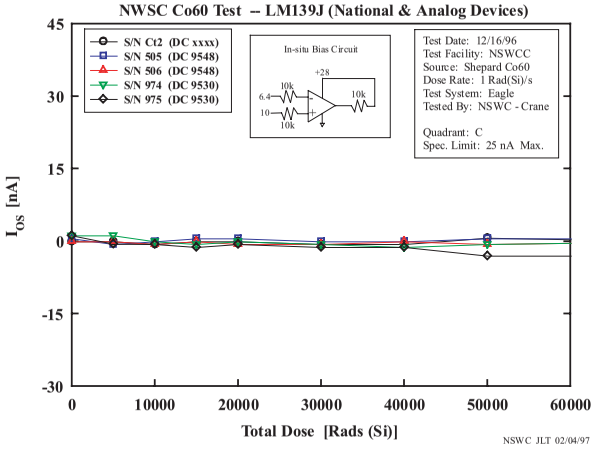

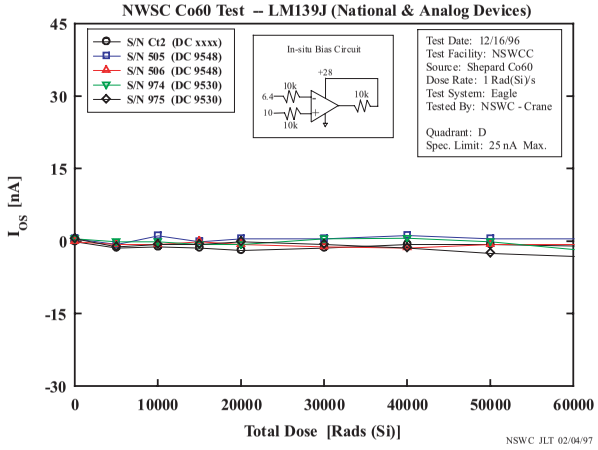

LM139 - Prop Delay (Co-60)

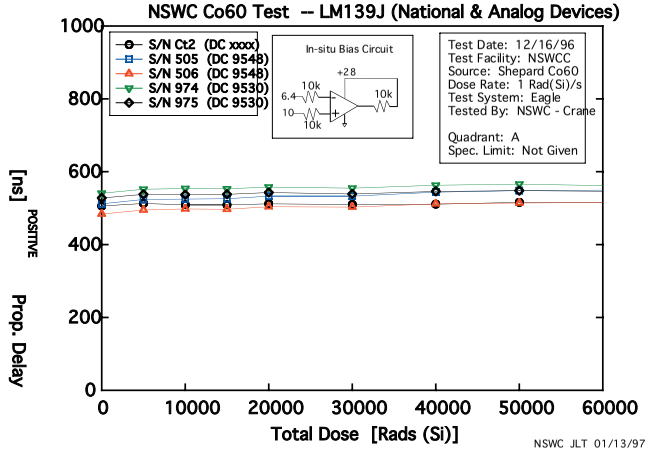

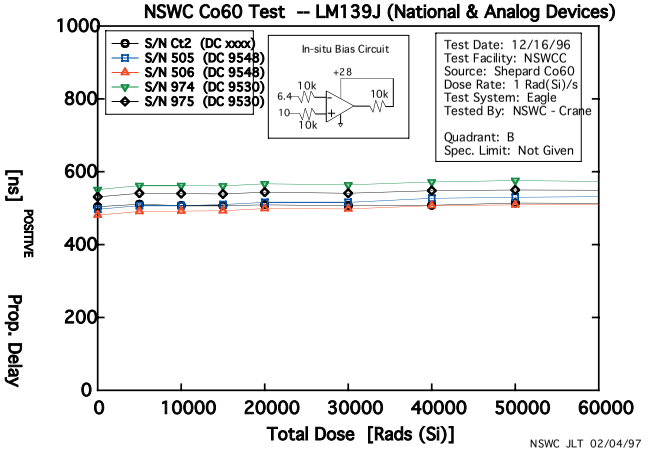

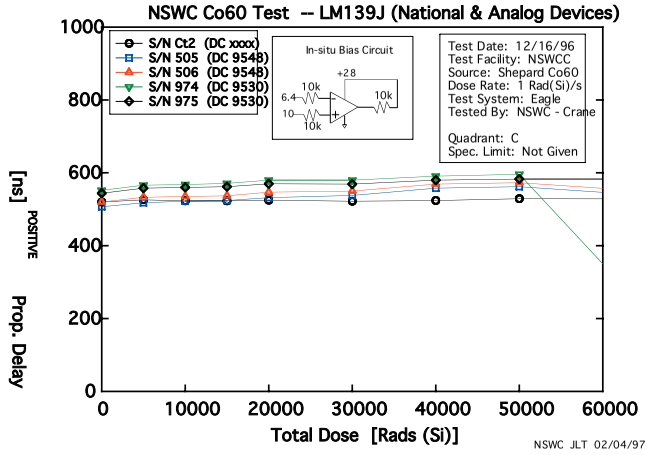

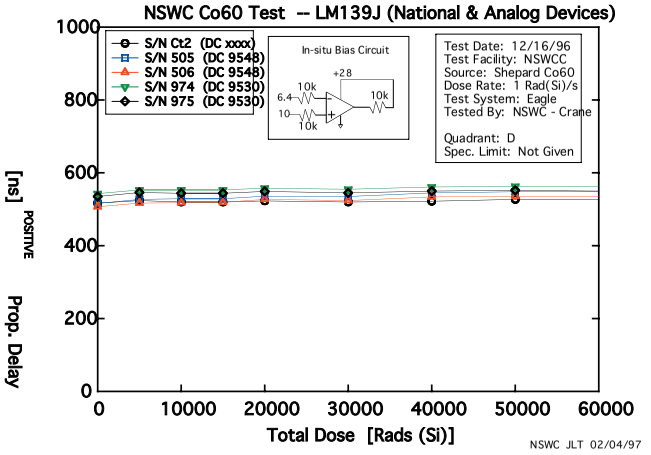

NAVSEA CRANE Surface Warfare Center Division

LM139 – Offset Voltage, Vos (Co-60)

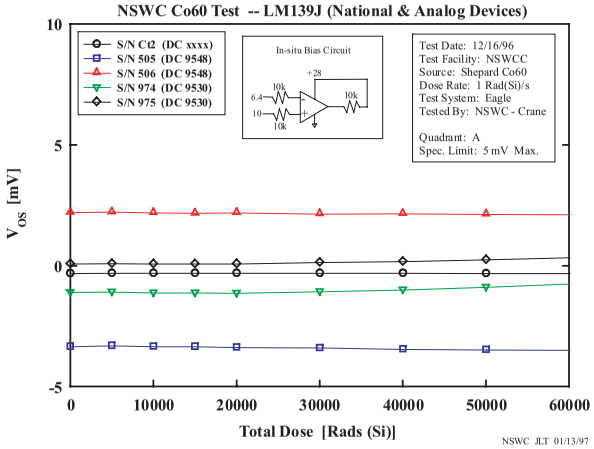

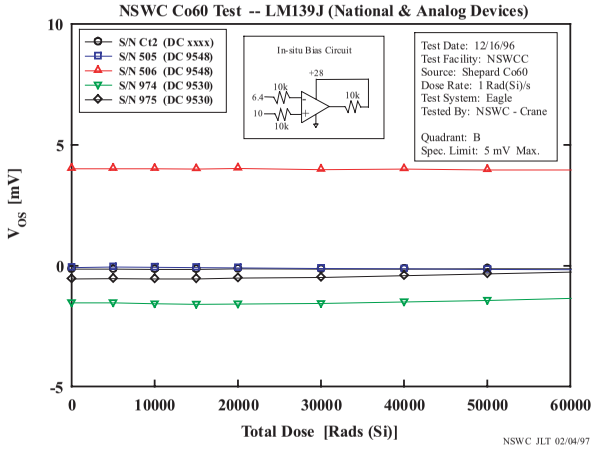

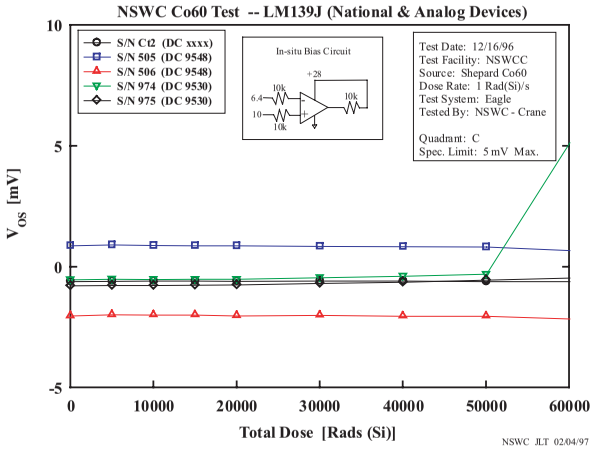

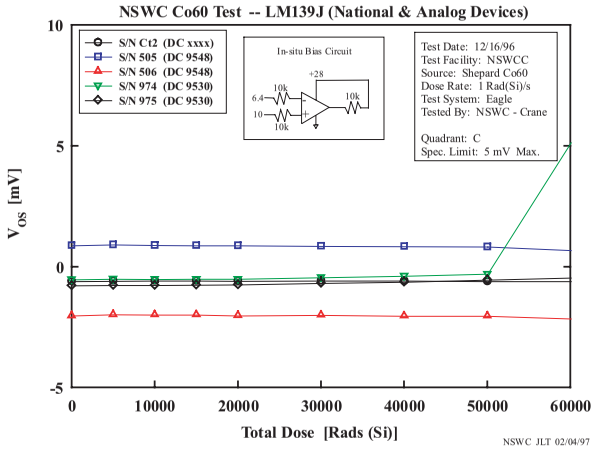

LM139 – Power Supply Current, Ips (Co-60)

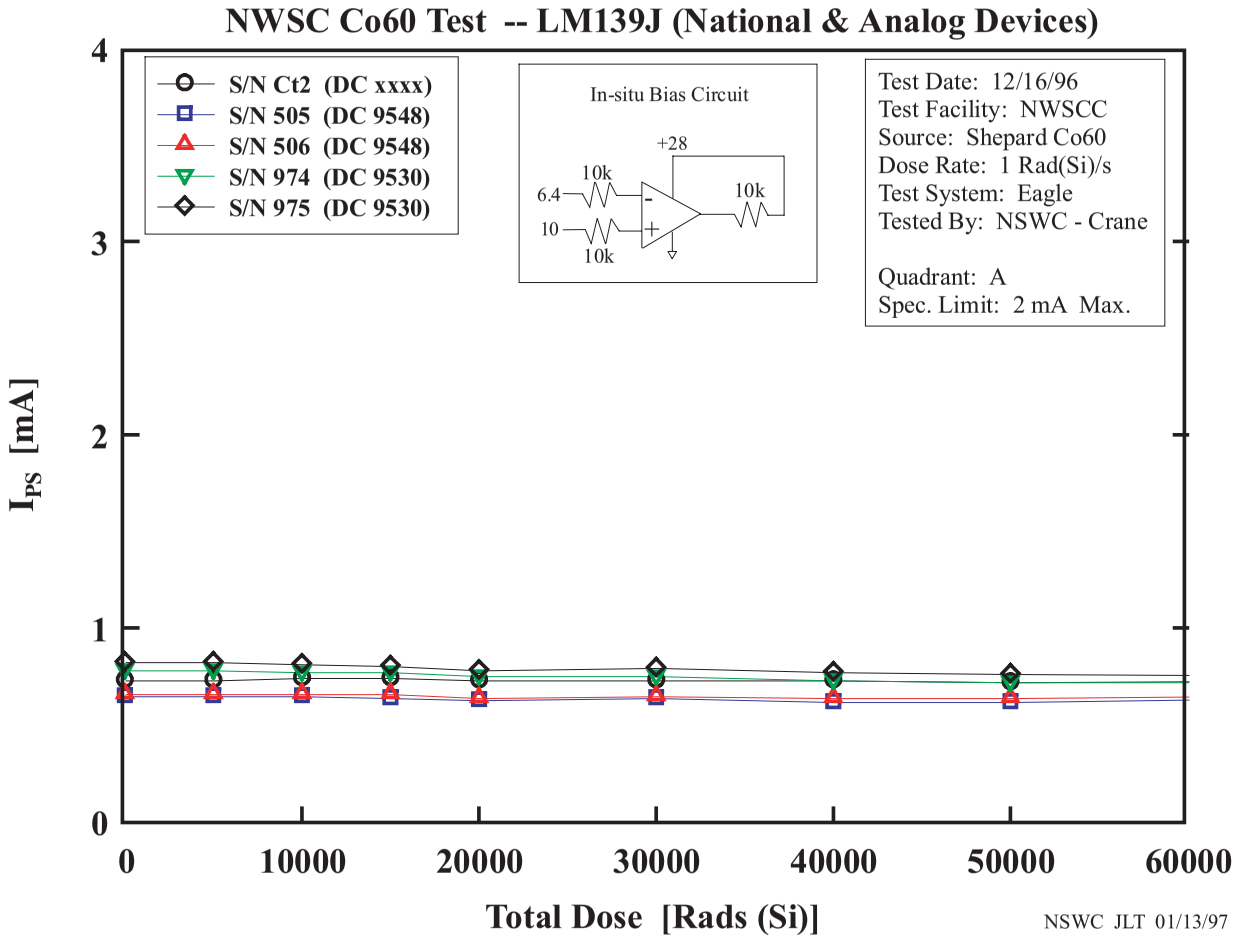

NAVSEA CRANE Surface Warfare Center Division

LM124 COTS and LM139

200 MeV Proton, 1 Rad(Si)/sec Data

(Low dose rate proton data is expensive and rare)

LM124 – Pos. Input Bias, Ibp (200-MeV Proton)

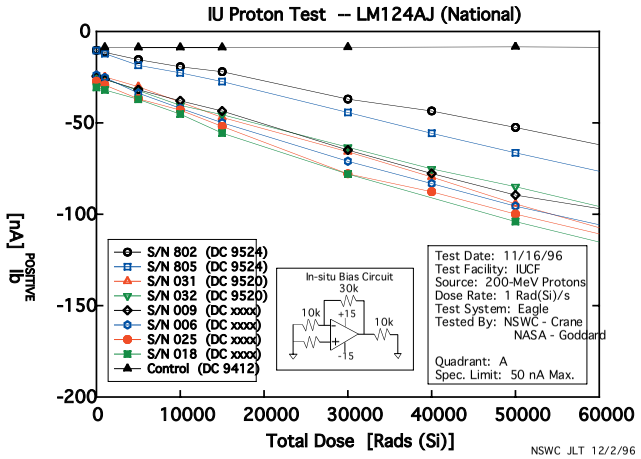

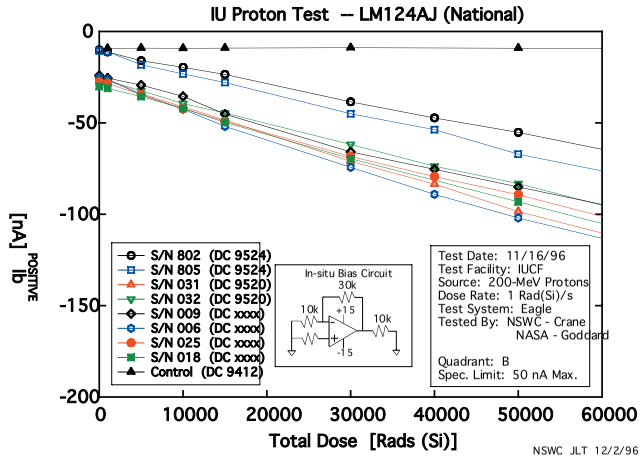

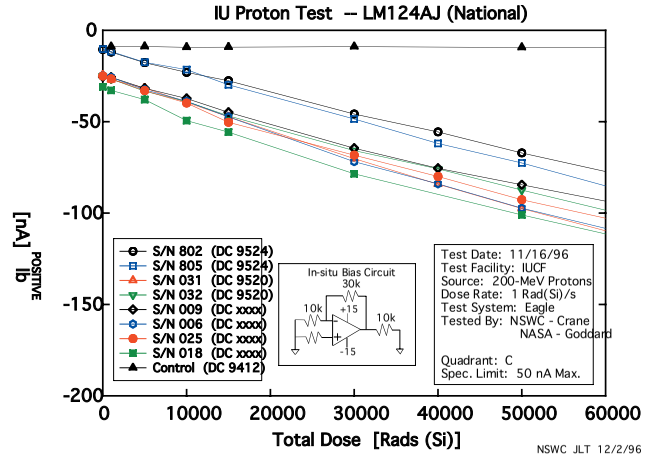

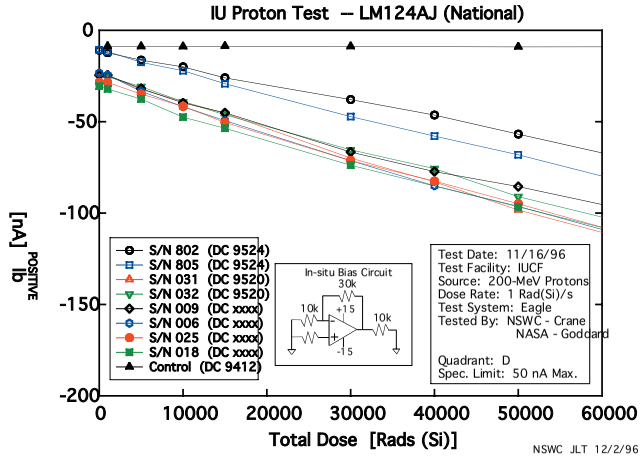

NAVSEA CRANE Surface Warfare Center Division

LM124 – Neg. Input Bias, Ibn (200-MeV Proton)

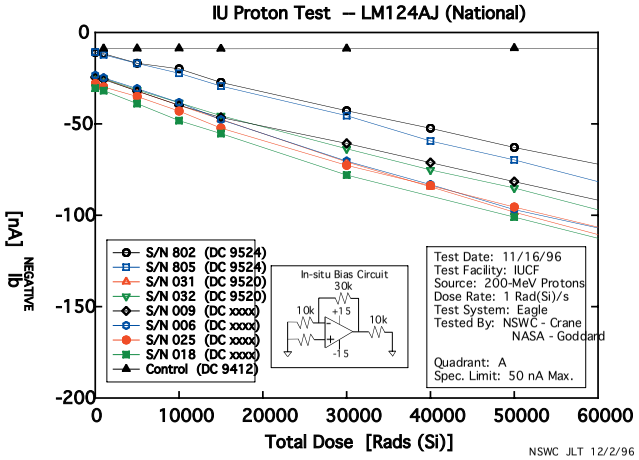

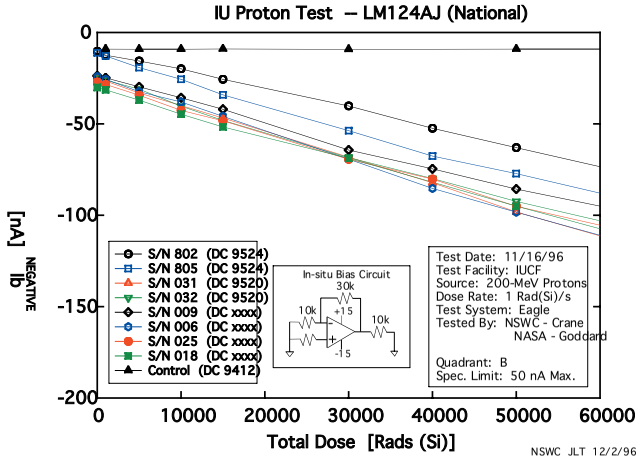

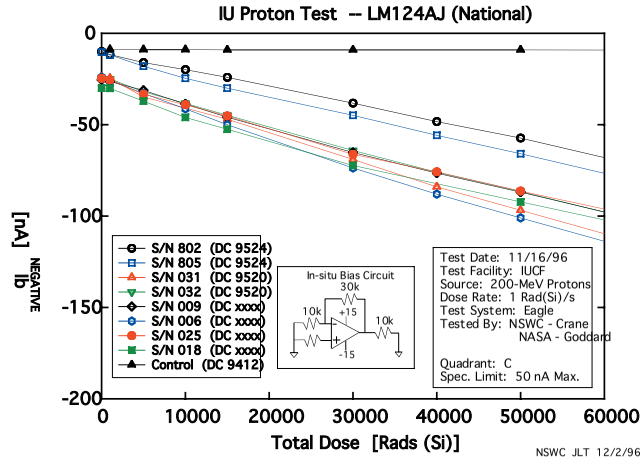

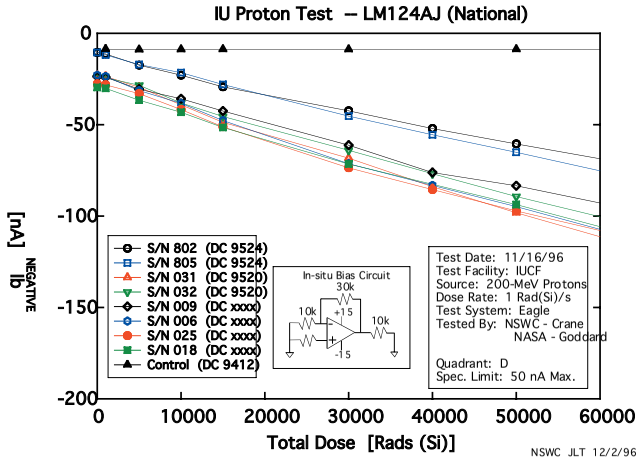

LM124 – Offset Current, Ios (200-MeV Proton)

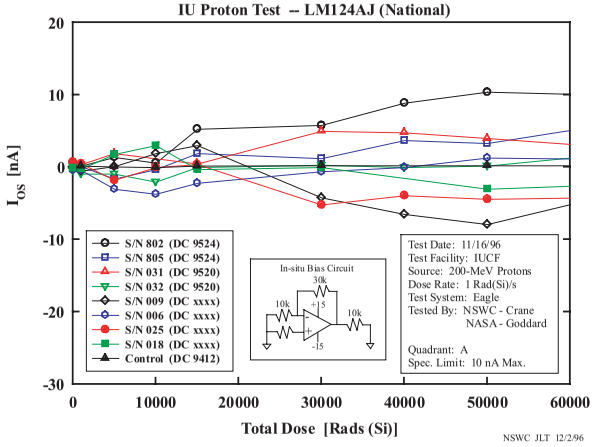

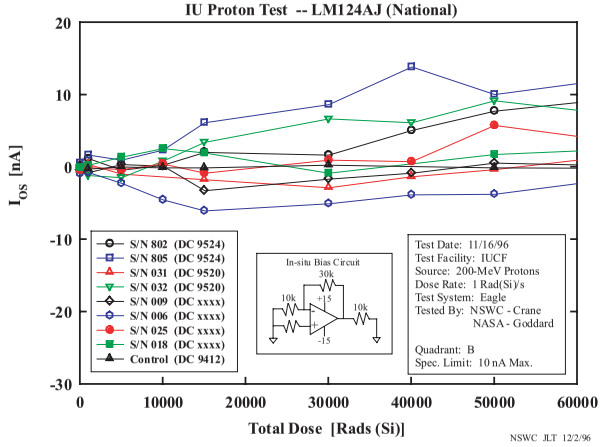

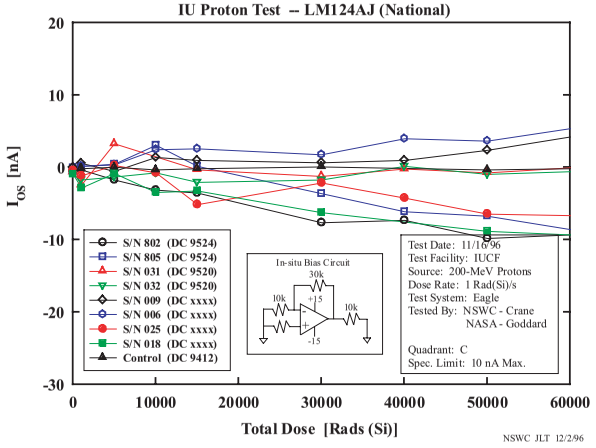

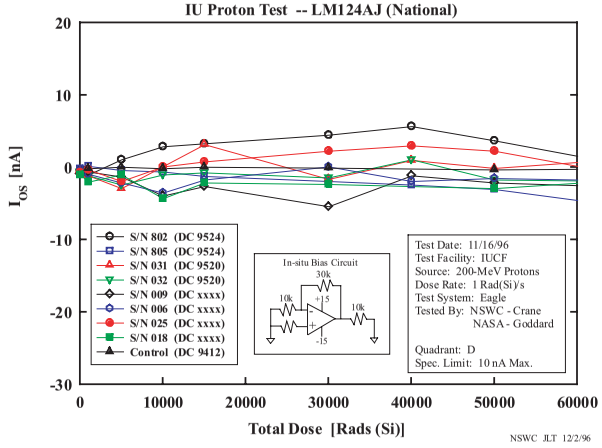

NAVSEA CRANE Surface Warfare Center Division

LM124 – Slew Rate (200-MeV Proton)

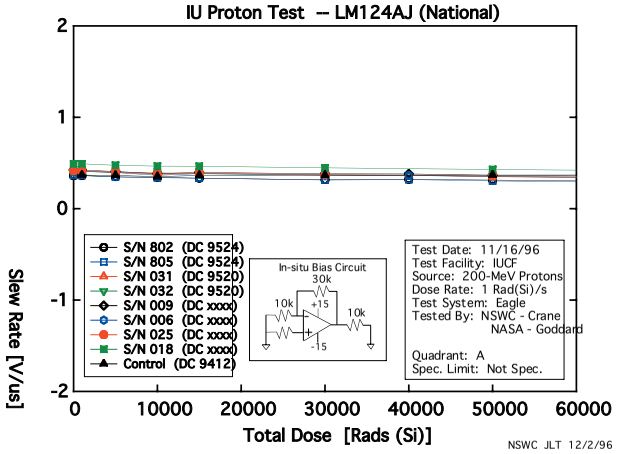

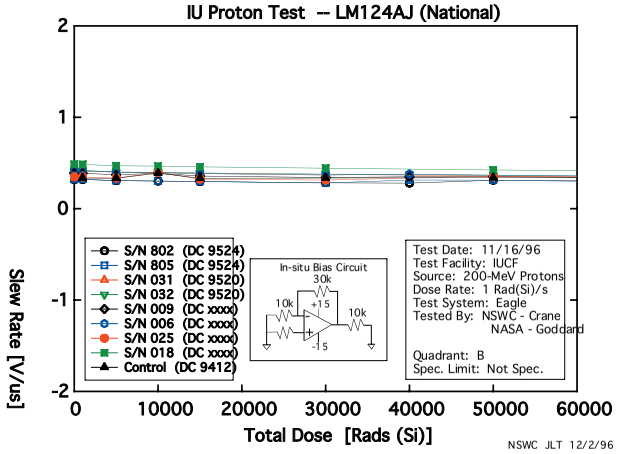

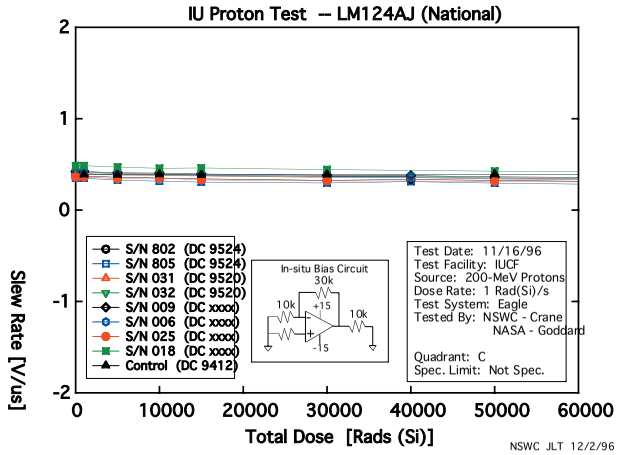

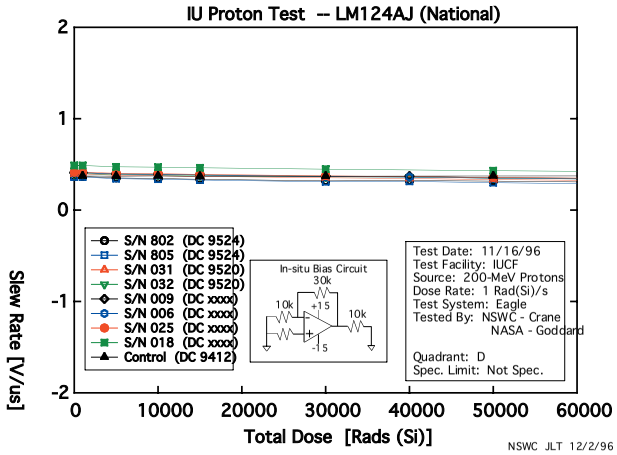

LM124 – Offset Voltage, Vos (200-MeV Proton)

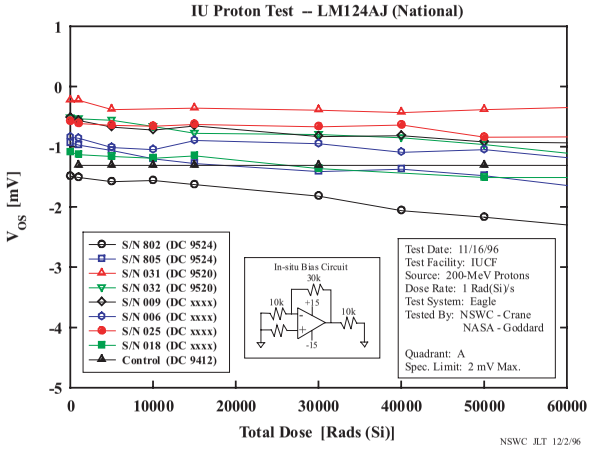

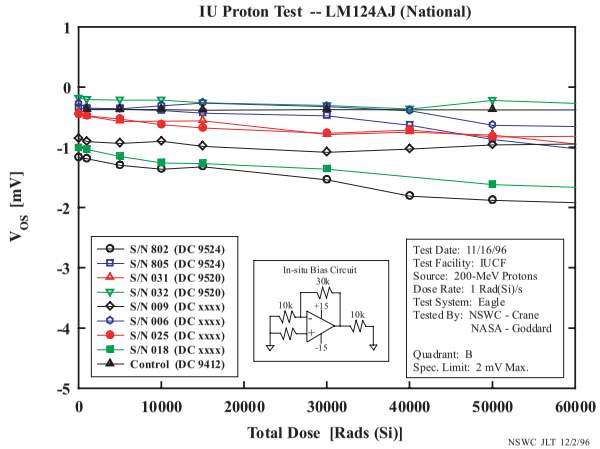

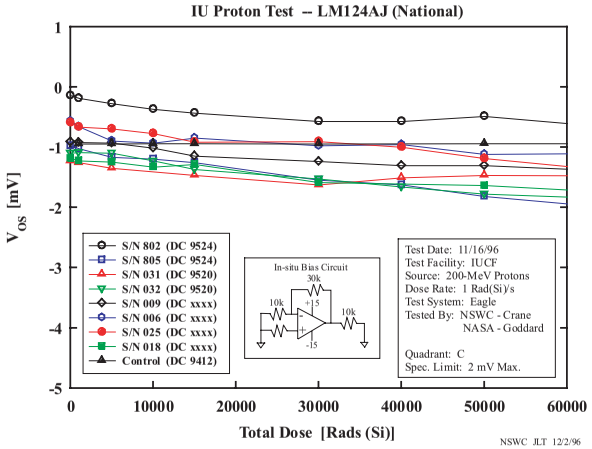

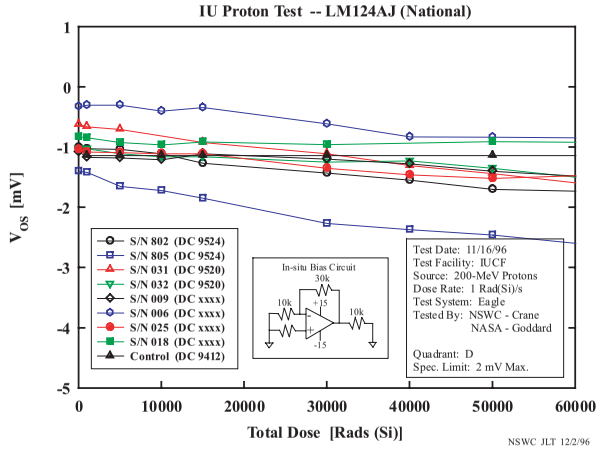

LM124 – Power Supply Current, Ips (200-MeV Proton)

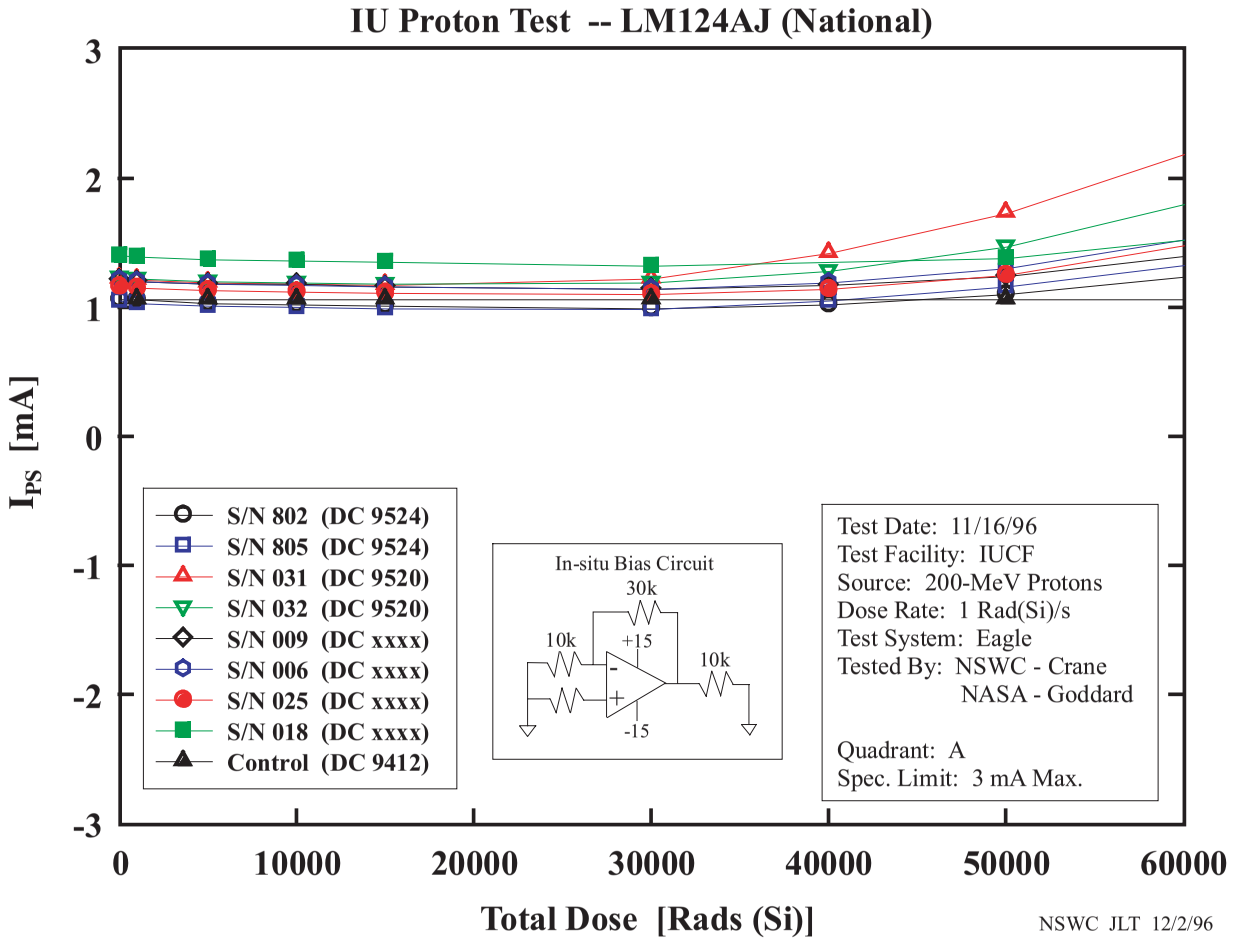

NSWC JLT 12/2/96

LM139 – Pos. Input Bias, Ibp (200-MeV Proton)

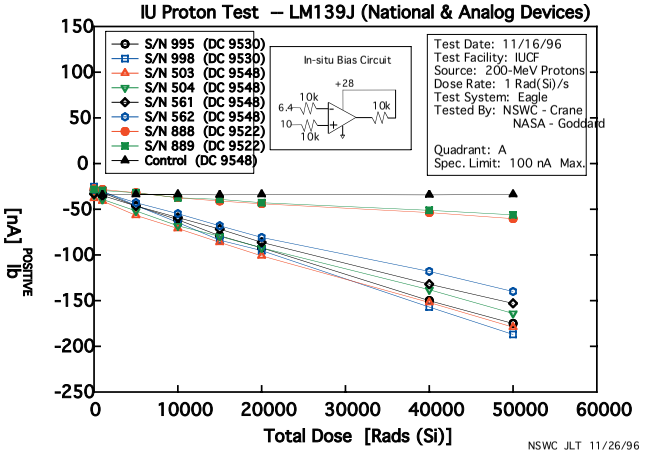

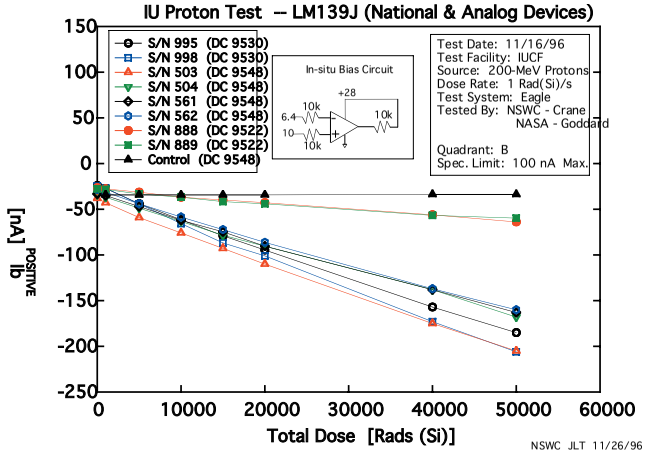

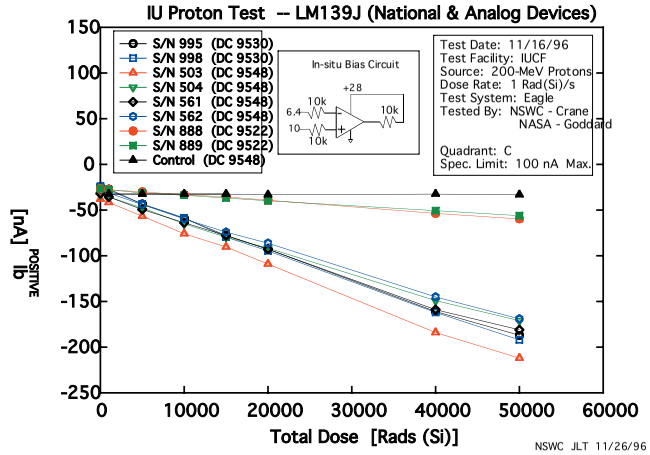

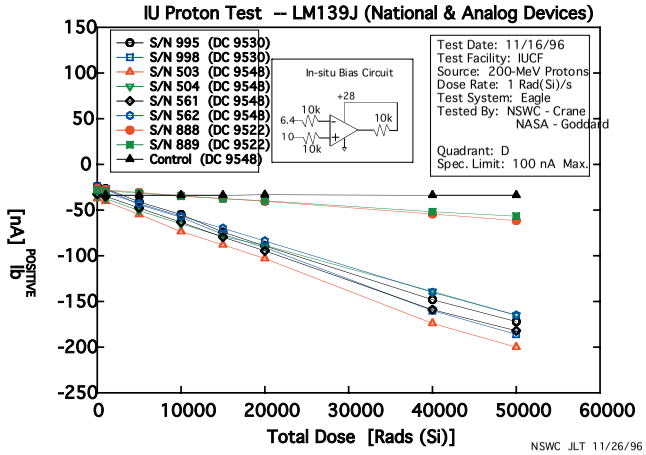

NAVSEA CRANE Surface Warfare Center Division

LM139 – Neg. Input Bias, Ibn (200-MeV Proton)

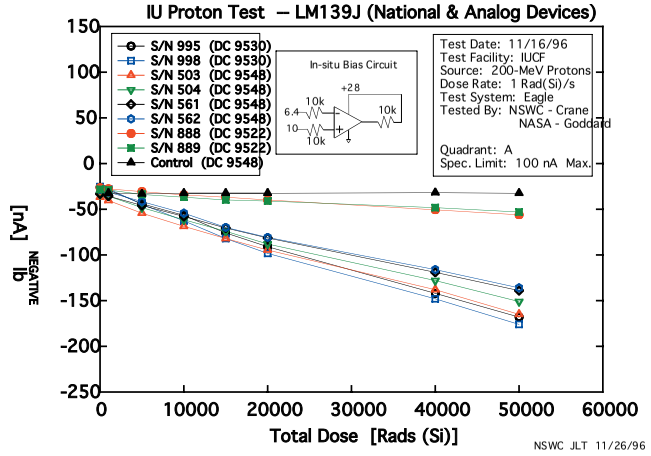

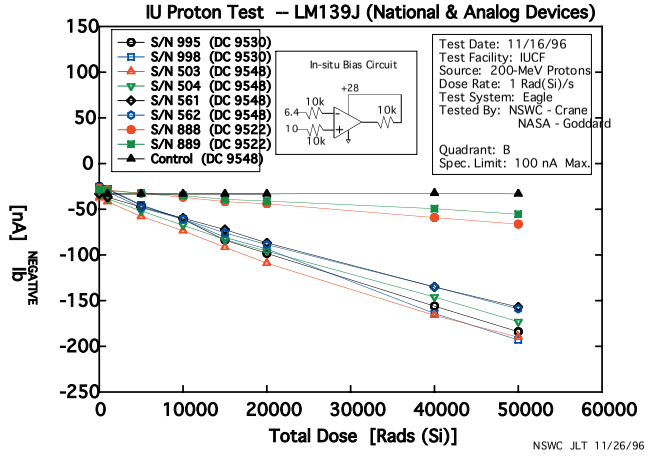

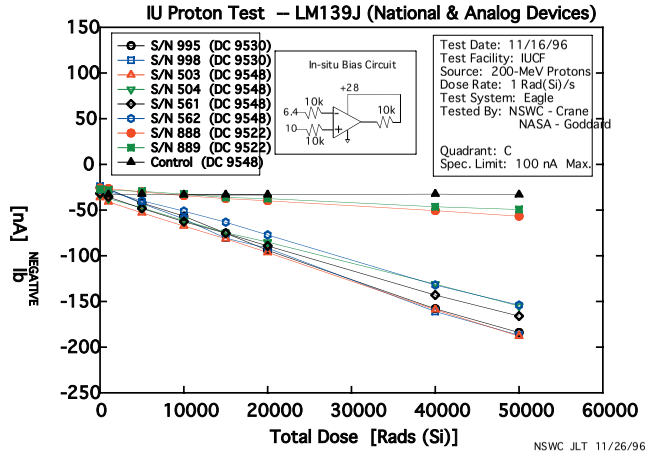

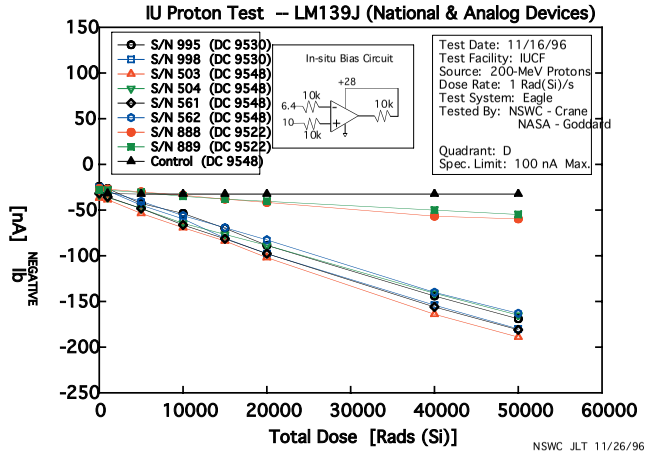

LM139 – Offset Current, Ios (200-MeV Proton)

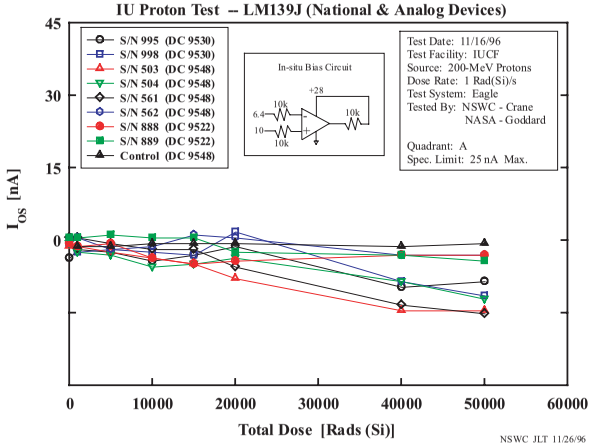

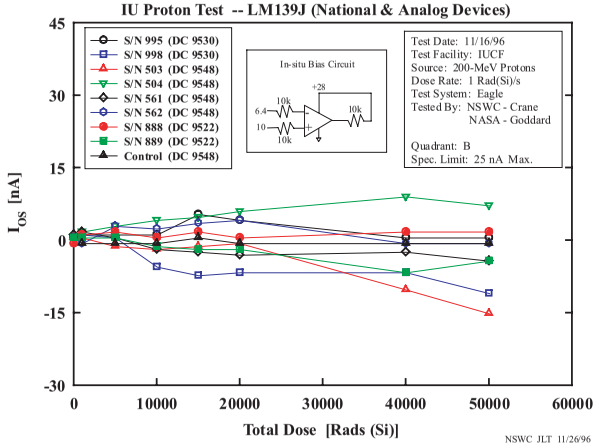

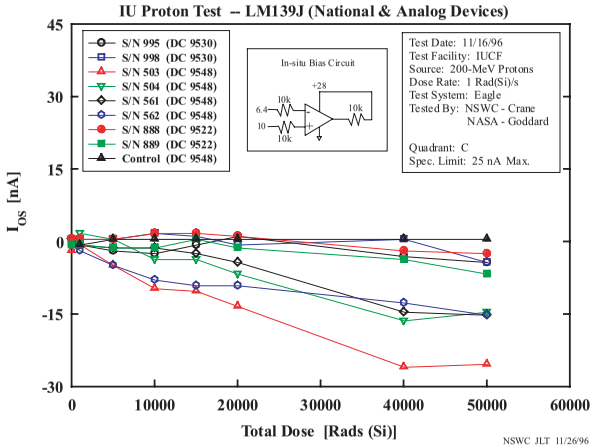

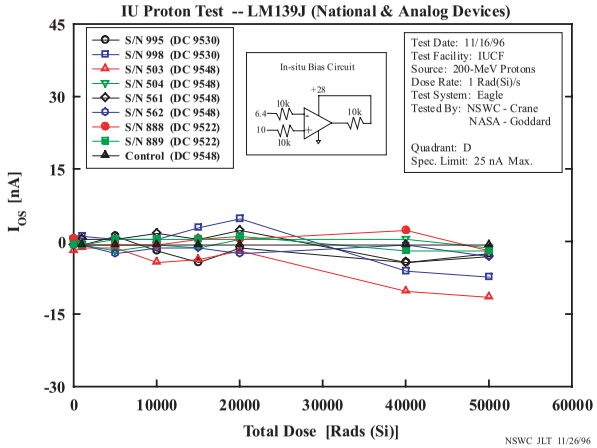

NAVSEA CRANE Surface Warfare Center Division

LM139 – Prop Delay (200-MeV Proton)

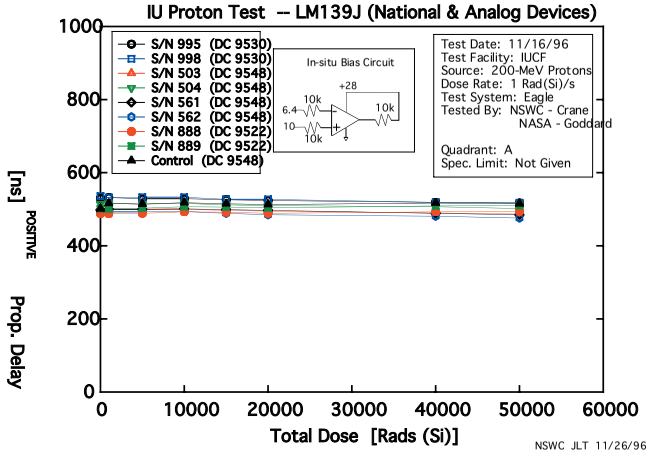

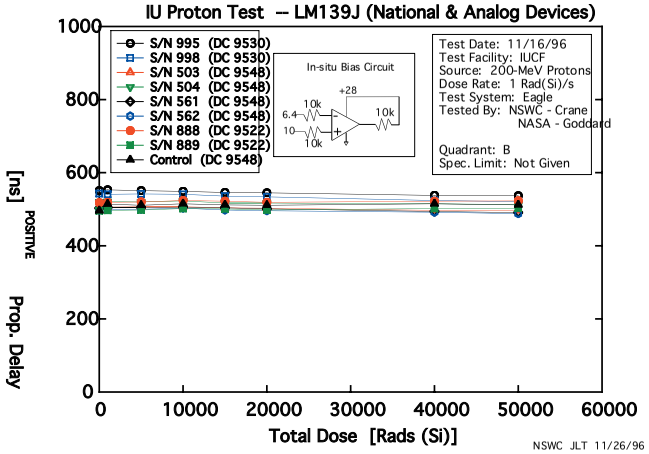

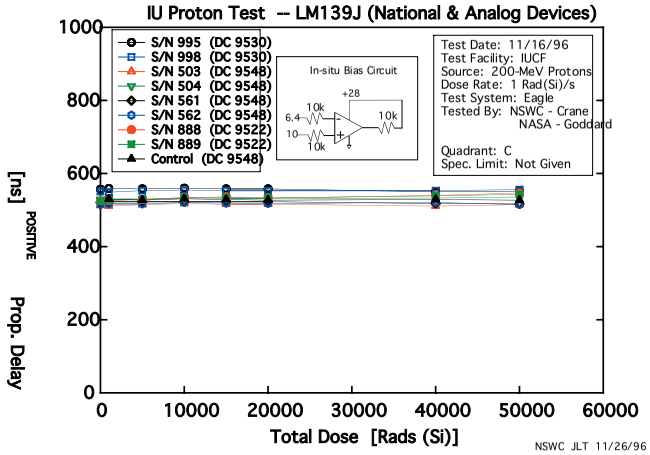

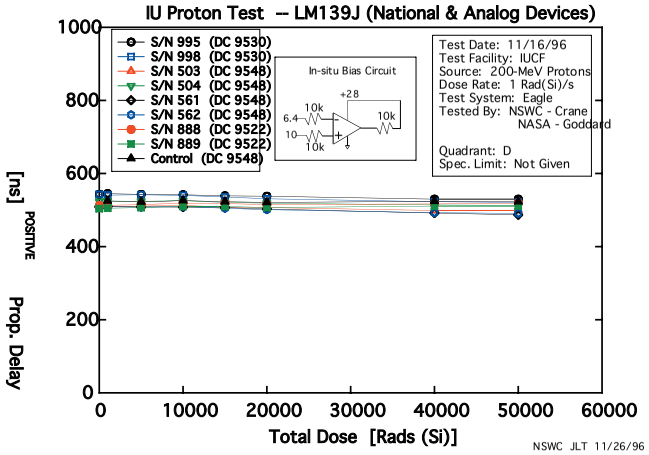

LM139 – Offset Voltage, Vos (200-MeV Proton)

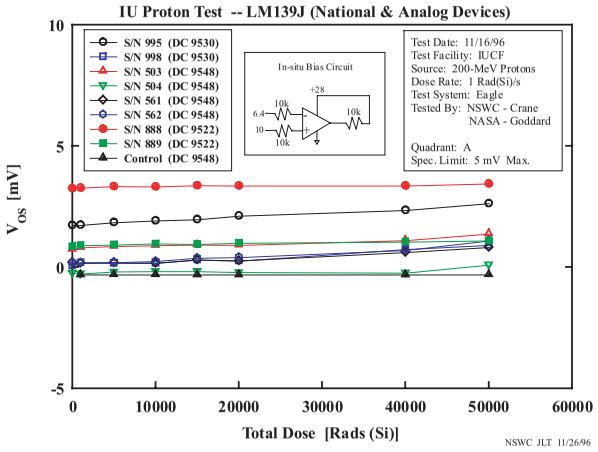

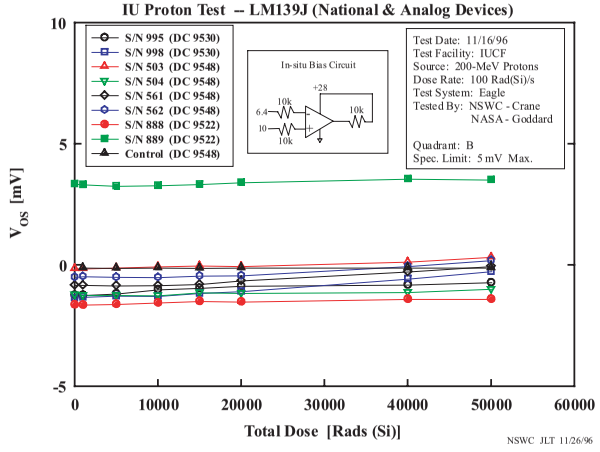

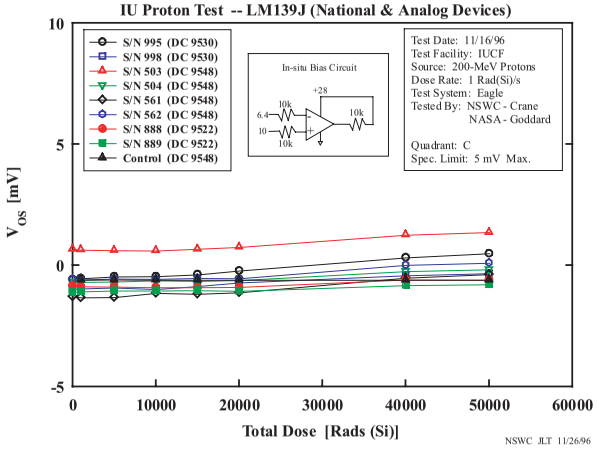

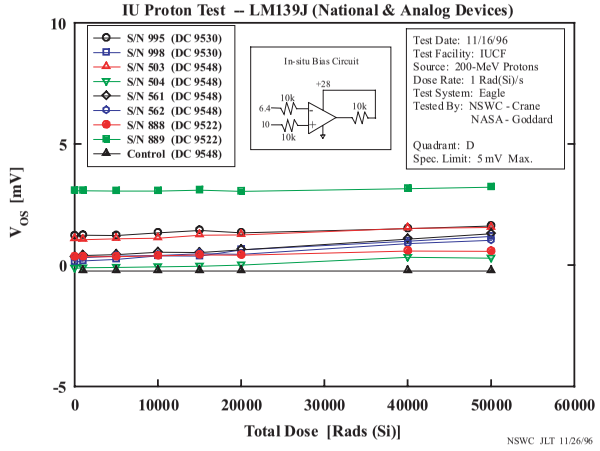

NAVSEA CRANE Surface Warfare Center Division

LM139 – Power Supply Current, Ips (200-MeV Proton)

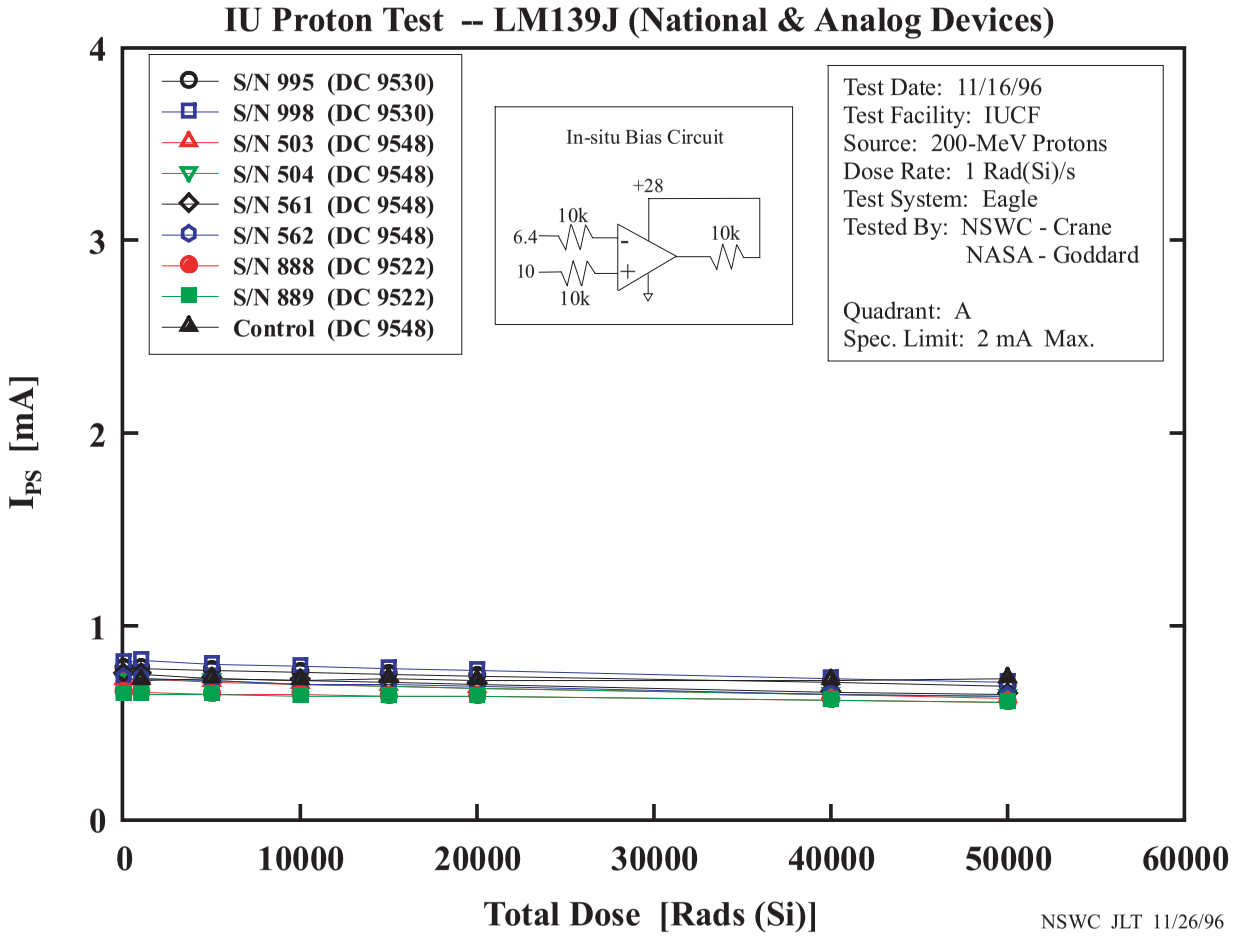

NAVSEA
CRANE
Surface Warfare Center Division

LM124 COTS and LM139

1 MeV equivalent Neutron Data

Graphs created in 2002 from 1996 data

Harnessing the Power of Technology for the Warfighter

NAVSEA CRANE Surface Warfare Center Division

Averaged Positive Input Bias (1-MeV Equiv. Neutron)

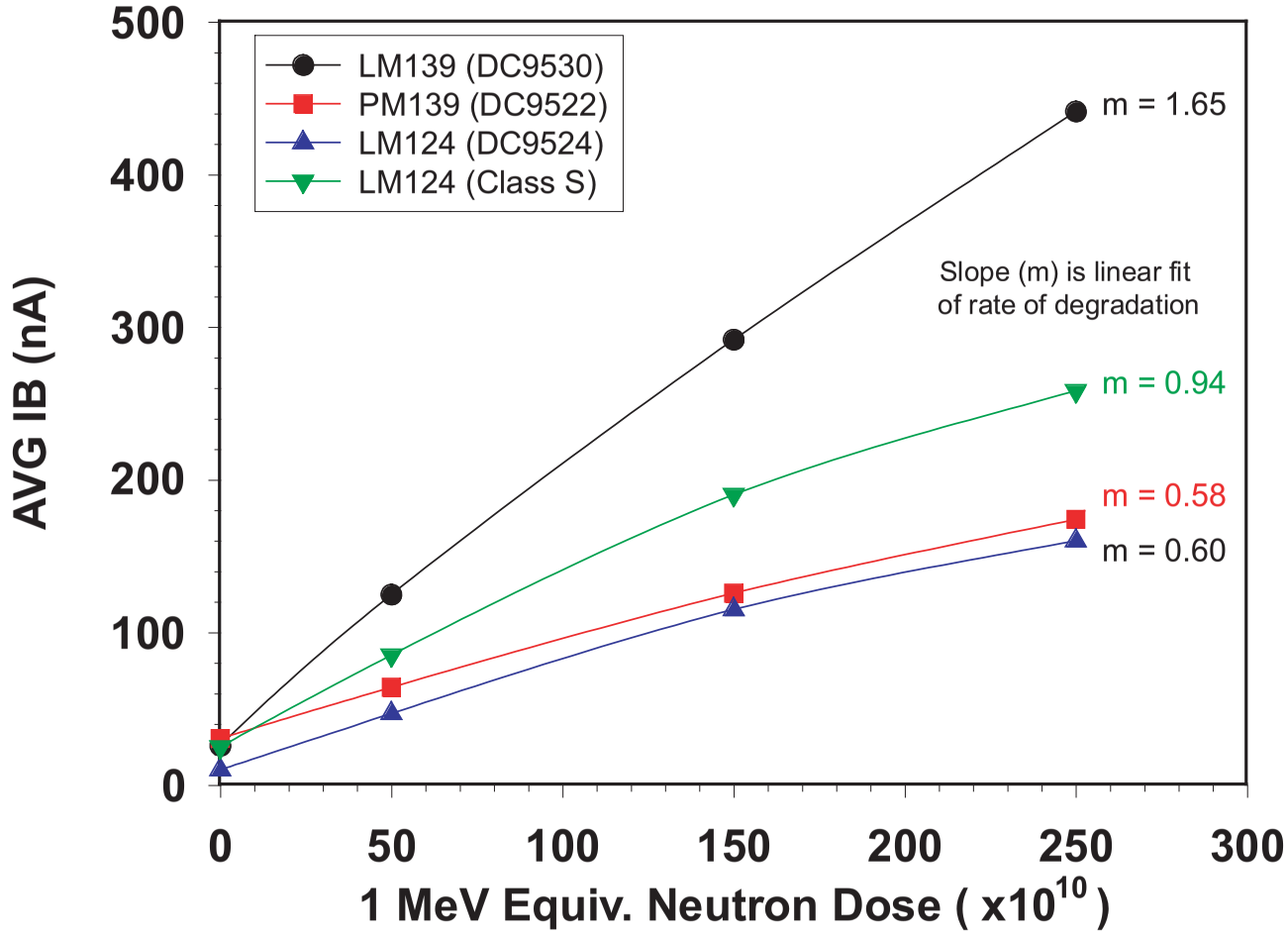

Averaged Offset Current (1-MeV Equiv. Neutron)

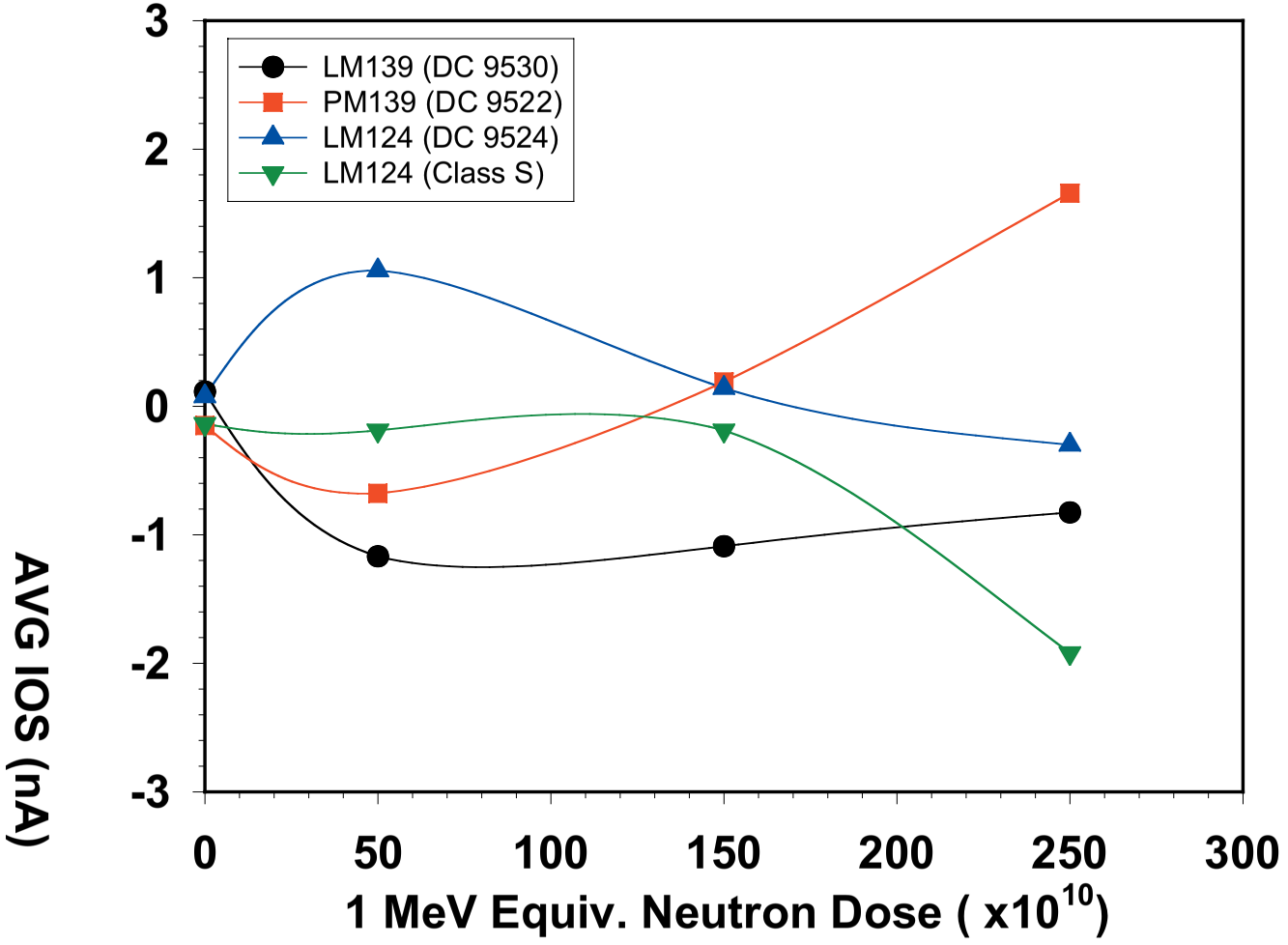

NAVSEA CRANE Surface Warfare Center Division

Averaged Positive Delay (1-MeV Equiv. Neutron)

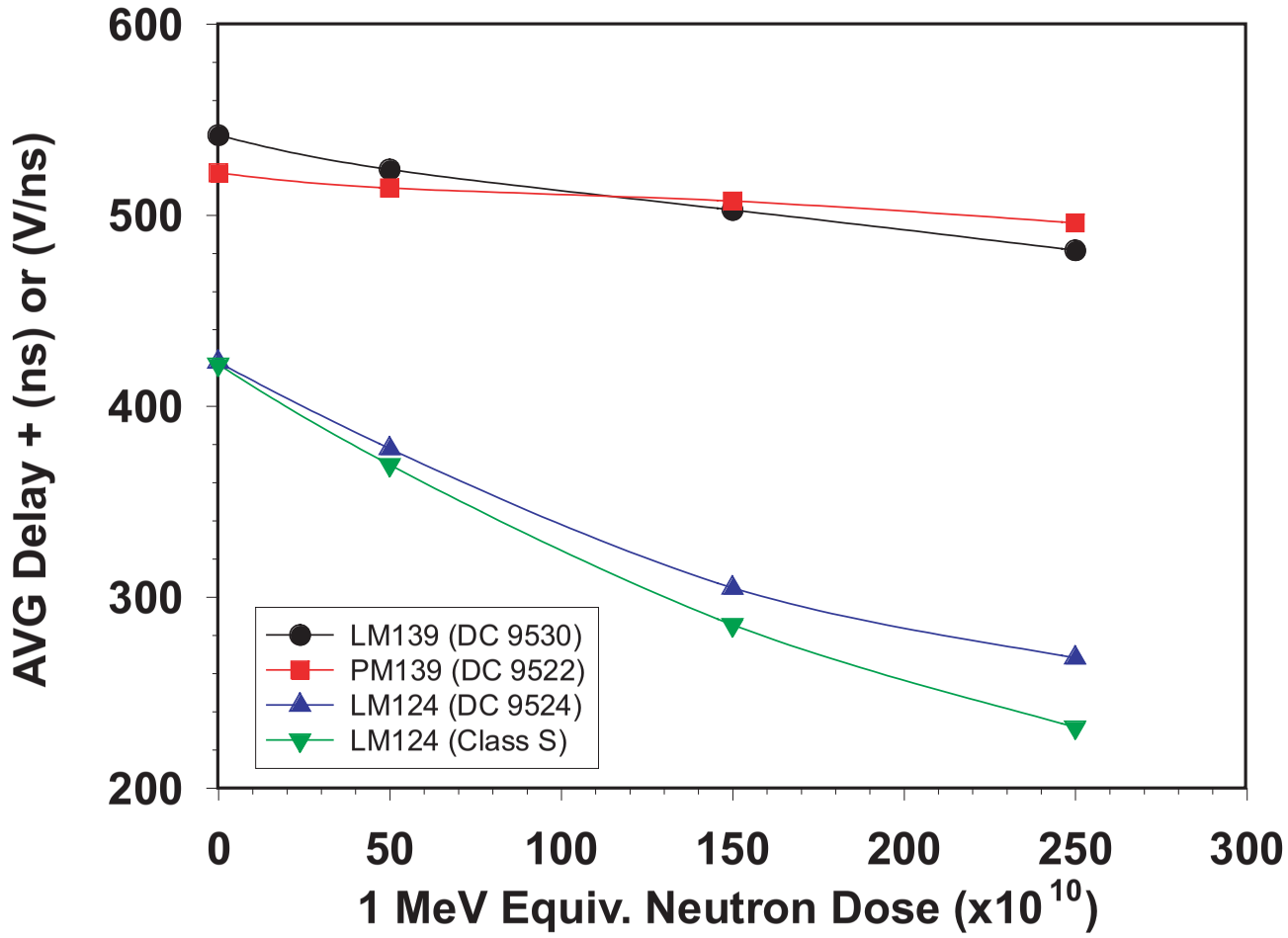

NAVSEA
CRANE
Surface Warfare Center Division

Averaged Offset Voltage (1-MeV Equiv. Neutron)

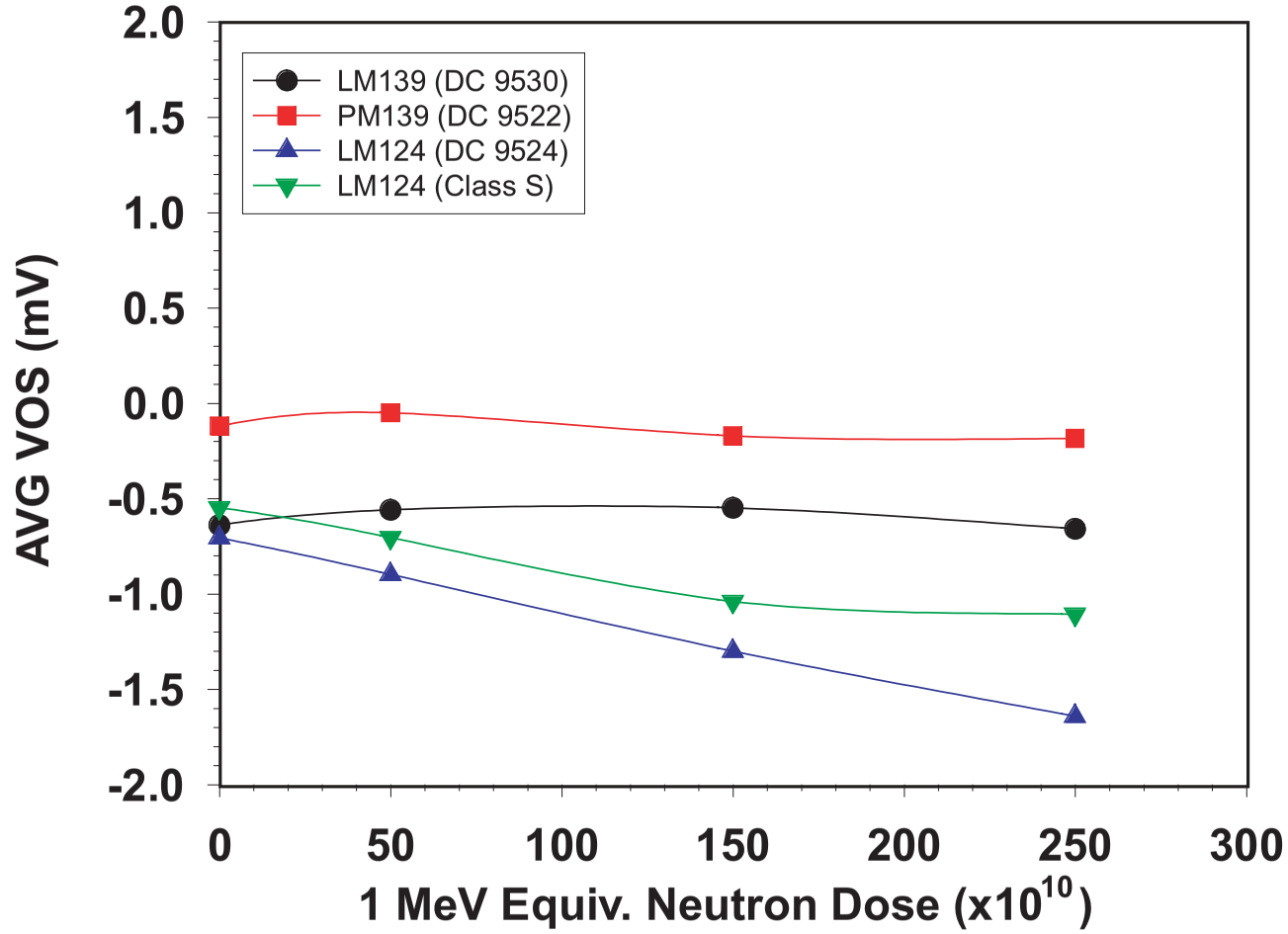

Harnessing the Power of Technology for the Warfighter

NAVSEA CRANE Surface Warfare Center Division

Averaged Pos. Supply Current (1-MeV Equiv. Neutron)

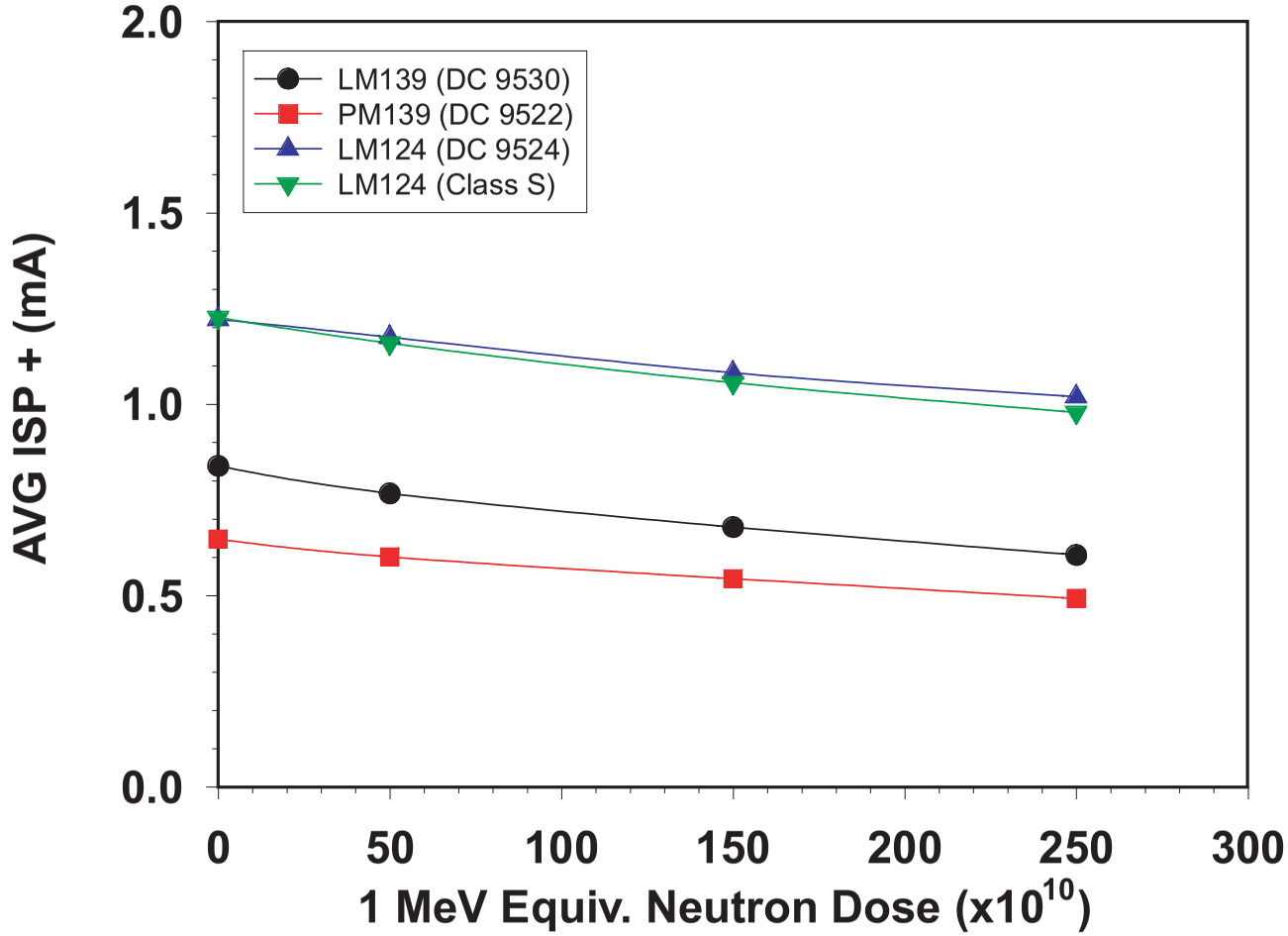

Averaged Neg. Supply Current (1-MeV Equiv. Neutron)

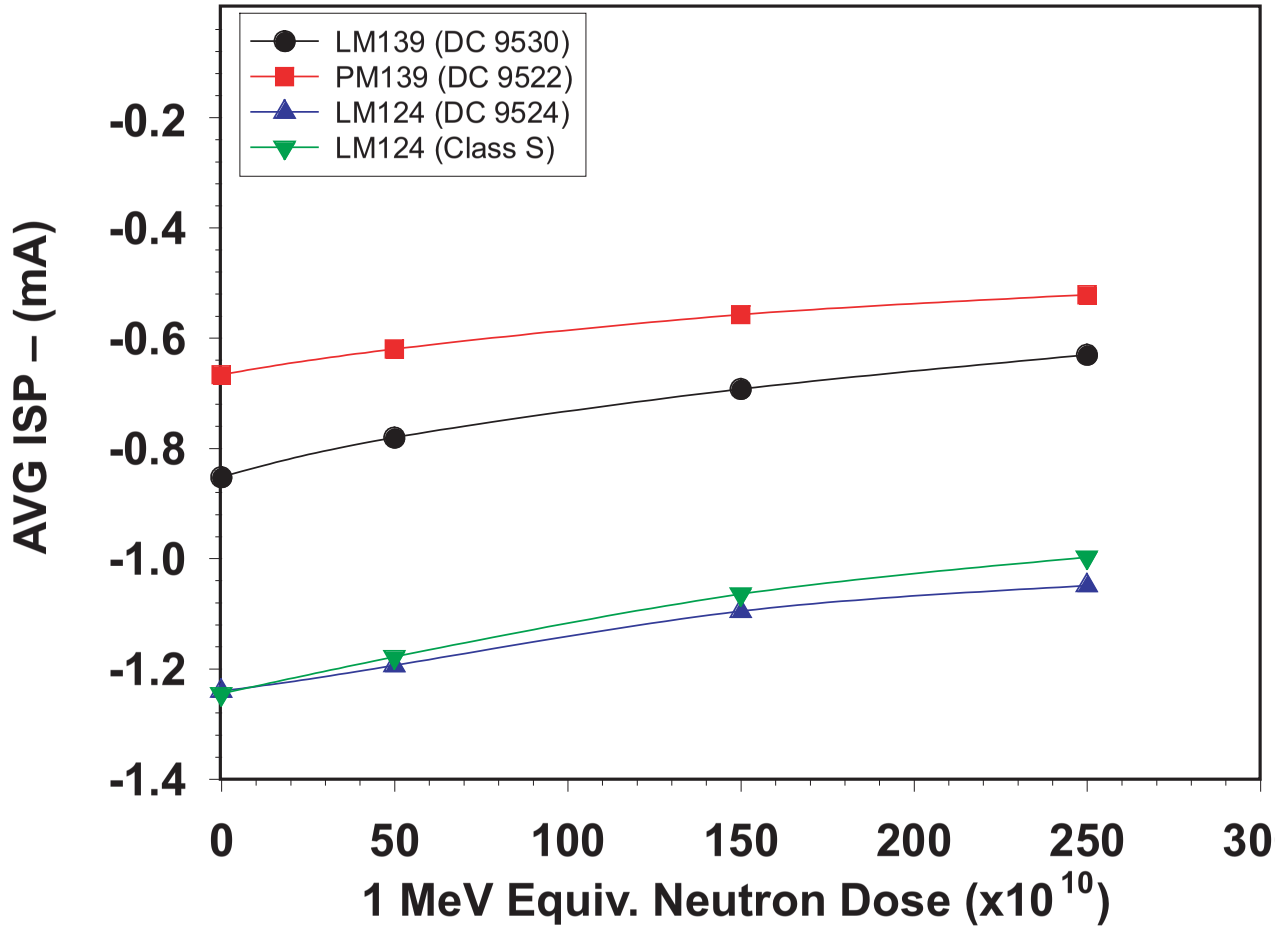

Harnessing the Power of Technology for the Warfighter

NAVSEA CRANE Surface Warfare Center Division

Averaged Output Current Low (1-MeV Equiv. Neutron)

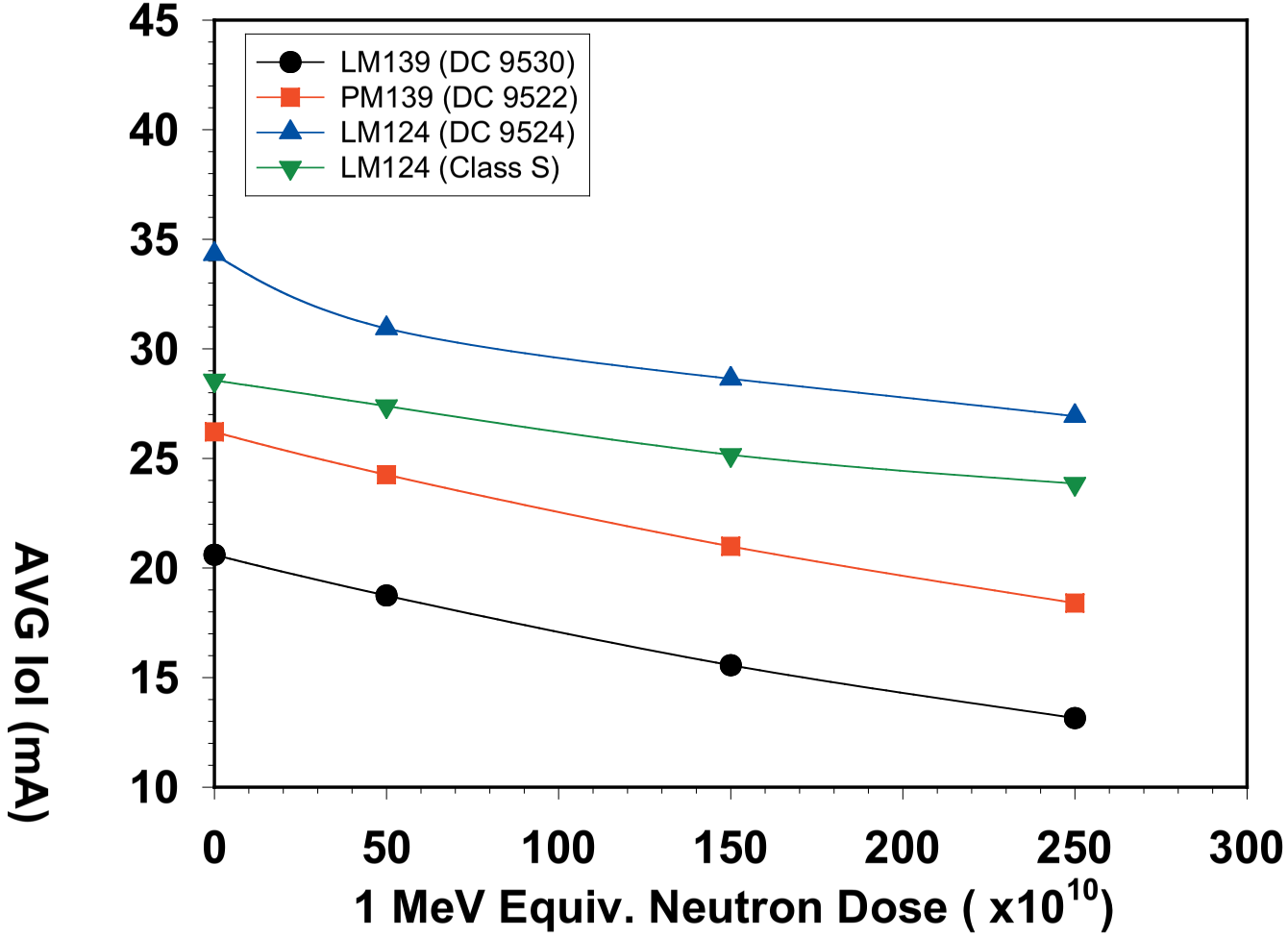

REFERENCES

1. Nowlin, R.N.; Enlow, E.N.; Schrimpf, R.D.; and Combs, W.E.: "Trends in the Total-Dose Response of Modern Bipolar Transistors," *IEEE Trans. Nucl. Sci.*, Vol. 39, No. 6, pp. 2026–2032, December 1992.

2. McClure, S.; Pease, R.L.; Will, E.; and Perry, G.: "Dependence of Total Dose Response of Bipolar Linear Microcircuits on Applied Dose Rate," *IEEE Trans. Nucl. Sci.*, Vol. 41, No. 6, pp. 2544–2549, December 1994.

3. Beaucour, J.T.; Carriere, T.; Gach, A.; et al.: "Total Dose Effects on Negative Voltage Regulator," *IEEE Trans. Nucl. Sci.*, Vol. 41, No. 6, pp. 2420–2426, December 1994.

4. Johnston, A.H.; Rax, B.G.; and Lee, C.I.: "Enhanced Damage in Linear Bipolar ICs at Low Dose Rates," *IEEE Trans. Nucl. Sci.*, Vol. 42, No. 6, pp. 1650–1659, December 1995.

5. Fleetwood, D.M.; Riewe, L.C.; Schwank, J.R.; et al.: "Radiation Effects at Low Electric Fields in Thermal, SIMOX, and Bipolar Base Oxides," *IEEE Trans. Nucl. Sci.*, Vol. 43, No. 6, pp. 2537–2543, December 1996.

6. Pease, R.L.; Cohn, L.M.; Fleetwood, D.M.; et al.: "A Proposed Hardness Assurance Test Methodology for Bipolar Linear Circuits and Devices in a Space Ionizing Radiation Environment," *IEEE Trans. Nucl. Sci.*, Vol. 44, No. 6, pp. 1981–1987, December 1997.

7. Montagner, X.; Briand, R.; Fouillat, P.; et al.: "Dose-Rate and Irradiation Temperature Dependence of BJT SPICE Model Rad-Parameters," *IEEE Trans. Nucl. Sci.*, Vol. 45, No. 3, pp. 1431–1437, June 1998.

8. Schmidt, D.M.; Fleetwood, D.M.; Schrimpf, R.D.; et al.: "Comparison of Ionizing-Radiation-Induced Gain Degradation in Lateral, Substrate, and Vertical PNP BJTs," *IEEE Trans. Nucl. Sci.*, Vol. 42, No. 6, pp. 1541–1549, December 1995.

9. Johnston, A.H.; Rax, B.G.; and Lee, C.I.: "Enhanced Damage in Linear Bipolar ICs at Low Dose Rates," *IEEE Trans. Nucl. Sci.*, Vol. 42, No. 6, pp. 1650–1659, December 1995.

10. Fitus, J.; Combs, W.; Turflinger, T.; et al.: "First Observations of Enhanced Low Dose Rate Sensitivity (ELDRS) in Space: One Part of the MPTB Experiment," *IEEE Trans. Nucl. Sci.*, Vol. 45, pp. 2673–2680, December 1998.

11. Titus, J.; Emily, D.; Krieg, J.; et al.: "Enhanced Low Dose Rate Sensitivity (ELDRS) of Linear Circuits in a Space Environment," *IEEE Trans. Nucl. Sci.*, Vol. 46, pp. 1608–1615, December 1999.

12. “Test Method 4001,” *MIL–STD–883*, Rev. E.

13. August, L.S.; Circle, J.C.; Ritter, J.C.; and Tobin, J.S.: “A MOS Dosimeter for Use in Space,” *IEEE Trans. Nucl. Sci.*, Vol. 30, pp. 508–511, Feburary 1983.

14. Dyer, C.; Truscott, P.; Sanderson, C.; et al.: “Radiation Environment Measurements From CREAM and CREDO During the Approach to Solar Maximum,” *IEEE Trans. Nucl. Sci.*, Vol. 47, pp. 2208–2217, December 2000.

15. Dyer, C.; Sanderson, C.; Mugford, R.; et al.: “Radiation Environment of the Microelectronics and Photonics Test Bed as Measured by CREDO–3,” *IEEE Trans. Nucl. Sci.,* Vol. 47, pp. 481–485, June 2000.

16. Stassinopoulos, E.G.; Van Gunten, O.; Brucker, G.J.; et al.: “Radiation Effects on MOS Devices: Dosimetry, Annealing, Iradiation Sequence and Sources,” *IEEE Trans. Nuc. Sci.,* Vol. 30, No. 3, pp. 1880–1884, June 1983.

17. Brucker, G.J.; Stassinopoulos, E.G.; Van Gunten, O.; et al.: “The Damage Equivalence of Electrons, Protons and Gamma Rays in MOS Devices,” *IEEE Trans. Nuc. Sci.*, Vol. 29, No. 6, pp. 1966–1969, December 1982.

18. August, L.S.: “Estimating and Reducing Errors in MOS Dosimeters Caused by Exposure to Different Radiations,” *IEEE Trans. Nuc. Sci.*, Vol. 29, No. 6, pp. 2000–2003, December 1982.

19. Dyer, C.S.; Sims, A.J.; Truscott, P.R.; et al.: “Measurements of the Radiation Environment From LEO to GTO Using the CREAM & CREDO Experiments,” *IEEE Trans. Nuc. Sci.*, Vol. 42, No. 6, pp. 1975–1982, December 1995.

20. Dyer, C.S.; Truscott, P.R.; Peerless, C.L.; et al.: “Updated Measurements From CREAM and CREDO and Implications for Environment and Shielding Models,” *IEEE Trans. Nuc. Sci.,* Vol. 45, No 3, pp. 1584–1589, June 1998.

21. Dyer, C.; Comber, C.; Truscott, P.; et al.: “Microdosimetry Code Simulations of Charge Deposition Spectra, Single Event Upsets and Multi-bit Upsets,” *IEEE Trans. Nucl. Sci.,* Vol. 46, pp. 1486–1493, December 1999.

22. Buchner, S.; Campbell, A.; Meehan, T.; et al.: “Investigations of Single-Ion Multiple Bit Upsets in Memories On Board a Space Experiment,” *IEEE Trans. Nucl. Sci.,* Vol. 47, pp. 705–711, June 2000.

23. Dyer, C.S.: “Radiation Effects on Spacecraft and Aircraft,” *Proc. SOLSPA*, ESA SP–477, pp. 505–512, March 2002.

24. Campbell, A.; Buchner, S.; Petersen, E.; et al.: “SEU Measurements and Predictions on MPTB for a Large Solar Event,” *Proc. RADECS01*; *IEEE Trans. Nucl. Sci.,* Vol. 49, pp. 1340–1344, June 2002.

25. Dyer, C.; Rodgers, D.; Clucas, S.; et al.: "Observation of Solar Particle Events From CREDO and MPTB During the Current Solar Maximum," Presented at the 2002 IEEE NSREC, Oral Paper B–4, Phoenix, AZ, July 15–19, 2002; *IEEE Trans. Nucl. Sci.*, accepted December 2002.

26. Blake, J.B.; Baker, D.N.; Turner, N.; et al.: "Correlation of Changes in the Outer-Zone Relativistic-Electron Population With Upstream Solar Wind and Magnetic Field Measurements," *Geophys. Res. Letts.*, Vol. 24, No. 8, pp. 927–929, April, 15 1997.

27. Fennell, J.F.; Koons, H.C.; and Blake, J.B.: "A Deep Dielectric Charging Environmental Specification for Geosynchronous and HEO/MOLNIYA Satellites," in *1999 Government Microcircuit Applications Conference (GOMAC) Digest*, pp. 823–826, March 1999.

28. Fennell, J.F.; Koons, H.C.; Chen, M.W.; and Blake, J.B.: "Internal Charging: A Preliminary Environmental Specification for Satellites," *IEEE Trans. Plasma Sci.,* Vol. 28, No. 6, pp. 2029–2036, December 2000.

29. Fennell, J.F.; Roeder, J.L.; Freidel, R.; et al.: "Open Field Line Region Boundary at High Altitudes," *Phys. and Chem. of Earth*, Vol. 24, pp. 129–134, 1999.

30. Fennell, J.F.; Blake, J.B.; Roeder, J.L.; et al.: "Tail Lobe and Open Field Line Region Entries at Mid to High Latitudes," *Adv. Space Res.*, Vol. 20, pp. 431–435, 1997.

31. Fennell, J.F.; Koons, H.C.; Roeder, J.L.; and Blake, J.B.: Spacecraft Charging: Observations and Relationship to Satellite Anomalies, Proceedings of 7th Spacecraft Charging Technology Conference, ESA SP–476, p. 279, November 2001.

32. Mazur, J.E.: "The Radiation Environment Outside and Inside a Spacecraft," Section II of "Radiation Effects–From Particles to Payloads," 2002 IEEE NSREC Short Course Notebook, pp. 1–69, July, 2002.

REPORT DOCUMENTATION PAGE

Form Approved
OMB No. 0704-0188

1. AGENCY USE ONLY (Leave Blank)	2. REPORT DATE	3. REPORT TYPE AND DATES COVERED
	August 2004	Technical Publication

4. TITLE AND SUBTITLE
Solar Variability and the Near-Earth Environment—Mining Enhanced Low Dose Rate Sensitivity Data From the Microelectronics and Photonics Test Bed Space Experiment

5. FUNDING NUMBERS

6. AUTHORS
T. Turflinger, W. Schmeichel, J. Krieg, J. Titus, A. Campbell,*
M. Reeves,* and P. Marshall**

7. PERFORMING ORGANIZATION NAMES(S) AND ADDRESS(ES)
NAVSEA Crane
300 Highway 361
Crane, IN 47522

8. PERFORMING ORGANIZATION REPORT NUMBER
M–1120

9. SPONSORING/MONITORING AGENCY NAME(S) AND ADDRESS(ES)
NASA's Space Environments and Effects (SEE) Program
George C. Marshall Space Flight Center
Marshall Space Flight Center, AL 35812

10. SPONSORING/MONITORING AGENCY REPORT NUMBER
NASA/TP—2004–213339

11. SUPPLEMENTARY NOTES
Prepared for NASA's Space Environments and Effects (SEE) Program by NAVSEA Crane
*Naval Research Laboratory, Washington, DC **Virginia
Technical Monitor: Donna Hardage, NASA Marshall Space Flight Center

12a. DISTRIBUTION/AVAILABILITY STATEMENT
Unclassified-Unlimited
Subject Category 93
Available: 301–621–0134

12b. DISTRIBUTION CODE

13. ABSTRACT (Maximum 200 words)

This effort is a detailed analysis of existing microelectronics and photonics test bed satellite data from one experiment, the bipolar test board, looking to improve our understanding of the enhanced low dose rate sensitivity (ELDRS) phenomenon. Over the past several years, extensive total dose irradiations of bipolar devices have demonstrated that many of these devices exhibited ELDRS. In sensitive bipolar transistors, ELDRS produced enhanced degradation of base current, resulting in enhanced gain degradation at dose rates <0.1 rd(Si)/s compared to similar transistors irradiated at dose rates >1 rd(Si)/s. This Technical Publication provides updated information about the test devices, the in-flight experiment, and both flight-and ground-based observations. Flight data are presented for the past 5 yr of the mission. These data are compared to ground-based data taken on devices from the same date code lots. Information about temperature fluctuations, power shutdowns, and other variables encountered during the space flight are documented.

14. SUBJECT TERMS
ELDRS, total dose, sensitivity, radiation, irradiation, bipolar devices, degradation

15. NUMBER OF PAGES
132

16. PRICE CODE

17. SECURITY CLASSIFICATION OF REPORT	18. SECURITY CLASSIFICATION OF THIS PAGE	19. SECURITY CLASSIFICATION OF ABSTRACT	20. LIMITATION OF ABSTRACT
Unclassified	Unclassified	Unclassified	Unlimited